Corso di Perfezionamento in Fisica

Topics in composite models and dark matter phenomenology

SCUOLA
NORMALE
SUPERIORE

Classe di Scienze

tesi di dottorato

SUPERVISOR:
Prof. Roberto Contino

CANDIDATO:
Alessandro Podo

XXXIII Ciclo
2017-2020

Abstract

We investigate models of composite dark matter in which the dark matter candidate arises naturally as an accidentally stable bound state of a confining dynamics and with observable signatures in a wide variety of experiments. In the first part of the thesis we introduce and explore a new class of models with dark fermions in the adjoint representation of the confining gauge group. The low energy dynamics and the cosmological history are peculiar and provide a dark matter candidate with properties much different from that of a canonical WIMP. The dark matter is heavy but has a large interaction range and can be tested primarily with indirect searches. In the second part of the thesis we classify and study models of composite dark matter with a strongly interacting chiral dark sector, in which all the mass scales are generated dynamically. In this case the candidate is a SM singlet dark pion with a thermal abundance whose low energy phenomenology can be thoroughly studied through chiral lagrangian techniques. We present an analysis of the low energy phenomenology, compute the radiatively generated masses of the light states and study the cosmological history of the model. The presence of partner states interacting with the SM offers the opportunity to test the model at colliders. In the last part of the thesis we present the phenomenological signatures of the models previously introduced and determine the current bounds. In doing so we also present a strategy to derive a limit on the lifetime of dark matter particles in generic models of particle dark matter from the observation of the 21 cm cosmological signal.

ai miei genitori,
Ermanno e Maria Grazia

Acknowledgments

It is a pleasure to thank my advisor, Roberto Contino, for his generous mentorship and his encouragement during the course of my Ph.D. His scientific rigour and deep knowledge of particle physics and quantum field theory have been an invaluable help and will always be an example for me.

I am grateful to Michele Redi for many fruitful discussions, crucial for the development of this work, and for collaboration on some of the topics presented in this thesis.

A special thank you to my collaborators and friends Andrea Mitridate and Filippo Revello: I have had a lot of fun and learned an incredible amount of physics from them.

During the course of my Ph.D. I have had the privilege to meet many extraordinary scientists who have shaped my understanding of physics. I deeply thank Lam Hui, Austin Joyce, Rashmish Mishra, Alberto Nicolis, Luca Santoni and Enrico Trincherini for discussions and collaboration and for sharing their knowledge and abilities, and Kaustubh Agashe, Dario Buttazzo, Gabriele Ferretti, Yann Gouttenoire, Andrei Mesinger, Cristina Mondino, Paolo Panci, Gabriele Rigo, Francesco Sgarlata, Alessandro Strumia, Luca Vecchi, Riccardo Rattazzi, Filippo Sala for useful conversations.

I am very grateful to my SNS colleagues and friends, especially Kevin Max, Carlo Heissenberg, Ivano Basile, Salvatore Bottaro, Sonali Verma, Leonardo Trombetta and Ling-Xiao Xu, for what we have shared during these years.

I wish to express my gratitude to the SNS theory and particle physics groups for the lively environment, and especially to Riccardo Barbieri, for being an example since my first year of undergraduate, and to Gigi Rolandi for introducing me to particle physics and guiding me during my first steps in the world of research.

Last, but not least, my warmest thanks go to my family and to my friends, for their extraordinary support during the difficult moments of graduate studies. I especially thank Daniele, Eugenio, Giacomo, Giammarco, Giorgio, Ludovico, Marco, Paola, Raffaele and Tommaso.

List of publications and other research

The research work presented in this Ph.D. thesis is based on the following references, in part reproduced [1, 2, 3, 4]:

- R. Contino, A. Mitridate and A. Podo, *Beyond the standard model with strong dynamics*, *Frascati Phys. Ser.* **65** (2017) 1.
- R. Contino, A. Mitridate, A. Podo and M. Redi, *Gluequark Dark Matter*, *JHEP* **02** (2019) 187 [1811.06975].
- R. Contino, A. Podo and F. Revello, *Composite dark matter from strongly-interacting chiral dynamics*, *to appear* (2020) [2008.10607] .
- A. Mitridate and A. Podo, *Bounds on Dark Matter decay from 21 cm line*, *JCAP* **05** (2018) 069 [1803.11169].

During his Ph.D. the author has also performed research on the vacuum alignment of chiral gauge theories with product gauge groups, in collaboration with Roberto Contino and Filippo Revello [5]. The author has spent a visiting research period of four months at the Columbia University in the City of New York performing research (to appear) on:

- the study of perturbations of slowly rotating black holes, in collaboration with Lam Hui, Luca Santoni and Enrico Trincherini;
- the study in Quantum Field Theory of bosonic and fermionic systems at finite chemical potential and zero temperature, in collaboration with Austin Joyce, Alberto Nicolis and Luca Santoni.

Contents

1 Introduction **8**

2 Gluequark dark matter **11**
2.1 Introduction . . . 11
2.2 The models . . . 12
2.3 Cosmological History . . . 18
2.3.1 Thermal freeze-out . . . 19
2.3.2 Dilution . . . 20
2.3.3 Reannihilation . . . 23
2.4 Estimate of the Relic density . . . 25
2.5 Summary . . . 29
2.A Dark Quark Annihilation Cross Section . . . 31
2.B Reannihilation . . . 31
2.B.1 Estimate of the Re-annihilation Cross Section . . . 33
2.B.2 Re-annihilation temperature . . . 37
2.C A model with hypercharge . . . 38

3 Chiral dark sector with SM interactions **40**
3.1 Introduction . . . 40
3.2 Analysis of minimal models . . . 42
3.3 The model with $SU(2)_{EW}$ doublets . . . 46
3.4 Phenomenological profile . . . 49
3.4.1 Dark Baryons . . . 49
3.4.2 Dark Pions and low-energy effective theory . . . 49
3.4.3 Decay channels . . . 51
3.4.4 Spectrum . . . 54
3.5 Cosmology . . . 55
3.5.1 Dark baryons . . . 55
3.5.2 Short-lived dark photons . . . 56
3.5.3 Long-lived dark photons . . . 57
3.5.4 Cosmologically stable dark photons . . . 62
3.5.5 Alternative choices of parameters and cosmological scenarios . . . 62
3.6 Discussion and outlook . . . 64
3.A Useful formulas for dark pions . . . 70
3.B Model with $SU(3)_c$ triplets . . . 70
3.C Boltzmann equations for long-lived dark photons . . . 71

3.D The Dark Photon 74

4 Phenomenology **77**
4.1 Constraints on the lifetime of dark matter from the 21 cm global signal . 77
4.1.1 The 21 cm cosmological signal 77
4.1.2 Bounds on Dark Matter decays 79
4.1.3 Comparison with the case of DM annihilations 82
4.2 Indirect searches 84
4.2.1 Cosmologically long-lived particles 84
4.2.2 Gluequark Annihilation and Decay 84
4.2.3 Chiral dark matter annihilation signals 88
4.3 Direct detection searches 89
4.3.1 Gluequark 89
4.3.2 Chiral DM 89
4.3.3 Limits on charged relics 91
4.4 Collider searches for gluequark models 91
4.5 Collider searches for models of chiral dark matter 95
4.5.1 Production and decays of NGB triplets 95
4.5.2 Bounds 97

5 Conclusions **105**

1 Introduction

The Standard Model (SM) of particle physics, with a small extension to account for neutrino oscillations, describes with striking accuracy and remarkable conceptual simplicity all the phenomena observed in laboratory tests of fundamental interactions and underlies the description of nuclear, atomic and condensed matter physics. Yet cosmological and astrophysical observations challenge its status as a complete theory, requiring explanations for the observed dark matter and dark energy components.

While dark energy may be explained within the SM by a cosmological constant, the problem of dark matter provides perhaps the strongest hint for the existence of new particles beyond the Standard Model. The properties of dark matter are still largely unknown and models of dark matter span an incredibly diverse variety of candidates ranging from ultralight bosons or axions [6, 7], to light fermionic dark matter [8, 9, 10, 11, 12], to weak scale particles [13, 14] and extending up to primordial black holes [15].

In the present thesis we try to take the properties of the Standard Model as a guideline to build models of dark matter with a motivated structure and that can be tested with a combination of observations, including colliders, laboratory experiments, astrophysical and cosmological observations.

From a modern point of view the SM is understood as an effective field theory with a very high ultraviolet cut-off, which appears renormalizable at energies currently probed in experiments. This feature notoriously gives rise to the SM hierarchy problem, but is also at the very origin of the attractive properties of the SM. In particular, global symmetries arise accidentally in the infrared and explain in the most economical way baryon and lepton number conservation, flavour and electroweak (EW) precision tests.

We consider these remarkable properties as paradigmatic, providing a compelling guidance to build possible extensions of the SM. In particular, the cosmological stability of Dark Matter (DM) can be elegantly explained in terms of accidental symmetries, in analogy with the stability of the proton following from baryon number conservation. This has to be contrasted with SM extensions where global symmetries are imposed ad hoc, like for example the case of R-parity in supersymmetry. A simple way to generate accidental symmetries without interfering with electroweak symmetry breaking is to extend the gauge theory structure of the SM by postulating a new confining dark color group whose dark fermions interact with the SM only through vectorlike gauge interactions.

This approach has been first proposed in Ref. [16] and models of Dark Matter based on it have been studied in Refs. [17, 18, 19, 20, 21, 22, 23, 24, 25, 26, 27]. A systematic classification of theories where the dark sector comprises new fermions transforming as real or vector-like representations under both the SM and dark gauge groups has been presented in Refs. [22, 25]. Such framework, known as Vector-Like Confinement [16], provides a safe non-trivial extension of the SM, since it gives small and calculable de-

viations to EW observables that are in full agreement with current data, and may lead to distinctive experimental signatures potentially observable at future colliders [28, 29]. Ref. [22] considered QCD-like theories with fermions in the fundamental representation of the dark gauge group in the regime where dark quark masses are below the dark color dynamical scale, $M_{\mathcal{Q}} < \Lambda_{DC}$, and found that a correct relic abundance can be obtained for baryonic DM candidates with masses of order 100 TeV. Lighter DM masses, down to $\mathcal{O}(10\,\text{TeV})$, are instead allowed if $M_{\mathcal{Q}} > \Lambda_{DC}$ [25]. Mesonic DM candidates can be even lighter and can arise for example as pseudo Nambu-Goldstone bosons (NGBs) of a spontaneously broken global symmetry of the dark dynamics.

In the first part of the thesis we continue this exploration by considering vectorlike models with fermions in the adjoint representation of the gauge group and vector-like or real representations of the SM. The dark matter candidate is a composite fermionic bound state of one dark fermion and dark gluons, that we call a gluequark. Similar candidates were previously considered in Ref. [30], where they couple to the SM sector through the neutrino portal, and in Refs. [31, 32], in the context of supersymmetric gauge theories. The gluequark has peculiar phenomenological properties deriving from an unusually large self-interaction range, *i.e.* larger than the Compton wavelength. In chapter 2 we provide a classification of the possible models of gluequarks with SM interactions and study their reach phenomenology.

In the second part of the thesis we try to go one step further by combining the previous approach to accidentally stable dark matter candidates with the question of the dynamical origin of the dark matter mass scale.

In the Standard Model (SM) of particle physics the mass spectrum of the theory, with the exception of neutrinos, is explained in terms of just two fundamental scales, i.e. the scale of QCD confinement and the electroweak (EW) scale. The QCD scale is generated through dimensional transmutation in terms of the QCD coupling and is thus dynamical. The EW scale, on the other hand, is set into the theory by hand through the Higgs mass term, and is moreover notoriously sensitive to UV corrections. This makes the SM description of the EW sector less predictive and compelling compared to the minimal and elegant characterization of the hadronic dynamics. Theories beyond the SM have been constructed – such as Composite Higgs [33, 34, 35, 36, 37, 38], SUSY with radiative EW symmetry breaking [39, 40], or Cosmological Relaxation [41]– where the electroweak scale is dynamically generated. The neutrino masses, which are generated by a dimension-5 operator in the SM effective theory, could be also set by a dynamical scale in a more complete theory, such as for example a Grand Unification Theory (GUT) or a theory with Dirac neutrinos.

If Dark Matter (DM) in our Universe is made of one (or more) new particle, it is natural to ask whether its mass is generated dynamically or if it entails yet another arbitrary fundamental scale. Theories where the DM mass is not dynamical (unless one considers a deeper layer of theoretical description), have been largely explored, including the previously discussed composite theories with vector-like fermions, since in that case bare mass terms can be larger than the dynamical scale and determine the masses of some of the physical states, possibly including the DM candidate [30, 25, 2]. Theories

where the DM mass is dynamical, on the other hand, have been less thoroughly studied and classified. While the possibility that the DM mass is set by the QCD or EW scales seems excluded by data, it is still possible –and in fact plausible– that the GUT scale or the dynamical scale from a new strongly-coupled gauge theory may play this role. The new strongly-coupled dynamics may be at the origin of electroweak symmetry breaking, as in Technicolor and Composite Higgs theories, or be comprised in a 'dark' or 'mirror' sector. Recent results along these directions are reviewed in Refs. [42] and [43, 44, 45], see also Ref. [46] and references therein. In the third chapter of this thesis we focus on confining, chiral dark gauge theories, in particular those with no fundamental dark scalar fields, which do not induce a dynamical breaking of the electroweak symmetry. Models of this kind with DM candidates appeared for example in Refs. [47, 48, 49]. In this class of theories the masses of all the dark states are generated dynamically, since no fermion mass term is allowed by gauge invariance. After an exploration of possible model building choices we have focused our attention on models with product gauge groups and studied in detail the phenomenology of a model with electroweak interactions. The chiral structure of the model provides an improved accidental stability for the DM candidates and an interesting low energy phenomenology with a SM singlet dark matter candidate accompanied by SM charged partner states, testable at colliders. The infrared dynamics of this model is well described by an effective chiral lagrangian, giving a good predictivity differently from the gluequark models.

In the last part of the thesis we discuss the experimental signatures of these models, analysing the complementarity of astrophysical searches and laboratory experiments, and identifying the different search strategies at colliders. We will see that indirect searches are the most promising for the gluequark dark matter candidate, while a large part of the parameter space of chiral dark matter models can be tested with a combination of present and future collider searches and indirect searches. In this chapter we also present and discuss a strategy to derive conservative bounds on the lifetime of dark matter particle from the observation of the monopole signal of the cosmological 21cm line, independently of the astrophysical parameter necessary to model in detail the re-ionization era.

The thesis is organized as follows. Chapter 2 provides a classification of models with adjoint fermions that can lead to a realistic DM candidate. We describe the cosmological history of the gluequark and present our estimate for the thermal relic abundance. After discussing a class of vector-like models, we turn our attention to chiral models in Chapter 3. We present a classification of chiral models with a product dark gauge group and SM charges, describe their infrared dynamics with chiral lagrangian techniques and investigate their cosmological history for various choices of parameters. Chapter 4 discusses a variety of bounds stemming from cosmological and astrophysical data, DM searches at colliders, direct and indirect detection experiments. We summarize and give our outlook in Chapter 5.

2 Gluequark dark matter

We introduce the gluequark Dark Matter candidate, an accidentally stable bound state made of adjoint fermions and gluons from a new confining gauge force. Such a scenario displays an unusual cosmological history where perturbative freeze-out is followed by a non-perturbative re-annihilation period with possible entropy injection. When the gluequark has electroweak quantum numbers, the critical density is obtained for masses as large as PeV. Independently of its mass, the size of the gluequark is determined by the confinement scale of the theory, leading at low energies to annihilation rates and elastic cross sections which are large for particle physics standards and potentially observable in indirect detection experiments.

2.1 Introduction

In this chapter we explore scenarios with a new kind of accidental composite DM candidate, the *gluequark*, which has properties different from those of dark baryons and mesons in several respects. Gluequarks are bound states made of one dark quark and a cloud of dark gluons in theories where the new fermions transform in the adjoint representation of dark color. They are accidentally stable due to dark parity, an anomaly free subgroup of dark fermion number, which is exact at the level of the renormalizable Lagrangian. Depending on the SM quantum numbers of the new fermions, violation of dark parity can arise from UV-suppressed dimension-6 operators thus ensuring cosmologically stable gluequarks for sufficiently large cut-off scales. Contrary to baryons and mesons, the physical size of the gluequark is determined by the confinement scale independently of its mass. In the regime of heavy quark masses, $M_{\mathcal{Q}} > \Lambda_{DC}$, this implies a physical size larger than its Compton wavelength, see Fig. 2.1. The annihilation cross section for such a large and heavy bound state can be geometric, much larger than the perturbative unitarity bound of elementary particles. This in turn modifies the thermal relic abundance and can lead to significant effects in indirect detection experiments. Also, the resulting cosmological history is non-standard and different from that of theories with baryon or meson DM candidates.

Bound states made of one dark fermion and dark gluons were considered in Ref. [30], where they couple to the SM sector through the neutrino portal. Similar DM candidates were also studied in Refs. [31, 32], in the context of supersymmetric gauge theories. There, bound states of one fermion (the dark gluino) and dark gluons arise as the partners of glueballs after confinement and were consequently called glueballinos. Ref. [31] showed that the observed DM abundance can be reproduced by a mixture of glueballs and glueballinos provided that the dark and SM sectors are decoupled very early on in their

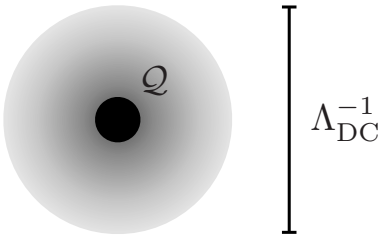

Figure 2.1: *Cartoon of the gluequark DM candidate. A heavy fermion in the adjoint of color gives rise to color singlet state surrounded by a gluon cloud of size* $1/\Lambda_{DC} \gg 1/M_{\mathcal{Q}}$.

thermal history. In such scenario the two sectors interact only gravitationally, the dark gluino being neutral under the SM gauge group. Notice that the stability of glueballs in this case does not follow from an accidental symmetry but is a consequence of the feeble interaction between the SM and dark sectors. In this work we will focus on the possibility that dark fermions are charged under the SM gauge group, so that the lightest states of the dark sector may be accessible through non-gravitational probes. In this case the dark and visible sectors stay in thermal equilibrium until relatively low temperatures, of the order of 1 GeV, and the thermal history of the Universe is rather different than that described in Refs. [31, 32]. In particular, we will argue that in our scenario dark glueballs cannot account for a sizeable fraction of DM because of BBN and CMB constraints.

Composite DM candidates from theories with adjoint fermions were also considered in the context of Technicolor models, see for example Refs. [50, 51]. Those constructions differ from ours in that technicolor quarks are assumed to transform as complex representations under the SM, but they can share common features with some of the models described in this work[1].

2.2 The models

We consider the scenario in which the SM is extended by a new confining gauge group G_{DC} (*dark colour*), and by a multiplet of Weyl fermions $\mathcal{Q}$ (*dark quarks*) transforming in the adjoint representation of G_{DC} and as a (possibly reducible) representation R under the SM group G_{SM}:

$$\mathcal{Q} \equiv (\text{adj}, R)\,. \tag{2.1}$$

In particular, we consider models where the dark quarks have quantum numbers under $\text{SU}(2)_L \times \text{U}(1)_Y$ but are singlets of $\text{SU}(3)_c$ color. New fermions colored under $\text{SU}(3)_c$ are an interesting possibility but are subject to very strong experimental constraints and their analysis deserves a separate study (see for example the recent discussion in

[1] Reference [51] for example considered gluequark DM in the context of the so-called Minimal Walking Technicolor model, but its estimate of the thermal relic abundance focuses on the perturbative freeze-out and does not include any of the non-perturbative effects described in this work.

Ref. [52]). We assume R to be a real or vector-like representation, so that the cancellation of G_{SM} anomalies is automatic and mass terms for the dark quarks are allowed.

We performed a classification of the minimal models, *i.e.* those with the smallest representations and minimal amount of fields, which give a consistent theory of DM. We refer to them as 'minimal blocks'. Each block is characterised by two parameters: the dark quark mass $M_{\mathcal{Q}}$ and the value of the dark gauge coupling $g_{\rm DC}$ at $M_{\mathcal{Q}}$. A CP-violating θ term can also be included but does not play an important role in what follows. The renormalizable lagrangian thus reads

$$\mathcal{L} = \mathcal{L}_{\rm SM} - \frac{1}{4g_{\rm DC}^2}\mathcal{G}_{\mu\nu}^2 + \mathcal{Q}^\dagger i\bar{\sigma}^\mu D_\mu \mathcal{Q} - \frac{M_{\mathcal{Q}}}{2}\left(\mathcal{Q}\mathcal{Q} + \mathcal{Q}^\dagger\mathcal{Q}^\dagger\right). \tag{2.2}$$

It is possible to combine more than one minimal block; in this case the number of parameters increases: each module can have a different mass and, depending on the SM quantum numbers, Yukawa couplings with the Higgs boson may be allowed.

As long as all dark quarks are massive, the theory described by (2.2) confines in the infrared forming bound states. The symmetry $\mathcal{Q} \to -\mathcal{Q}$, *dark parity*, is an accidental invariance of the renormalizable Lagrangian. The physical spectrum is characterized by states that are either even or odd under dark parity. The gluequark, denoted by χ in the following, is the lightest odd state and has the same SM quantum numbers of its constituent dark quark, thus transforming as an electroweak multiplet. Radiative corrections will induce a mass splitting among different components, with the lightest state being accidentally stable at the renormalizable level thanks to its odd dark parity. The mass difference computed in Ref. [14] shows that the lightest component is always the electromagnetically neutral one, which therefore can be a DM candidate provided it has the correct relic density.

We select models with a suitable gluequark DM candidate by requiring them to be free of Landau poles below 10^{15} GeV. This is a minimal assumption considering that, as discussed below, astrophysical and cosmological bounds on the gluequark lifetime can be generically satisfied only for a sufficiently large cut-off scale. It is also compatible with Grand Unification of SM gauge forces. The ultraviolet behaviour of each model is dictated by the number of dark colors $N_{\rm DC}$ and by the dimension of the SM representation R, i.e. by the number of Weyl flavors N_f. Models with too large N_f or $N_{\rm DC}$ imply too low Landau poles for G_{SM}, and are thus excluded from our analysis. The list of minimal blocks that satisfy our requirements is reported in Table 2.1 for $\mathrm{SU}(N_{\rm DC})$, $\mathrm{SO}(N_{\rm DC})$ and $\mathrm{Sp}(N_{\rm DC})$ dark color groups. Each block is characterized by its accidental symmetry (that can be larger than the dark parity) and by the dimensionality of the lowest-lying operator $\mathcal{O}_{\rm dec}$ which violates it. The latter has the form

$$\mathcal{O}_{\rm dec} = \mathcal{O}_{\rm SM}\mathcal{G}^a_{\mu\nu}\sigma^{\mu\nu}\mathcal{Q}^a, \tag{2.3}$$

where $\mathcal{O}_{\rm SM}$ is a SM composite operator matching the $\mathrm{SU}(2)_L \times \mathrm{U}(1)_Y$ quantum numbers of the dark quark $\mathcal{Q}$. The operator (2.3) can in general induce the mixing of the gluequark with SM leptons, providing an example of partial compositeness. As long as the theory is not in the vicinity of a strongly-coupled IR fixed point at energies $E \gg M_{\mathcal{Q}}, \Lambda_{DC}$,

N_f	Quantum numbers SU(2) × U(1)	N_{DC} SU	SO	Sp	Accidental Symmetry	$\mathcal{O}_{\rm dec}$	Classical $[\mathcal{O}_{\rm dec}]$
1	$N \equiv 1_0$	All	All	All	$\mathbb{Z}_2$	$\ell H \mathcal{G}_{\mu\nu}\sigma^{\mu\nu} N$	6
3	$V \equiv 3_0$	$\leqslant 3$	$\leqslant 4$	1	$\mathbb{Z}_2$	$\ell H \mathcal{G}_{\mu\nu}\sigma^{\mu\nu} V$	6
4	$L \equiv 2_{1/2} \oplus \bar{L} \equiv 2_{-1/2}$	$\leqslant 4$	$\leqslant 6$	$\leqslant 2$	U(1)	$\ell \mathcal{G}_{\mu\nu}\sigma^{\mu\nu} L$	5
6	$T \equiv 3_1 \oplus \bar{T} \equiv 3_{-1}$	2	3	1	U(1)	$\ell H^c \mathcal{G}_{\mu\nu}\sigma^{\mu\nu} T$	6

Table 2.1: *M*inimal building blocks for models of gluequark DM. We require that a multiplet contains an electromagnetic neutral component and that the gauge couplings do not have Landau poles below 10^{15} GeV, assuming a representative mass of 100 TeV for the dark quarks. We denote with ℓ the SM lepton doublets.

the dimension of $\mathcal{O}_{\rm dec}$ is simply given by $[\mathcal{O}_{\rm dec}] = 7/2 + [\mathcal{O}_{\rm SM}]$, as reported in the sixth column of Table 2.1. Among the minimal blocks, the $L\bar{L}$ model has $[\mathcal{O}_{\rm dec}] = 5$ classically. In this case the naive suppression of the gluequark decay rate is not enough to guarantee cosmological stability, although a stable DM candidate can still be obtained through additional dynamics, see the discussion in Appendix 2.C. In the remaining minimal blocks the classical dimension of $\mathcal{O}_{\rm dec}$ is 6 and the gluequark can be sufficiently long lived. Indirect detection experiments and data from CMB and 21 cm line observations set important constraints on these models which will be discussed in Chapter 4.

The behaviour of the theory at energies above the confinement scale depends largely on the number of dark flavors N_f and on the value of the dark coupling $g_{\rm DC}$ at the scale $M_{\mathcal{Q}}$. One can identify two regimes. In the first, $g_{\rm DC}(M_{\mathcal{Q}})$ is perturbative and this necessarily implies a confinement scale smaller than the quark mass, $\Lambda_{DC} < M_{\mathcal{Q}}$; we will call this the 'heavy quark' regime. In this case, depending on the value of N_f, there are three possible behaviours. For $N_f \geqslant N_f^{\rm AF} = 11/2$ the theory is not asymptotically free, hence starting from the UV the coupling gets weaker at lower scales until one reaches the quark mass threshold below which the dynamics becomes strong and confines [2]. For $N_f^c \leqslant N_f < N_f^{\rm AF}$, where N_f^c is the non-perturbative edge of the conformal window, the theory flows towards an IR fixed point at low energies until the quark mass threshold is passed, below which one has confinement. Finally, if $N_f < N_f^c$ the coupling grows strong quickly in the infrared and confinement is triggered without delay. Only for this latter range of values of N_f the confinement scale can be larger than the quark mass, $M_{\mathcal{Q}} < \Lambda_{DC}$; we will refer to this as the 'light quark' regime. The physical spectrum, the phenomenology and the thermal history are rather different in the two regimes.

The infrared behaviour of SU(N_{DC}) gauge theories with fermions in the adjoint representation was extensively studied through lattice simulations, see for example [53, 54, 55, 56, 57, 58, 59, 60, 61, 62] and references therein. There seems to be sufficient evidence for an infrared conformal phase of theories with $N_{\rm DC} = 2$ colors and $N_f = 4, 3$ massless Weyl flavors, while results with $N_f = 2$ are more uncertain though still compatible with a conformal regime. Theories with $N_f = 1$ are supersymmetric and have been shown

[2] Notice that the value of $N_f^{\rm AF}$, in the case of adjoint fermions, does not depend on the gauge group.

to be in the confining phase. The case with $N_{\rm DC} = 3$ colors is much less studied and no firm conclusion can be drawn on the conformal window. Notice that, independently of the number of colors, asymptotic freedom is lost for $N_f \geqslant 6$, while the existence of a weakly-coupled infrared fixed point can be established for $N_f = 5$ by means of perturbation theory. Besides determining which phase the massless theory is in, simulations give also information on the spectrum of bound states. In particular, information on the gluequark mass in the limit of heavy quark masses ($M_{\mathcal{Q}} \gg \Lambda_{DC}$) can be obtained from lattice simulations with adjoint static sources, see for example Refs. [63, 64].

Heavy quark regime: In the heavy quark regime, the lightest states in the spectrum are glueballs, while those made of quarks are parametrically heavier. The value of the glueball mass is close to the one of pure gauge theories. Lattice results for pure glue SU(3) theories show that the 0^{++} state is the lightest with mass $m_{0^{++}} \sim 7\Lambda_{DC}$, see for example [65]. Similar values are found for SU(N_{DC}) with different number of colors. The gluequark is expected to be the lightest state made of quarks, with a mass $M_\chi \sim M_{\mathcal{Q}}$. Other states made of more dark quarks (collectively denoted as mesons) quickly decay to final states comprising glueballs and gluequarks, depending on their dark parity.

The gluequark lifetime can be accurately estimated by computing the decay of its constituent heavy quark, similarly to spectator calculations for heavy mesons in QCD. In the minimal blocks where the dark parity-violating operator has dimension 6 the main decay channel for the lightest gluequark χ^0 is $\chi^0 \to h\nu + n\Phi$ (where Φ indicates a glueball and $n \geqslant 1$). In the V model of Table 2.1 with three dark flavors transforming as an EW triplet, the dim-6 operator

$$\frac{g_{UV}^2}{\Lambda_{UV}^2}\left(H^{c\dagger}\sigma^i \ell\, \mathcal{G}_{\mu\nu}\sigma^{\mu\nu}\mathcal{Q}^i + h.c.\right)$$

induces the decay of the gluequark with inverse lifetime

$$\frac{1}{\tau(\chi_0)} \simeq \frac{g_{UV}^4}{4096\pi^3}\frac{M_{\mathcal{Q}}^5}{\Lambda_{UV}^4} \simeq 10^{-28} g_{UV}^4 \left(\frac{M_{\mathcal{Q}}}{100\,\text{TeV}}\right)^5 \left(\frac{10^{18}\,\text{GeV}}{\Lambda_{UV}}\right)^4 \text{s}^{-1}\,. \tag{2.4}$$

Similar results apply for the N and $T \oplus \bar{T}$ minimal blocks.

Glueballs can decay to SM particles through loops of dark quarks. In particular, since the latter are assumed to have electroweak charges, glueballs can always decay to photons through dimension-8 operators of the form $\mathcal{G}_{\mu\nu}\mathcal{G}^{\mu\nu}W_{\alpha\beta}W^{\alpha\beta}$ generated at the scale $M_{\mathcal{Q}}$. For all the minimal models in Table 2.1 this is the lowest-dimensional operator which induces glueball decay. The partial width into photons is determined to be [66, 67] [3]

$$\Gamma(\Phi \to \gamma\gamma) \simeq 0.7\,\text{s}^{-1}\left(\frac{N_{\rm DC}}{3}\right)^2 \left(\frac{M_\Phi}{500\,\text{GeV}}\right)^9 \left(\frac{100\,\text{TeV}}{M_{\mathcal{Q}}}\right)^8. \tag{2.5}$$

[3] To derive this and the following decay rates we used the value of the matrix element $\langle 0|\mathcal{G}_{\mu\nu}\mathcal{G}^{\mu\nu}|\Phi\rangle$ computed on the lattice for $SU(3)$, see Ref. *e.g.* [68].

When phase space allows, the decay channels $Z\gamma$, W^+W^- and ZZ open up producing one order-of-magnitude smaller lifetime. Relatively long-lived glueballs, as implied by the estimate (2.5), are subject to cosmological and astrophysical constraints as discussed in Chapter 4.

Models with Yukawa couplings to the Higgs doublet can be obtained combining minimal blocks. In this case 1-loop radiative effects at the scale $M_{\mathcal{Q}}$ generate the dimension-6 effective operator $|H|^2\mathcal{G}^2_{\mu\nu}$, inducing a much shorter lifetime. If their mass is high enough, $M_\Phi > 2m_h$, glueballs predominantly decay to two Higgs bosons with a decay width

$$\Gamma(\Phi \to hh) \simeq 10^{12}\,\mathrm{s}^{-1} \left(\frac{N_{\rm DC}}{3}\right)^2 \left(\frac{y_1 y_2}{0.1}\right)^2 \left(\frac{M_\Phi}{500\,\mathrm{GeV}}\right)^5 \left(\frac{100\,\mathrm{TeV}}{\bar{M}_{\mathcal{Q}}}\right)^4 , \tag{2.6}$$

where $\bar{M}_{\mathcal{Q}} = (M_{\mathcal{Q}_1} M_{\mathcal{Q}_2})^{1/2}$, and $y_{1,2}$, $M_{\mathcal{Q}_{1,2}}$ are respectively the Yukawa couplings and masses of the dark quarks circulating in the loop. Lighter glueballs can decay through the mixing with the Higgs boson; as for the Higgs, the dominant channel for $M_\Phi < 150\,\mathrm{GeV}$ is that into bottom quarks, with a corresponding partial width[4]

$$\Gamma(\Phi \to b\bar{b}) \simeq 3 \cdot 10^{7}\,\mathrm{s}^{-1} \left(\frac{N_{\rm DC}}{3}\right)^2 \left(\frac{y_1 y_2}{0.1}\right)^2 \left(\frac{M_\Phi}{50\,\mathrm{GeV}}\right)^7 \left(\frac{10\,\mathrm{TeV}}{\bar{M}_{\mathcal{Q}}}\right)^4 . \tag{2.7}$$

Light quark regime: If dark quarks are lighter than Λ_{DC}, the physical spectrum is radically different and one expects spontaneous breaking of the global $SU(N_f)$ symmetry down to $\mathrm{SO}(N_f)$. The lightest states are thus the (pseudo) Nambu-Goldstone bosons φ, while the DM candidate is the gluequark, accidentally stable and with a mass of the order of the confinement scale Λ_{DC}. As discussed in section 2.4, and similarly to the baryonic DM theories of Ref. [22], reproducing the correct DM relic density in this regime fixes $\Lambda_{DC} \sim 50\,\mathrm{TeV}$. The NGBs with SM quantum numbers get a mass from 1-loop electroweak corrections, which is predicted to be $\mathcal{O}(10\,\mathrm{TeV})$ for the value of Λ_{DC} of interest. Besides such a radiative correction, the quark mass term breaks explicitly the $\mathrm{SU}(N_f)$ global symmetry and gives an additional contribution. Including both effects, the NGB mass squared is given by

$$m^2_\varphi = c_0 M_{\mathcal{Q}} \Lambda_{DC} + c_1 \frac{3\alpha_2}{4\pi} I(I+1)\Lambda^2_{DC} , \tag{2.8}$$

where I is the weak isospin of the NGB and $c_{0,1}$ are $\mathcal{O}(1)$ coefficients.

For fermions in the adjoint representations, only models with $N_f < 5$ light quarks can be in the regime $M_{\mathcal{Q}} < \Lambda_{DC}$, since those with more fermions are either IR conformal or IR free. Therefore, among the minimal blocks of Table 2.1 only two are compatible with the light quark regime, *i.e.* the V model and the $L \oplus \bar{L}$ model. The V model has a global symmetry breaking $\mathrm{SU}(3) \to \mathrm{SO}(3)$ which leads to five NGBs transforming as an electroweak quintuplet. In the $L \oplus \bar{L}$ model one has $\mathrm{SU}(4) \to \mathrm{SO}(4)$ and nine NGBs transforming as $3_\pm, 3_0$ of $\mathrm{SU}(2)_{\rm EW} \times \mathrm{U}(1)_Y$.

[4] The scaling $\Gamma(\Phi \to b\bar{b}) \sim M^7_\Phi$ is approximately correct for $M_\Phi \ll m_h$, though eq. (2.7) is a good numerical estimate for $m_h \sim M_\Phi < 150\,\mathrm{GeV}$ as well.

The limit of very small quark masses, $M_{\mathcal{Q}}\Lambda_{DC} \ll m_\varphi^2$, is experimentally interesting, since NGBs have predictable masses. In general, the lightest NGBs decay to SM final states through anomalies or Yukawa couplings, as in the case of the V model. In some cases, however, some of the NGBs are accidentally stable due to unbroken symmetries of the renormalizable Lagrangian. An explicit violation of such accidental symmetries is expected to arise from higher-dimensional operators, possibly resulting into long-lived particles. An example of this kind is given by the $L \oplus \bar{L}$ model, where NGBs made of LL or $\bar{L}\bar{L}$ constituents have $U(1)$ number ± 2 and are stable at the renormalizable level, see Appendix 2.C.

Since we assumed the dark quarks to transform as real or vectorlike representations under the SM gauge group, the fermion condensate responsible for the global symmetry breaking in the dark sector can be aligned along an $(SU(2)_L \times U(1)_Y)$-preserving direction (in non-minimal models, Yukawa interactions can generate a vacuum misalignment leading to Higgs partial compositeness, see [33, 69]). As the strong dynamics preserves the EW gauge symmetry of the SM, it also affects electroweak precision observables through suppressed corrections which are easily compatible with current constraints for sufficiently high values of Λ_{DC}, as required to reproduce the DM relic abundance [16, 25, 28].

Besides the NGBs, the physical spectrum comprises additional bound states with mass of order Λ_{DC}. These include the gluequarks, which are expected to be the lightest states with odd dark parity, and mesons (i.e. bound states made of more than one dark quark)[5]. Except for the lightest gluequark, which is cosmologically stable, all the other states promptly decay to final states comprising NGBs and gluequarks, depending on their dark parity. In the minimal blocks where dark parity is broken by the dimension-6 operator $\ell H \mathcal{G}_{\mu\nu}\sigma^{\mu\nu}\mathcal{Q}$, the most important decay channels of the gluequark are $\chi^0 \to h\nu$ and $\chi^0 \to h\nu + \varphi$. The two-body decay dominates at large-$N_{\rm DC}$ and gives a lifetime of order

$$\frac{1}{\tau(\chi_0)} \sim \frac{g_{UV}^4}{8\pi}\frac{M_\chi^3 f_\chi^2}{\Lambda_{UV}^4} = 4\times 10^{-26} g_{UV}^4 \left[\frac{M_\chi}{100\,\text{TeV}}\right]^3 \left[\frac{f_\chi}{25\,\text{TeV}}\right]^2 \left[\frac{10^{18}\,\text{GeV}}{\Lambda_{UV}}\right]^4 \text{s}^{-1} \qquad (2.9)$$

where f_χ is the decay constant of the gluequark[6].

To summarize our discussion on models, Table 2.1 reports the minimal blocks which have a potentially viable DM candidate and a sufficiently high cut-off, above 10^{15} GeV, as required for SM Grand Unification and to suppress the DM decay rate. In particular, the requirement on the absence of Landau poles restricts the list of possible models to a

[5] The existence of stable baryons in theories with adjoint fermions was investigated in Refs. [70, 71], where stable skyrmion solutions were identified and conjectured to correspond to composite states with mass of $O(N_{\rm DC}^2)$, interpolated from the vacuum by non-local operators. We will not include these hypothetical states in our analysis. In the light quark regime they are expected to annihilate with a geometric cross section and contribute a fraction of DM relic density comparable to that of the gluequarks.

[6] This has been defined by $\langle 0|\mathcal{G}_{\mu\nu}\sigma^{\mu\nu}\mathcal{Q}|\chi(p,r)\rangle = f_\chi M_\chi u_r(p)$, and scales as $f_\chi \sim M_\chi(N_{\rm DC}/4\pi)$ in the large-$N_{\rm DC}$ limit.

few candidates. As mentioned before, the case of the singlet was studied already in the literature [31, 32], and it will not be considered further in this work. We find that in all the other minimal blocks of Table 2.1 the $SU(3)_c \times SU(2)_L \times U(1)_Y$ gauge couplings unify with much lower precision than in the SM. Making the dark sector quantitatively compatible with SM Grand Unification thus requires extending these minimal blocks by including additional matter fields. Also, it would be interesting to explore the possibility of unifying both the visible and dark gauge couplings. We leave this study to a future work.

In the next sections we will discuss the thermal history of the Universe and try to estimate the DM relic density: section 3 explains the general mechanisms at work and is largely independent of the details of the models; section 4 gives a concrete example, adopting as a benchmark the V model of Table 2.1, i.e. the minimal block with an $SU(2)_L$ triplet. For a discussion of the $L \oplus \bar{L}$ model see Appendix 2.C.

2.3 Cosmological History

The Universe undergoes different thermal histories in the light and heavy quark regimes. We first give a brief overview of such evolution, followed by a more detailed discussion with quantitative estimates.

In the light quark regime the thermal history is relatively simple and similar to that described for baryonic DM in Ref. [22]. Dark color confines when dark quarks are relativistic and in thermal equilibrium. After confinement the gluequarks annihilate into NGBs with a non-perturbative cross section $\sigma v_{\rm rel} \sim \pi/\Lambda_{DC}^2$, while glueballs are heavy and unstable. At temperatures $T \sim M_\chi/25$ the annihilation processes freeze out and the gluequarks start behaving as ordinary thermal relics.

In the heavy quark regime the thermal history is more complex and characterized by three different stages. Before confinement ($T \gtrsim \Lambda_{DC}$), free dark quarks annihilate into dark gluons and undergo perturbative freeze-out at $T \sim M_\mathcal{Q}/25$ (see section 2.3.1). At confinement ($T \sim \Lambda_{DC}$), the vast majority of the remaining dark quarks hadronizes into gluequarks, while the plasma of dark gluons is converted into a thermal bath of non-relativistic glueballs. The formation of mesons is suppressed by the low density of dark quarks compared to the ambient dark gluons. Glueballs overclose the Universe if they are cosmologically stable, therefore we consider the region of the parameter space where their lifetime is sufficiently short. As first pointed out in [72, 73, 74], and recently reconsidered in [75, 76, 77], decays of non-relativistic particles with a large and non-thermal energy density – like the glueballs – can modify the standard relation between the scale factor and the temperature during the cosmological evolution. If the glueballs are sufficiently long lived and dominate the energy density of the Universe at some stage of the cosmological evolution, the standard scaling $a \propto T^{-1}$ is modified into $a \propto T^{-8/3}$. During this early epoch of matter domination, the Universe expands faster than in the radiation-dominated era, leading to an enhanced dilution of the DM relic density (see section 2.3.2). Finally, interactions among gluequarks can lead to a second stage of DM

annihilation through the process

$$\begin{aligned} \chi + \chi \to \mathcal{Q}\mathcal{Q}^* + \Phi/V \\ \hookrightarrow \mathcal{Q}\mathcal{Q} \to \text{SM} \end{aligned} \tag{2.10}$$

where $\mathcal{Q}\mathcal{Q}^*$ is an excited bound state of dark quarks and V stands for a SM vector boson or possibly a Higgs boson in models with Yukawa interactions. An analogous mechanism was first discussed in Ref. [78, 79, 80] and more recently by Ref. [81, 52, 82]. The process (2.10) proceeds in two steps. Initially, an excited bound state $\mathcal{Q}\mathcal{Q}^*$ with size $\mathcal{O}(1/\Lambda_{DC})$ is formed by a collision of two χ's through a recombination of the constituent heavy quarks. This is similar to what happens for example in hydrogen anti-hydrogen scattering [83]. As a consequence of the large size of the gluequark (see the discussion in section 2.3.3), the corresponding recombination cross section is expected to be large $\sigma_{\rm rec} \approx \pi/\Lambda_{DC}^2$. Once formed, the $\mathcal{Q}\mathcal{Q}^*$ can either decay ($\mathcal{Q}\mathcal{Q}^* \to \mathcal{Q}\mathcal{Q} + V \to$ SM) or be dissociated back into two gluequarks by interactions with the SM and glueball baths ($\Phi/V + \mathcal{Q}\mathcal{Q} \to \chi + \chi$). A naive estimate shows that the latter process typically dominates. This is because the largest contribution to the total cross section comes from scatterings with large impact parameters, $b \sim 1/\Lambda_{DC}$, in which the $\mathcal{Q}\mathcal{Q}^*$ is produced with a large angular momentum, $\ell \sim M_{\mathcal{Q}} v b$. Bound states with $\ell \gg 1$ take more time to de-excite to lower states, and dissociation can happen before they reach the ground state. The annihilation of gluequarks through recombination is therefore inefficient as long as the glueball bath is present. Only when the glueballs decay away, a second stage of DM annihilation can take place through the process (2.10).

2.3.1 Thermal freeze-out

Thermal freeze-out is the first (only) phase of the cosmological evolution in the regime with heavy (light) quarks. In this stage the number density of free dark quarks (for $M_{\mathcal{Q}} > \Lambda_{DC}$) or of gluequarks (for $M_{\mathcal{Q}} < \Lambda_{DC}$) is reduced until it becomes so low that chemical equilibrium is no longer attained and freeze-out takes place. The number density at freeze-out is approximately given by

$$n(T_{\rm f.o.}) \simeq \frac{H(T_{\rm f.o.})}{\langle \sigma_{\rm ann} v_{\rm rel} \rangle}\,, \tag{2.11}$$

where H is the Hubble parameter, and afterwards it is diluted by the Universe expansion.

In the heavy quark regime, free dark quarks annihilate with a perturbative cross section into dark gluons and into pairs of SM particles (vector bosons, Higgs bosons and fermions). The freeze-out temperature is of order $T_{\rm f.o.} \approx M_{\mathcal{Q}}/25$. A general expression for the annihilation cross section is reported in Appendix 2.A, see eq. (2.41). For the V model with $N_{DC} = 3$ analysed in the next section, the annihilation cross section into dark gluons and SM fields is

$$\langle \sigma_{\rm ann} v_{\rm rel} \rangle = \frac{\pi \alpha_{\rm DC}^2}{M_{\mathcal{Q}}^2} \left(\frac{27}{96} + \frac{1}{8} \left(1 + \frac{25}{12} \right) \frac{\alpha_2^2}{\alpha_{\rm DC}^2} + \frac{1}{2} \frac{\alpha_2}{\alpha_{\rm DC}} \right) \left(\frac{1}{6} S_3 + \frac{1}{3} S_{3/2} + \frac{1}{2} S_{-1} \right)\,, \tag{2.12}$$

neglecting the mass of final states. The term from annihilation into SM particles separately shows the contribution of vectors and fermions plus longitudinal gauge bosons.

Terms in the second parenthesis encode the Sommerfeld enhancement from dark gluon exchange: S_3, $S_{3/2}$, S_{-1} refer respectively to the 1, 8 and 27 color channels and are given by [84, 85]

$$S_n = \frac{\alpha_{\rm DC}}{v_{\rm rel}} \frac{2\pi n}{1 - e^{-2\pi n \alpha_{\rm DC}/v_{\rm rel}}} \,. \tag{2.13}$$

In the light quark regime gluequarks annihilate into NGBs with a cross section that is expected to scale naively as

$$\langle \sigma_{\rm ann} v_{\rm rel} \rangle \sim \frac{\pi}{\Lambda_{DC}^2} \,, \tag{2.14}$$

in analogy with nucleon-nucleon scattering in QCD [86]. Nambu-Goldstone bosons are unstable and later decay into SM particles.

2.3.2 Dilution

As well known, the number density of DM particles today is related to the number density at freeze-out by

$$n_{\rm DM}(T_0) = n_{\rm DM}(T_{\rm f.o}) \left(\frac{a_{\rm f.o.}}{a_0} \right)^3 \,. \tag{2.15}$$

This relation is usually rewritten in terms of temperatures assuming that between freeze-out and today the standard scaling $a \propto T^{-1}$ holds. However, the validity of the standard scaling relies upon the assumption that entropy is conserved in the SM sector, i.e. that no energy is injected into the SM plasma. In presence of large entropy injection one can have an epoch during which a grows faster than $a \propto T^{-1}$. In this case the relation between $n_{\rm DM}(T_0)$ and $n_{\rm DM}(T_{\rm f.o})$ is given by:

$$n_{\rm DM}(T_0) = n_{\rm DM}(T_{\rm f.o}) \left(\frac{T_0}{T_{\rm f.o.}} \right)^3 \left(\frac{a\,(T_i)}{a\,(T_f)} \frac{T_i}{T_f} \right)^3 \,, \tag{2.16}$$

where T_i and T_f defines the temperature interval during which the non-standard scaling holds (see Fig. 2.2). The last term in parenthesis accounts for the suppression with respect to the naive relict density which would be obtained using the standard scaling. In the following we will show that late-time decays of dark glueballs can give rise to a non-standard scaling of the form $a \propto T^{-\alpha}$ with $\alpha > 1$. The corresponding suppression factor thus reads:

$$\mathcal{F} \equiv \left(\frac{a\,(T_i)}{a\,(T_f)} \frac{T_i}{T_f} \right)^3 = \left(\frac{T_f}{T_i} \right)^{3\alpha - 3} \,. \tag{2.17}$$

After dark color confinement, the energy density of the Universe can be divided into a relativistic component, ρ_R, containing all the SM relativistic particles, and a non-relativistic one, ρ_M, containing all the dark-sector long-lived degrees of freedom (i.e. dark

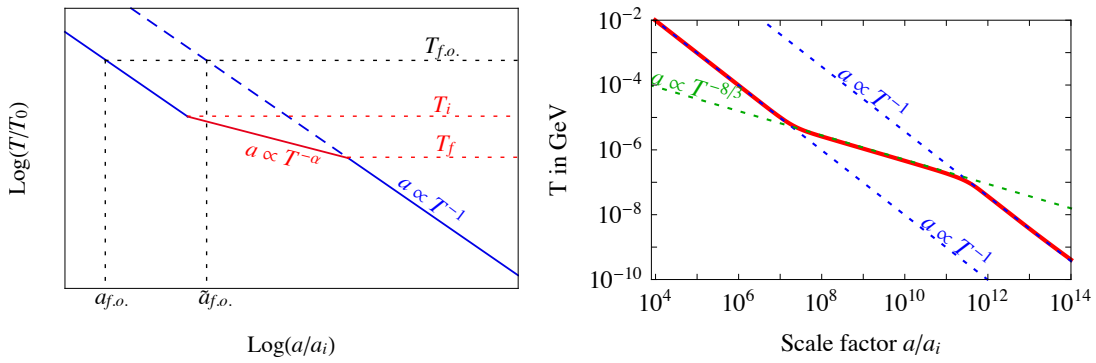

Figure 2.2: *Left: Sketch of the non-standard $a(T)$ scaling. Values of $\alpha > 1$ in eq.(2.17) imply a scale factor at freeze-out, $a_{f.o.}$, smaller than the one obtained from a standard cosmology, $\tilde{a}_{f.o.}$. This in turn leads to a suppression of the relic density by a factor $(a_{f.o.}/\tilde{a}_{f.o.})^3 = (T_f/T_i)^{3\alpha-3}$. Right: Scaling obtained by solving numerically (2.18) and (2.19) for $M_{\mathcal{Q}} = 100\,\text{TeV}$ and $T_{dc} = \Lambda_{DC} = 10\,\text{GeV}$. There exists an epoch during which the $a(T)$ scaling is very well approximated by a power law $a \propto T^{-\alpha}$ with $\alpha = 8/3$.*

glueballs and gluequarks). In particular, the energy density of glueballs at confinement is much larger than the corresponding thermal energy density for a non-relativistic species, and this can lead to an early epoch of matter domination. Neglecting the subleading contribution of gluequarks to ρ_M, the evolution of $\rho_{M,R}$ is governed by[7]

$$\begin{cases} \dot{\rho}_M = -3H\rho_M - \Gamma_\Phi\,\rho_M \\ \dot{\rho}_R = -4H\rho_R + \Gamma_\Phi\,\rho_M \end{cases} \tag{2.18}$$

where Γ_Φ is the glueball decay rate and the Hubble parameter H is given by the Friedmann equation:

$$H^2 = \frac{8\pi G}{3}\,(\rho_R + \rho_M)\ . \tag{2.19}$$

Since in the relevant region of the parameter space the dark and SM sectors are in thermal equilibrium at dark confinement, the initial conditions at $T = T_{dc} \approx \Lambda_{DC}$ are given by

$$\rho_M(T_{dc}) = \xi\,\rho_R(T_{dc}) \qquad \text{with} \qquad \xi \equiv \frac{g_D(T_{dc})}{g_*(T_{dc})}\,, \tag{2.20}$$

where $g_D(T)$ and $g_*(T)$ count the number of relativistic degrees of freedom in the dark and SM sector respectively. Furthermore, assuming that the decay products thermalize

[7]Here we omit the contribution of glueball annihilations into SM vector bosons to the evolution of $\rho_{M,R}$. This contribution is negligible in the region of the parameter space where dilution is sizeable. Both the rate of glueball annihilation at temperatures of order Λ_{DC} and the glueball decay rate scale as $\Lambda_{DC}^9/M_{\mathcal{Q}}^8$, so that the former, similarly to the latter, is expected to be smaller than Hubble when dilution is relevant. We have checked this naive expectation by verifying that after confinement the estimated annihilation rate is smaller than Hubble on branch 1 of Fig. 2.4.

fast enough, the temperature of the Universe below T_{dc} is related to the relativistic energy density by:

$$\rho_R \equiv \frac{\pi^2}{30} g_* \, T^4 \qquad (T < T_{dc}) \, . \tag{2.21}$$

The evolution during the early matter-dominated epoch, if the latter exists, can be described by solving analytically eq. (2.18) at leading order in ρ_R/ρ_M for cosmic times $t \ll 1/\Gamma_\Phi$ [75]:

$$\rho_M = \bar{\rho}_M \left(\frac{\bar{a}}{a}\right)^3 e^{-\Gamma_\Phi (t-\bar{t})} \tag{2.22a}$$

$$\rho_R \simeq \bar{\rho}_R \left(\frac{\bar{a}}{a}\right)^4 + \frac{2}{5}\sqrt{\frac{3}{8\pi}} \Gamma_\Phi \, M_{\rm Pl} \, \bar{\rho}_M^{1/2} \left[\left(\frac{\bar{a}}{a}\right)^{3/2} - \left(\frac{\bar{a}}{a}\right)^4\right] . \tag{2.22b}$$

Here $\bar{\rho}_{M,R}$ and $\bar{a}$ denote the initial conditions at some time $\bar{t}$ much after the beginning of the matter-dominated epoch. The relativistic energy density is given by the sum of $\bar{\rho}_R$ (first term in eq.(2.22b)), diluted as a^{-4}, and the energy injected by glueball decays (second term in eq.(2.22b)), diluted as $\sim a^{-3/2}$. Initially the first term dominates and the standard scaling $a \propto T^{-1}$ is obtained; as long as the glueball lifetime is long enough, the second term will start to dominate at some temperature T_i, implying a non-standard scaling $a \propto T^{-8/3}$ (see Fig. 2.2). The value of T_i can be found by equating the first and second terms of eq.(2.22b) and by using eqs.(2.19),(2.20):

$$T_i \simeq T_{dc}\, \xi \times \left[\frac{\Gamma_\Phi M_{\rm Pl}}{4.15\sqrt{g_*}\, T_{dc}^2\, \xi^2 + \Gamma_\Phi M_{\rm Pl}}\right]^{2/5} . \tag{2.23}$$

The non-standard scaling ends when almost all the glueballs are decayed, *i.e.* around $(t - t_{dc}) \sim \Gamma_\Phi^{-1}$, where t_{dc} is the time at dark confinement. Using eqs. (2.19) and (2.20), one can translate this condition in terms of a temperature finding:

$$T_f \simeq \sqrt{M_{\rm Pl}\Gamma_\Phi} \, . \tag{2.24}$$

From eq.(2.17) it follows that late-time decays of glueballs dilute the naive relic density by a factor

$$\mathcal{F} = \left(\frac{T_f}{T_i}\right)^5 = \frac{0.28}{g_*^{5/4}} \frac{M_{\rm Pl}^{5/2}\Gamma_\Phi^{5/2}}{T_{dc}^5\, \xi^5} \left(\frac{4.15\sqrt{g_*}\, T_{dc}^2\, \xi^2 + \Gamma_\Phi M_{\rm Pl}}{\Gamma_\Phi M_{\rm Pl}}\right)^2 , \tag{2.25}$$

where $\mathcal{O}(1)$ numerical factors omitted in eq.(2.24) have been included. When the glueballs are sufficiently long lived to give a sizeable dilution, the second term in the numerator inside the parenthesis of eq.(2.25) can be neglected and $\mathcal{F}$ is very well approximated by:

$$\mathcal{F} \simeq \frac{4.82}{g_*^{1/4}} \frac{\sqrt{M_{\rm Pl}\Gamma_\Phi}}{T_{dc}\, \xi} \, . \tag{2.26}$$

While the analytic formulas (2.22b)-(2.26) turn out to be quite accurate, in our estimate of the relic density performed in section 2.4 we will solve eq. (2.18) numerically without making any approximation.

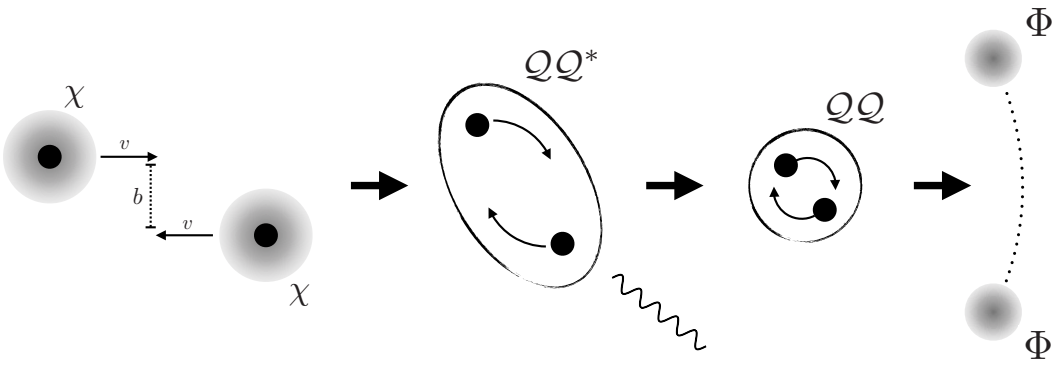

Figure 2.3: *Cartoon of the re-annihilation processes occurring after dark confinement. First, free quarks combine into color singlets gluequarks. Next, fast collisions form excited $\mathcal{Q}\mathcal{Q}^*$ states that at sufficiently low temperatures fall into the ground state and decay.*

2.3.3 Reannihilation

At $T = T_{dc} \sim \Lambda_{DC}$ the theory confines and the dark degrees of freedom reorganize into singlets of dark color. In the heavy quark regime, the number density of gluons is much larger than the one of fermions and the vast majority of free quarks $\mathcal{Q}$ hadronize into gluequarks. These can then collide and recombine in excited $\mathcal{Q}\mathcal{Q}^*$ states by emitting an electroweak gauge boson (or a Higgs boson in theories with Yukawa couplings) or a glueball when kinematically allowed, see eq. (2.10). The process goes through a recombination of the constituent heavy quarks, while the direct annihilation of these latter has a small and perturbative rate. Given that gluequarks have a size of order $1/\Lambda_{DC}$, one expects naively a recombination cross section of order $\sigma_{\rm rec} \sim 1/\Lambda_{DC}^2$. This value can in fact be reduced by kinematic constraints and the actual total cross section depends ultimately on the temperature at which the process takes place. A detailed discussion and estimates for the recombination cross section are given in Appendix 2.B.

Once formed, $\mathcal{Q}\mathcal{Q}^*$ states with mass $M(QQ^*) > 2M_{\mathcal{Q}}$ will promptly decay back to two gluequarks. Lighter states, on the other hand, can either de-excite and thus decay into SM particles through the emission of a SM vector boson or a glueball ($\mathcal{Q}\mathcal{Q}^* \to \mathcal{Q}\mathcal{Q} + V/\Phi \to$ SM), or be dissociated by interactions with the glueball and SM plasmas ($\Phi/V + \mathcal{Q}\mathcal{Q}^* \to \chi + \chi$), see Fig. 2.3.

If de-excitation occurs faster than dissociation, a second era of efficient DM annihilation can take place, reducing the gluequark number density. While re-annihilation processes can be active over a long cosmological time interval, it is the last stage during which the re-annihilation cross section gets its largest value $\sigma_{\rm rea}$ that is most important to determine the final gluequark density. This last stage happens relatively quickly and can be characterized by a re-annihilation temperature T_R. The exact value of T_R depends on the rate of dissociation and is difficult to estimate. The largest uncertainties arise from the calculation of the de-excitation rate, which can vary over several orders of magnitude. We performed a thorough analysis taking into account the many dynamical

ingredients which play a role in determining both the re-annihilation cross section and temperature. A detailed account is reported in Appendix 2.B. We find that, under the most reasonable assumptions, dissociation of the most excited QQ^* states occurs faster than de-excitation, as long as the glueball bath originating from dark gluons confinement is present; therefore, the re-annihilation temperature is approximately equal to the one at which glueballs decay ($T_R \approx T_D$). Besides this most probable scenario, in the following we will also consider the other extreme possibility where re-annihilation occurs right after confinement ($T_R = \Lambda_{DC}$). The comparison between these two opposite scenarios will account for the theoretical uncertainties intrinsic to the determination of the non-perturbative dynamics characterizing our DM candidate.

In both benchmark scenarios considered above the last stage of the re-annihilation epoch occurs while entropy is conserved in the Universe and can thus be described by a set of standard Boltzmann equations given in eq. (2.43). They reduce to a single equation for sufficiently large de-excitation or glueball decay rates. This reads

$$\frac{dY_\chi}{dz} = -\frac{s\langle\sigma_{\rm rea} v\rangle}{Hz} Y_\chi^2 \,, \tag{2.27}$$

where $z = M_{\mathcal{Q}}/T$, $Y_\chi \equiv n_\chi/s$ and s is the entropy density of the Universe. The equilibrium term can be neglected since $T_R \leqslant \Lambda_{DC} \ll M_{\mathcal{Q}}$. Assuming a re-annihilation cross section which is constant and velocity independent[8], eq. (2.27) can be easily integrated analytically; one obtains (for $T < T_R$)

$$Y_\chi(T)^{-1} = Y_\chi(T_R)^{-1} + \frac{2}{3}\left(\frac{s\sigma_{\rm rea} v}{H}\right)_{T_R}\left[1 - \left(\frac{T}{T_R}\right)^{3/2}\right] . \tag{2.28}$$

Late-time annihilation significantly affects the gluequark relic density when the second term in the above equation dominates, *i.e.* roughly when

$$n_\chi \sigma_{\rm rea} v \gg H \qquad \text{at } T = T_R \,, \tag{2.29}$$

in agreement with a naive expectation. When condition (2.29) is met, any dependence from the previous stages of cosmological evolution, encoded in $Y_\chi(T_R)$, is washed out and the asymptotic value of the relic density is set only by re-annihilation. For temperatures T sufficiently smaller than T_R (but higher than a possible subsequent period of dilution, in the case $T_R \sim \Lambda_{DC}$), eq.(2.28) can be recast in terms of the gluequark relic density as follows:

$$n_\chi(T) \simeq 1.4\, \frac{(M_{\mathcal{Q}} T_R)^{3/2}}{M_{\mathcal{Q}} M_{\rm Pl}} \frac{g_{\rm SM}(T)^{1/2}}{\sigma_{\rm rea}} \left(\frac{T}{T_R}\right)^3 \qquad \text{for } \; T \ll T_R \,. \tag{2.30}$$

[8] As explained in Appendix 2.B, the last stage of re-annihilation can be effectively described by a constant cross section; the latter turns out to be also velocity independent in the relevant region of the parameter space of our theories.

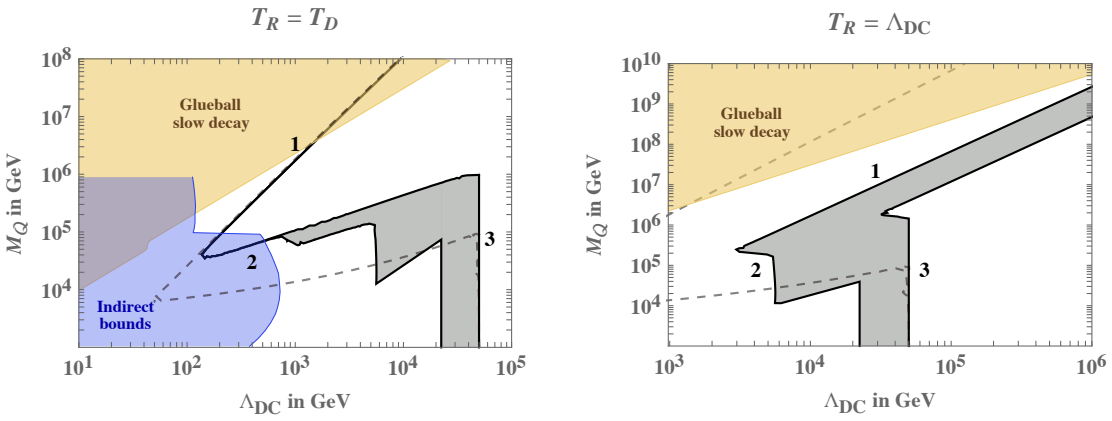

Figure 2.4: *On the black solid line* $\Omega_\chi = \Omega_{\rm DM}$. *We also report (dashed line) the isocurve* $\Omega_\chi = \Omega_{\rm DM}$ *for the case where re-annihilation is not considered. The numbers indicate the three thermal histories described in the text. In the yellow region the glueballs are either stable or have a lifetime bigger than* 1 s. *In the first case they will over-close the Universe while in the latter they will spoil BBN, both cases are therefore forbidden. The blue region is ruled out by indirect searches, namely modifications of the CMB power spectrum, 21-cm line observables and indirect detection (see section 4.2.2).*

2.4 Estimate of the Relic density

The cosmological evolution of gluequarks is determined by the interplay of the mechanisms described in the previous section and depends on the two fundamental parameters M_Q and Λ_{DC}. For each point in the plane (Λ_{DC}, M_Q) one can thus in principle reconstruct the thermal history of the Universe and compute the DM abundance Ω_χ. In this section we will sketch the different possible thermal histories and give an estimate for Ω_χ. As a reference model we consider the minimal module with a triplet of $\mathrm{SU}(2)_L$ (see Table 2.1). We will assume the theory to be outside its conformal window, so that the regime of light dark quarks is well defined. We will discuss at the end how the picture changes for different SM representations and when the theory is in the conformal window or is not asymptotically free.

We will try to quantify the large uncertainties that arise in the determination of the cosmological evolution and of the relic density as a consequence of the non-perturbative nature of the processes involved. As anticipated in section 2.3.3, one of the largest uncertainties comes from the identification of the re-annihilation temperature T_R. We will consider the two previously discussed benchmarks: $T_R = T_D$, the most plausible one according to our estimates, and $T_R = T_{dc}$. We reconstruct for each of them the different possible cosmological evolutions obtained by varying M_Q and Λ_{DC}. Our estimate of the DM abundance for both benchmarks is reported in Fig. 2.4, where we show the isocurve $\Omega_\chi h^2 = 0.119$ reproducing the experimentally observed density.

Let us consider first the case $T_R = T_D$. There are three possible thermal histories that

can be realized (they are correspondingly indicated in the left plot of Fig. 2.4):

1. For very large $M_{\mathcal{Q}}/\Lambda_{DC}$ the Universe undergoes a first perturbative freeze-out at $T_{\rm f.o.} \sim M_{\mathcal{Q}}/25$, then dark confinement occurs at $T \sim \Lambda_{DC}$ followed by an epoch of dilution between T_i and $T_f = T_D = T_R$ [9]. Glueballs decay at $T \lesssim T_D$, and the number density of gluequarks is too small, as a consequence of the dilution, to ignite a phase of non-perturbative re-annihilation. The DM density is therefore given by

$$\Omega_{\rm DM} \simeq \frac{n(T_{\rm f.o.})M_\chi}{\rho_{\rm crit}} \left(\frac{T_0}{T_{\rm f.o.}}\right)^3 \mathcal{F}\,, \tag{2.31}$$

where the number density at freeze-out is estimated by solving the Boltzmann equations numerically and approximately given by eq. (2.11). By using the dilution factor reported in eq. (2.26), setting $M_\chi = M_{\mathcal{Q}}$, $T_{\rm f.o.} = M_{\mathcal{Q}}/25$, and $T_{dc} = \Lambda_{DC}$ as indicated by lattice studies [87], one obtains

$$\Omega_{\rm DM}h^2 \sim 0.1 \left(\frac{0.1}{\alpha_{\rm DC}}\right)^2 \left(\frac{\Lambda_{DC}}{\rm TeV}\right)^{3/2} \left(\frac{100\,\Lambda_{DC}}{M_{\mathcal{Q}}}\right)^2\,, \tag{2.32}$$

which describes well the slope of the upper part of the relic density isocurve in the left panel of Fig. 2.4. Because of the extreme dilution happening during the early epoch of matter domination, the experimental DM abundance is reproduced in this case for very large DM masses, of order of hundreds of TeV or more, above the naive unitarity bound.

2. For smaller values of $M_{\mathcal{Q}}/\Lambda_{DC}$ (but still with $M_{\mathcal{Q}}/\Lambda_{DC} \gtrsim 25$), the dilution between $T_{\rm f.o.}$ and T_D is not enough to prevent re-annihilation (*i.e.* condition (2.29) is met). The latter thus occurs at $T \simeq T_D$, washing out any dependence of Ω_χ from the previous stages of cosmological evolution; the corresponding DM relic density is

$$\Omega_{\rm DM} \simeq \frac{n_\chi(\bar{T})M_\chi}{\rho_{\rm crit}} \left(\frac{T_0}{\bar{T}}\right)^3 \qquad \text{for } T_0 < \bar{T} \ll T_R. \tag{2.33}$$

The first factor corresponds to the gluequark energy density at the end of the re-annihilation (given by eq.(2.30)), and the second one encodes the standard dilution due to the Universe expansion. We evaluate the re-annihilation cross section by using the semiclassical model described in Appendix 2.B.1; this gives

$$\sigma_{\rm rea}^{model} = \frac{4\pi}{\Lambda_{DC}^2}\left[\varepsilon_\Phi(\Lambda_{DC}, M_{\mathcal{Q}}, T_R) + \alpha_2\,\varepsilon_V(\Lambda_{DC}, M_{\mathcal{Q}}, T_R)\right]\,. \tag{2.34}$$

The parameters ε_Φ and ε_V are smaller than 1 and encode the suppression from energy and angular momentum conservation respectively for the recombination processes $\chi\chi \to QQ^* + \Phi$ and $\chi\chi \to QQ^* + V$. While eq.(2.34) is the result of

[9] Here we are implicitly assuming that the re-heating temperature at the end of inflation is larger than $M_{\mathcal{Q}}$, so that the number density of dark quarks after the perturbative freeze-out is thermal.

a rather sophisticated analysis of the re-annihilation dynamics and represents our best estimate for $\sigma_{\rm rea}$, it is subject to large theoretical uncertainties, as discussed in Appendix 2.B.1. We thus also consider the extreme situation where the re-annihilation cross section is always large and saturated by its geometric value

$$\sigma_{\rm rea}^{geo} = \frac{4\pi}{\Lambda_{DC}^2}\,. \tag{2.35}$$

Varying $\sigma_{\rm rea}$ between the values in eqs.(2.34) and (2.35) will quantify the uncertainty on $n_\chi(\bar{T})$. By using eq.(2.30) and setting $M_\chi = M_\mathcal{Q}$ and $T_R = T_D \sim \sqrt{M_{\rm Pl}\Gamma_\Phi}$, eq. (2.33) takes the form:

$$\Omega_{\rm DM}h^2 \sim 0.1 \left(\frac{\Lambda_{DC}}{\rm GeV}\right)^{11/4} \left(\frac{M_\mathcal{Q}}{1000\,\Lambda_{DC}}\right)^{15/2} \frac{4\pi/\Lambda_{DC}^2}{\sigma_{\rm rea}(M_\mathcal{Q},\Lambda_{DC})}\,. \tag{2.36}$$

This formula describes the intermediate part of the isocurve in the left plot of Fig. 2.4. Initially (*i.e.* for $150\,{\rm GeV} \lesssim \Lambda_{DC} \lesssim 800\,{\rm GeV}$) the re-annihilation is dominated by the process $\chi\chi \to QQ^* + \Phi$ and $\varepsilon_\Phi \simeq 1$; in this case the last factor in (2.36) can be well approximated with 1 (the electroweak contribution to $\sigma_{\rm rea}^{model}$ is small) and the estimated uncertainty on the gluequark relic density is negligible. For larger Λ_{DC} re-annihilation into QQ^* plus a glueball becomes kinematically forbidden in our semiclassical model, and ε_Φ quickly drops to zero (see Appendix 2.B.1). In this region $\varepsilon_V \simeq 1/10$ and varying $\sigma_{\rm rea}$ between $\sigma_{\rm rea}^{model}$ and $\sigma_{\rm rea}^{geo}$ spans the gray region. The extension of the latter quantifies the uncertainty of our estimate of the relic density.

3. When $M_\mathcal{Q}/\Lambda_{DC} \leqslant 25$, the perturbative freeze-out does not take place. If $M_\mathcal{Q}$ is bigger than Λ_{DC}, then the Universe undergoes a first epoch of annihilation of dark quarks for $T \gtrsim M_\mathcal{Q}$, followed after confinement by the annihilation of gluequarks, until thermal freeze-out of these latter occurs at $T \simeq M_\chi/25$. If $M_\mathcal{Q} < \Lambda_{DC}$, on the other hand, the theory is in its light quark regime and the only epoch of annihilation is that of gluequarks after dark confinement, again ending with a freeze-out at $T \simeq M_\chi/25$. Afterwards n_χ is diluted by the Universe expansion without any enhancement from the decay of glueballs (these are too short lived to give an early stage of matter domination). The expression for the DM relic density is formally the same as in eq.(2.31) with $\mathcal{F} = 1$. Setting $T_{\rm f.o.} = M_\chi/25$, one obtains

$$\Omega_{\rm DM}h^2 \approx 0.1\,\frac{4\pi/\Lambda_{DC}^2}{\sigma_{\rm ann}} \left(\frac{\Lambda_{DC}}{100{\rm TeV}}\right)^2\,. \tag{2.37}$$

For $1 \lesssim M_\mathcal{Q}/\Lambda_{DC} \lesssim 25$ the non-perturbative annihilation of gluequarks proceeds through the same recombination processes of eq.(2.10). According to the model of Appendix 2.B.1, only the final state with a vector boson is kinematically allowed, and $\varepsilon_V \simeq \alpha_2/10$. This implies $\sigma_{\rm ann} \simeq (\alpha_2/10)\,4\pi/\Lambda_{DC}^2$, so that the DM relic density turns out to be independent of $M_\mathcal{Q}$. If instead the re-annihilation

cross section is estimated by eq.(2.35), then by continuity with the previous cosmological evolution one must take $\sigma_{\rm ann} \simeq 4\pi/\Lambda_{DC}^2$, which also corresponds to a relic density independent of $M_{\mathcal{Q}}$. Varying $\sigma_{\rm ann}$ between these two values gives the largest vertical portion of the gray region in the left plot of Fig. 2.4.

As soon as one enters the light quark regime, $M_{\mathcal{Q}} < \Lambda_{DC}$, the annihilation of gluequarks proceeds through the direct annihilation of their constituents (the theory at $M_{\mathcal{Q}}$ is non-perturbative) with a cross section $\sigma_{\rm ann} = 4\pi c/\Lambda_{DC}^2$, where c is an order 1 coefficient. We vary $1/5 < c < 1$ to quantify the uncertainty in this last non-perturbative process. We thus obtain the narrower vertical portion of the gray region in the left plot of Fig. 2.4, which extends down to arbitrarily small $M_{\mathcal{Q}}$. The observed relic density in this regime is reproduced for $\Lambda_{DC} \simeq 50\,\text{TeV}$, similarly to the light quark regime in baryonic DM models [22].

Let us turn to the case $T_R = T_{dc} = \Lambda_{DC}$. As for $T_R = T_D$ one can identify three possible thermal histories (correspondingly indicated in the right panel of Fig. 2.4):

1. For $M_{\mathcal{Q}}/\Lambda_{DC} \gg 25$ the Universe goes first through a perturbative freeze-out of dark quarks at $T_{\rm f.o.} \simeq M_{\mathcal{Q}}/25$, then re-annihilation occurs right after confinement for $T \simeq \Lambda_{DC}$. Finally, dilution takes place between T_i and the temperature of the glueball decay T_D. The DM relic density is given by the expression in eq.(2.33) times the dilution factor $\mathcal{F}$. Numerically one has

$$\Omega_{\rm DM}h^2 \simeq 5\cdot 10^{-2}\,\frac{\Lambda_{DC}^4}{\xi\, M_{\mathcal{Q}}^{5/2}}\,\frac{4\pi/\Lambda_{DC}^2}{\sigma_{\rm rea}(M_{\mathcal{Q}},\Lambda_{DC})}\,. \tag{2.38}$$

   In this case, our semiclassical model estimates $\varepsilon_\Phi \simeq 1/100$ throughout the parameter space of interest. By varying $\sigma_{\rm rea}$ between $\sigma_{\rm rea}^{model}$ and $\sigma_{\rm rea}^{geo}$ we thus obtain the upper portion of the gray region in the right plot of Fig. 2.4.

2. For smaller $M_{\mathcal{Q}}/\Lambda_{DC}$ (but still with $M_{\mathcal{Q}}/\Lambda_{DC} > 25$), the glueballs are too short lived to ignite the dilution, and the DM relic density is given by eq.(2.33). Setting $T_R = \Lambda_{DC}$ one obtains

$$\Omega_{\rm DM}h^2 \simeq 10^{-10}\,\frac{\Lambda_{DC}M_{\mathcal{Q}}}{\text{GeV}^2}\left(\frac{M_{\mathcal{Q}}}{\Lambda_{DC}}\right)^{1/2}\frac{4\pi/\Lambda_{DC}^2}{\sigma_{\rm rea}(M_{\mathcal{Q}},\Lambda_{DC})}\,. \tag{2.39}$$

3. When $M_{\mathcal{Q}}/\Lambda_{DC} < 25$ the cosmological evolution of the Universe is the same as thermal history 3 in the case $T_R = T_D$. The DM relic density is given by eq.(2.37), corresponding to the vertical gray regions of the right plot of Fig. 2.4.

The plots of Fig. 2.4 graphically summarize our estimate of the DM relic density including the uncertainty from the value of T_R (left vs right panel), and from the value of the cross sections for gluequark re-annihilation and annihilation in the light-quark regime (gray region). Reducing substantially the uncertainty on the re-annihilation process (both the cross section and the value of T_R) is not simple and would require

a dedicated and in-depth study of the recombination and de-excitation rates, and an extensive study of the system of Boltzmann equations, which we do not attempt in this work. An improved precision in the context of our semiclassical model, on the other hand, could be obtained from a more accurate knowledge of the spectrum of states in the strong sector, in particular of the masses of the glueball and gluequark; this can be obtained through dedicated lattice simulations. Notice also that the plots of Fig. 2.4 have been obtained by assuming a dark color gauge group $SU(3)$, for which the confinement temperature T_{dc} and the non-perturbative matrix element relevant for the glueball decay rate are known from lattices studies. Extending our results to other dark gauge groups would in general require to determine these inputs with dedicated simulations, in absence of which there would be further theoretical uncertainties (both in the estimate of the DM relic density, through the expression of the dilution factor in eq. (2.26), and in the exclusion region from the glueball lifetime).

As a last remark we notice that the qualitative picture derived in this section is largely independent of the details of the specific model. However, the quantitative results can change significantly in models with Yukawa couplings, where the glueball lifetime is much shorter. In particular, the exclusion region from the glueball lifetime moves further up left and branch 1, where dilution occurs, becomes vertical (so that the relic density is uniquely fixed in terms of Λ_{DC}). Finally, models that, in the limit of zero quark masses, are infrared free or in the conformal window are constrained to be in the regime $M_{\mathcal{Q}} > \Lambda_{DC}$.

2.5 Summary

In this work we continued the systematic study of gauge theories with fermions in real or vector-like representations, initiated in Ref. [22], where a DM candidate arises as an accidentally stable bound state of the new dynamics. We considered in detail the gluequark DM candidate, a bound state of adjoint fermions with a cloud of gluons, stable due to dark fermion number. What makes this scenario special in the context of accidental DM is that the physical size of DM, that controls the low-energy interactions, is determined by the dynamical scale of the gauge theory independently of its mass. In the heavy quark regime the DM mass and size can be vastly separated leading to an interesting interplay of elementary and composite dynamics. In particular, cross sections much larger than the perturbative unitarity bound of elementary particles can arise, modifying the thermal abundance and producing potentially observable signals in indirect detection experiments. Gluequarks display a rich and non-standard cosmological history and could be as heavy as PeV if their abundance is set by thermal freeze-out.

Our estimates show that the observed DM density can be reproduced by gluequarks both in the light and heavy quark regimes. The mass of the DM is of order 100 TeV or larger, which makes the models difficult to be directly tested at present and future colliders. On the other hand, indirect experiments sensitive to the decay and the annihilation of the DM are a powerful probes of gluequark theories, as will be discussed in Chapter 4. Anticipating the results, we found that these experiments can already set

important limits, excluding part of the curve which reproduces the observed DM density, depending on the value of the annihilation cross section and if the naive estimate for the gluequark decay rate is assumed (see Fig. 4.5). This suggests that gluequark theories in the very heavy quark regime require non-generic UV completions to ensure the accidental stability of the DM at the level of dimension-6 operators. For example, the dark parity could be gauged in the UV (see Appendix 2.C), or its violation could be generated only by non-perturbative gravitational effects in a weakly-coupled UV completion. Similar arguments are put forward also in the context of axion models concerning the quality of the Peccei-Quinn symmetry, see [88]. Assuming that an appropriate UV completion exists, gluequark models are interesting examples where the DM density can be generated thermally after inflation by very heavy particles. This can be contrasted with other scenarios, such as Wimpzillas [89], where ultra heavy DM candidates are never in thermal equilibrium.

The low-energy dynamics and the spectrum of gluequarks are non-perturbative and we were only able to give rough estimates of various effects. In particular, in the heavy quark regime, the quantitative estimate of the re-annihilation relevant for the thermal relic abundance and indirect detection of DM is highly uncertain, as it depends on the details of the spectrum and on the rates of non-perturbative transitions. A more firm conclusion would require a better knowledge of the recombination cross sections and of the de-excitation rates of bound states, as well as an extensive study of the system of Boltzmann equations. In the light-quark regime, a non-perturbative calculation of the annihilation cross section would lead to a sharp prediction of the dynamical scale of the dark sector. The precise knowledge of the spectrum of gluequarks, mesons and pions would then give valuable information for indirect detection and collider studies.

In this work we studied gluequarks as thermal relic candidates and focused on the simplest, minimal theories of Tab. 2.1. Investigating non-minimal models would be certainly interesting and important under several aspects. For example, SM gauge couplings unify at high energies with less precision in the minimal blocks of Tab. 2.1 than in the SM. Achieving precision unification thus necessarily requires extending the models to include additional matter with SM quantum numbers. Furthermore, while the thermal relic abundance hints to a large DM mass, this conclusion can be modified in more general gluequark theories where the DM is asymmetric (this requires a larger accidental symmetry than dark parity) or where the DM abundance is determined by the decay of unstable heavier states. These theories would have a smaller mass gap and could be tested at the LHC and at future colliders.

2.A Dark Quark Annihilation Cross Section

In this section we report the formulas for the annihilation cross section of dark quarks, which are useful to study the perturbative freeze-out and DM indirect detection.

Dark quarks can annihilate into dark gluons and into SM final states (mainly VV, Vh, hh and $\psi\bar{\psi}$, where $V = W, Z, \gamma$). These latter contribute significantly to the total cross section in the case of perturbative freeze-out whenever $M_{\mathcal{Q}}/\Lambda_{DC} \gg 1$ and thus the dark color interaction strength does not exceed much the electroweak one. Final states into SM particles are also expected to be important for direct detection even though they have a smaller rate compared to DM annihilation into glueballs.

The tree-level annihilation cross-section of dark quarks $\chi_i\chi_j$ in a representation $(A_{\rm DC}, R_{\rm SM})$ of the dark color and $\mathrm{SU}(2)_L$ groups into massless vectors at low energy reads,

$$\begin{aligned} \langle\sigma v_{\rm rel}\rangle_{ij\to VV} &= \frac{A^1_{ij} + A^2_{ij}}{16\pi}\frac{1}{M^2_{\mathcal{Q}}} \\ A^1_{ij} &\equiv \left[T^a T^a T^b T^b\right]_{ij}, \qquad A^2_{ij} \equiv \left[T^a T^b T^a T^b\right]_{ij} \end{aligned} \tag{2.40}$$

where the generators are written as $T \equiv (g_{\rm DC} T_{\rm DC}\otimes 1)\oplus(1\otimes g_{\rm SM} T_{\rm SM})$. Selecting the neutral component in the equation above and averaging over dark color gives the perturbative annihilation cross-section of DM today. Averaging over all initial states as required for the thermal freeze-out one finds [25],

$$\begin{aligned} \langle\sigma v_{\rm rel}\rangle_{\rm ann} = \frac{\pi}{M^2_{\mathcal{Q}}}\Bigg[&\frac{\alpha^2_{\rm DC}}{d(R_{\rm SM})}\frac{K_1(R_{\rm DC}) + K_2(R_{\rm DC})}{g_\chi d(R_{\rm DC})^2} + \frac{\alpha_2^2}{d(R_{\rm DC})}\frac{K_1(R_{\rm SM}) + K_2(R_{\rm SM})}{g_\chi d(R_{\rm SM})^2} \\ &+ \alpha_{\rm DC}\alpha_2\frac{4C(R_{\rm DC})C(R_{\rm SM})}{g_\chi d(R_{\rm SM}) d(R_{\rm DC})}\Bigg], \end{aligned} \tag{2.41}$$

where

$$K_1(R) = d(R)C(R)^2, \quad K_2(R) = K_1(R) - \frac{d(A)C(A)T(R)}{2}, \quad d(R) = dim(R)\,. \tag{2.42}$$

and A stands for the adjoint representation. $T(R)$ and $C(R)$ are respectively the Dynkin index and the quadratic Casimir of the representation R, and $g_\chi = 2(4)$ for real (complex) representations.

Dark quarks can also annihilate into final states with SM fermions and Higgs bosons through their SM gauge and Yukawa interactions. These channels have been included in eq. (2.12).

2.B Reannihilation

As discussed in section 2.3.3, a second stage of annihilation involving gluequarks can occur after confinement. The annihilation can proceed in a single step into glueballs or SM vector and Higgs bosons:

- $\chi + \chi \to n\Phi/nV$: in the heavy quark regime this process has a perturbative cross section; indeed the exchanged momentum in the interaction is of $\mathcal{O}(M_{\mathcal{Q}})$ with $M_{\mathcal{Q}} \gg \Lambda_{DC}$, thus the interaction strength is governed by $g_{\rm DC}(M_{\mathcal{Q}})$ which is perturbative.

Alternatively, it can take place in two steps, a non-perturbative recombination followed by de-excitation and decay into SM particles:

- $\chi + \chi \to \mathcal{Q}\mathcal{Q}^*$ $\dashrightarrow$ SM: the recombination is two to one and energy conservation implies $M_{\mathcal{Q}\mathcal{Q}^*} > 2M_\chi$, therefore the opposite decay process is always allowed. The matrix element for the inverse decay is non-perturbative and the corresponding rate is expected to be much larger than the rate of the de-excitation process $\mathcal{Q}\mathcal{Q}^* \to \mathcal{Q}\mathcal{Q} + n\Phi/nV$.

- $\chi + \chi \to \mathcal{Q}\mathcal{Q}^* + \Phi/V$ $\dashrightarrow$ SM: the recombination takes place with the emission of one electroweak gauge boson or, if kinematically allowed, one glueball. Bound states with $M_{\mathcal{Q}\mathcal{Q}^*} < 2M_\chi$ will in general be formed which cannot decay back into gluequarks. They can de-excite and decay into SM particles. The corresponding re-annihilation rate is expected to be non-perturbative and potentially large.

Only the last of the three processes described above can ignite an epoch of re-annihilation. The dynamics of re-annihilation is described by a set of coupled Boltzmann equations of the form

$$\begin{aligned}
\frac{dY_\chi}{dz} &= -\frac{s\langle\sigma_{\rm rec}v\rangle}{Hz}\left(Y_\chi^2 - Y_{\chi,eq}^2\,\frac{Y_{\mathcal{Q}\mathcal{Q}^*}\,Y_\Phi}{Y_{\mathcal{Q}\mathcal{Q}^*}^{eq}\,Y_\Phi^{eq}}\right)\,,\\
\frac{dY_{\mathcal{Q}\mathcal{Q}^*}}{dz} &= \frac{1}{2}\frac{s\langle\sigma_{\rm rec}v\rangle}{Hz}\left(Y_\chi^2 - Y_{\chi,eq}^2\frac{Y_{\mathcal{Q}\mathcal{Q}^*}Y_\Phi}{Y_{\mathcal{Q}\mathcal{Q}^*}^{eq}Y_\Phi^{eq}}\right) - \frac{\Gamma_{\mathcal{Q}\mathcal{Q}^*}}{Hz}(Y_{\mathcal{Q}\mathcal{Q}^*} - Y_{\mathcal{Q}\mathcal{Q}^*}^{eq})\\
\frac{dY_\Phi}{dz} &= \frac{1}{2}\frac{s\langle\sigma_{\rm rec}v\rangle}{Hz}\left(Y_\chi^2 - Y_{\chi,eq}^2\frac{Y_{\mathcal{Q}\mathcal{Q}^*}Y_\Phi}{Y_{\mathcal{Q}\mathcal{Q}^*}^{eq}Y_\Phi^{eq}}\right) - \frac{\Gamma_\Phi}{Hz}(Y_\Phi - Y_\Phi^{eq})\,.
\end{aligned} \tag{2.43}$$

These expressions are simplified in that the actual system of equations involves the number densities of all possible $\mathcal{Q}\mathcal{Q}^*$ bound states. Furthermore, we have omitted the effect of the recombination into EW vector bosons and of the corresponding inverse process. Equation (2.43) will be however sufficient for our discussion, and the generalization to the full case is straightforward.

In order to annihilate into SM particles with an unsuppressed rate, an excited $\mathcal{Q}\mathcal{Q}^*$ bound state needs to reach first a state with low angular momentum. Consequently, re-annihilation is efficient only when the rate of de-excitation is larger than the one of dissociation[10].

Obtaining a precise estimate of the ratio between the de-excitation and dissociation rates is difficult because: *i)* the dynamics of these processes is non perturbative and the

[10] In the opposite regime of fast dissociation, and much before the glueball decay, the last term in the second and third lines of eq. (2.43) can be neglected. The solution to the Boltzmann equations is thus given by non-thermal equilibrium values for the three populations which are close to their initial conditions at dark confinement.

lifetime depends on the different initial and final $\mathcal{Q}\mathcal{Q}^*$ states considered; *ii)* the rate of the dissociation process initiated by EW vector bosons depends on their energy, which follows a thermal distribution and thus varies with the temperature. The result is that the re-annihilation process can be efficient for some of the QQ^* states and inefficient for others, and it becomes more and more efficient as the temperature decreases.

This can be effectively described as a non-perturbative re-annihilation process happening with a temperature-dependent cross section that saturates to a maximal value when dissociation becomes inefficient for all the bound states. Since the evolution of the relic density takes place on relatively short time scales, the final abundance after this second freeze-out can be approximately characterized by two parameters: the final (maximal) value of the cross section, and the temperature at which this final cross section is reached. These two quantities will be dubbed respectively as the re-annihilation cross section, $\sigma_{\rm rea}$, and the re-annihilation temperature, T_R.

During the last stage of re-annihilation, for sufficiently large Γ_Φ or $\Gamma_{\mathcal{Q}\mathcal{Q}^*}$, the system of equations given in eq. (2.43) simplifies. The abundance of gluequarks can be described by a single equation, see eq. (2.28).

2.B.1 Estimate of the Re-annihilation Cross Section

In this section we try to estimate $\sigma_{\rm rea}$ using considerations based on energy and angular momentum conservation and simplified phenomenological models.

First of all, it is useful to determine if (depending on value of the temperature, Λ_{DC} and $M_{\mathcal{Q}}$) the recombination process takes place in a semiclassical or fully quantum regime. If the De Broglie wavelength of the particle $\lambda = h/p$ is of order or larger than the typical interaction range $R \sim 1/\Lambda_{DC}$ the collision is fully quantum mechanical, otherwise a semiclassical picture can be adopted. The condition for a semiclassical behaviour can be recast as $l_{\rm max} \sim M_\chi v R \gg 1$, where $l_{\rm max}$ is the maximum angular momentum of the process given the short-range nature of the interaction. We find that the processes occurring in the very early Universe (at $T = T_R$) are always in the semiclassical regime in the region of parameter space where the DM experimental density can be reproduced. Recombination processes occurring at the CMB or at later times, instead, turn out to be quantum mechanical because of the much lower gluequark velocity.

In the quantum regime, the lowest partial wave is expected to dominate in the low momentum limit $k \to 0$. In the case of exothermic reactions[11], as the one considered here, general arguments of scattering theory suggest that the cross section scales as $1/k$ for $k \to 0$ if the process can take place in s-wave [90]. In the non-relativistic limit we thus expect a cross section $\sigma \propto 1/v$. Since the process is non-perturbative it is not possible to compute this cross section from first principles; furthermore, since two different scales ($M_{\mathcal{Q}}$ and Λ_{DC}) appear in the problem, it is not clear what is the cross section scaling[12].

[11] Exothermic reactions are those where the particles in the final states are lighter than those in the initial state.

[12] The electroweak process $\chi + \chi \to QQ^* + V$ has a close nuclear analogue given by $p + n \to d + \gamma$. Explicit calculations reproduce the expected $1/v$ velocity dependence [91]. The non-perturbative constant in that case can be predicted using elastic nucleon scattering data.

In light of this we adopt two different benchmark scenarios:

$$\langle \sigma_{\rm ann} v_{\rm rel} \rangle \sim \begin{cases} \dfrac{1}{\Lambda_{DC}^2} \\ \\ \pi R_B^2 \approx \dfrac{\pi}{(\alpha_{\rm DC}^2 M_{\mathcal{Q}}^2)} \,. \end{cases} \tag{2.44}$$

In the first one the cross-section is controlled by the size of the gluequark while in the latter is the size of the s-wave ground state which fixes the cross section.

In the semiclassical regime we estimate the re-annihilation cross section using a simple dynamical model. We first discuss the process $\chi + \chi \to QQ^* + \Phi$ and then analyse the recombination into EW vector bosons. Our semiclassical model is defined in terms of the following simplified assumptions:

- The gluequarks are modelled as hard spheres with radius of order $R \sim 1/\Lambda_{DC}$, colliding with impact parameter b and thermal velocity v.
- The interaction is short range, therefore the maximum impact parameter for which an interaction occurs is $b_{\rm max} = 2R \sim 2/\Lambda_{DC}$. We define a corresponding geometric total cross section
$$\sigma_{\rm total} = \pi b_{\rm max}^2 = \frac{4\pi}{\Lambda_{DC}^2} \,. \tag{2.45}$$
For thermal velocities, $b_{\rm max}$ can be converted into a maximum angular momentum $l_{\rm max} = b_{\rm max} M_\chi v \sim 2(M_\chi/\Lambda_{DC})\sqrt{3T/M_\chi}$ for the colliding particles.
- Energy conservation implies that only some bound states can be formed. Among these we identify the states with maximum angular momentum l_* allowed by energy conservation and by the short range constraint $l_* \leqslant l_{\rm max}$.
- Angular momentum conservation implies that only interactions with impact parameter smaller than $b_* \approx (l_*+1)/(M_\chi v)$ can lead to bound state formation[13]. The short range interaction constraint then forces $b_* \leqslant b_{\rm max}$. If no bound state is allowed by energy conservation we take $b_* = 0$.
- The recombination cross section is estimated by the geometrical value $\sigma = \pi b_*^2$.

The model predicts a re-annihilation cross section into glueballs that can be conveniently expressed in terms of a suppression factor ε_Φ as follows:

$$\sigma_{{\rm rea},\Phi} = \pi b_*^2 = \left(\frac{b_*}{b_{\rm max}}\right)^2 \sigma_{\rm total} \equiv \varepsilon_\Phi \, \sigma_{\rm total} \,, \tag{2.46}$$

[13]The factor (l_*+1) takes into account the quantization of l_* and ensures that the cross section is not underestimated for small angular momenta.

where ε_Φ is computed to be

$$\varepsilon_\Phi = \begin{cases} 1 & \text{if} \quad l_* > l_{\max} - 1, \\ \dfrac{\Lambda_{DC}^2}{4} \dfrac{(l_*+1)^2}{M_\chi^2 v^2} & \text{if} \quad l_* < l_{\max} - 1, \\ 0 & \text{if} \quad l_* \text{ does not exist.} \end{cases} \tag{2.47}$$

Notice that ε_Φ is a function of $M_\mathcal{Q}$, Λ_{DC} and indirectly of the temperature through the value of l_* and v.

In order to determine l_* we use the energy balance equation in the center-of-mass frame:

$$2M_\chi + 2K_\chi \geqslant M_{\mathcal{Q}\mathcal{Q}^*} + M_\Phi \,, \tag{2.48}$$

where K_χ is the kinetic energy of the colliding gluequarks. The gluequark mass can be written in terms of the quark mass plus a binding energy B_χ:

$$M_\chi = M_\mathcal{Q} + B_\chi \,. \tag{2.49}$$

Similarly, the mass of the di-quark bound state is decomposed as

$$M_{\mathcal{Q}\mathcal{Q}^*} = 2M_\mathcal{Q} + B_{\mathcal{Q}\mathcal{Q}^*} \,. \tag{2.50}$$

We set the gluequark binding energy to the value computed in QCD lattice simulations of SU(3) gauge theories: $B_\chi = 3.5\,\Lambda_{DC}$ [64] [14]. The binding energy of the $\mathcal{Q}\mathcal{Q}^*$ bound state, $B_{\mathcal{Q}\mathcal{Q}^*}$, is instead approximated by the energy levels of a confining model with a Coulomb potential plus a linear term [92]

$$V(r) = -\frac{\alpha_{\text{eff}}}{r} + \sigma r, \tag{2.51}$$

with $\alpha_{\text{eff}} = \alpha_{\text{DC}}(M_\mathcal{Q})$ and $\sigma = 2.0\, N_{DC} \Lambda_{DC}^2$. Therefore, $B_{\mathcal{Q}\mathcal{Q}^*}$ is computed numerically as a function of the principal and orbital quantum numbers of the bound state. The energy balance of eq.(2.48) can be rewritten as

$$B_{\mathcal{Q}\mathcal{Q}^*} \leqslant 2B_\chi + 2K_\chi - M_\Phi \,, \tag{2.52}$$

and implies a constraint on the maximal angular momentum l_* (as well as on the principal number). In general one should also impose the additional condition $M_{QQ*} < 2M_\chi$,

[14] The bare quark mass and binding energy are renormalization scheme dependent. Here we quote the result of reference [64] valid in the RS scheme which, according to the authors, smoothly converges to the $\overline{MS}$ scheme in the perturbative regime. Since we are interested in just an order-of-magnitude determination of the relic density, we neglect the scheme dependence of B_χ in what follows. We notice however that our numerical estimate of the re-annihilation cross section is rather sensitive to the value of B_χ, hence the scheme dependence can have a strong impact. We take such theoretical uncertainty effectively into account by considering different benchmark scenarios, as explained in section 2.3.3.

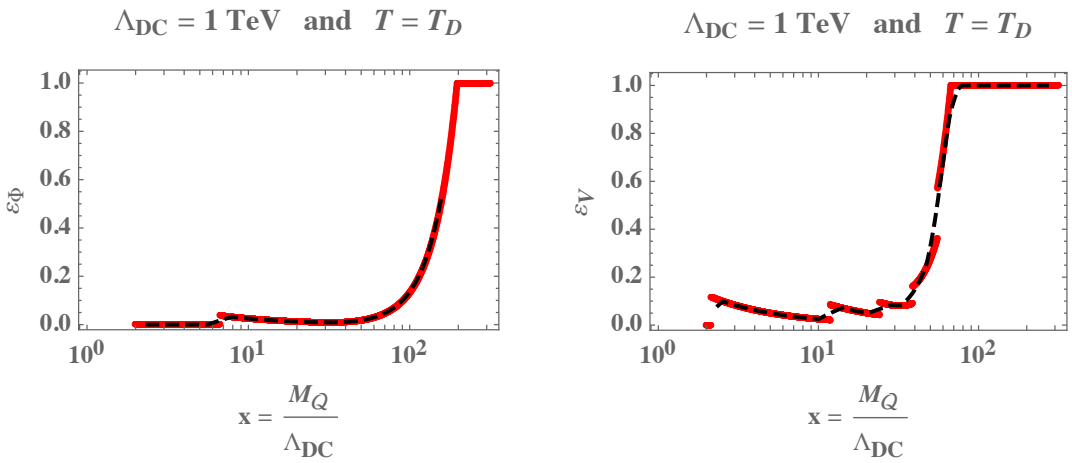

Figure 2.5: *Suppression factors ε_Φ (left panel) and ε_V (right panel) at $T = T_D$ as a function of the ratio $M_\mathcal{Q}/\Lambda_{DC}$ for $\Lambda_{DC} = 1\,\text{TeV}$. In red the results of the numerical computation and in black the interpolation used to compute the relic density. Discontinuities in the numerical results are due to the integer nature of l_*.*

to ensure that the decay of the QQ^* state back into gluequarks is kinematically forbidden. In terms of binding energies, this condition reads

$$B_{\mathcal{Q}\mathcal{Q}^*} < 2B_\chi\,. \tag{2.53}$$

The average gluequark kinetic energy in eq. (2.52) is of order of the temperature, which in turn is smaller than Λ_{DC}. We set the glueball mass to its value computed on the lattice in SU(3) Yang-Mills theories, $M_\Phi \simeq 7\Lambda_{DC}$, and thus find $2K_\chi - M_\Phi < 0$. As a consequence, the condition (2.52) is always stronger than (2.53).

Since eq. (2.52) depends on the gluequark kinetic energy, which we set to $K_\chi = T$ in our numerical computation, the value of l_* will have a dependence on T. For illustration we show in Fig. 2.5 the value of ε_Φ as a function of $M_\mathcal{Q}/\Lambda_{DC}$ obtained at $T = T_D$ for $\Lambda_{DC} = 1\,\text{TeV}$. Changing Λ_{DC} while keeping the temperature fixed leads to very small variations of ε_Φ. For $T = \Lambda_{DC}$, on the other hand, ε_Φ turns out to be small and of order of a few$\times 10^{-2}$ in the region of interest ($100\,\text{GeV} < \Lambda_{DC} < 10\,\text{TeV}$ and $1 < M_\mathcal{Q}/\Lambda_{DC} < 100$).

In the case of the recombination with the emission of a vector boson, $\chi + \chi \to QQ^* + V$, we expect the re-annihilation cross section to be suppressed by at least a factor α_2. Clearly, this process becomes relevant only when the recombination with glueball emission is strongly suppressed or forbidden for kinematic reasons. The transitions $\chi + \chi \to QQ^* + V$ that are relevant for re-annihilation are those where the QQ^* is sufficiently light so that it cannot decay back in two χ's. Such bound states satisfy the condition (2.53), which requires the kinetic energy of the emitted vector boson to be larger than the sum of the kinetic energies of the colliding gluequarks ($K_V > 2K_\chi$). The

re-annihilation cross section can be written as

$$\sigma_{\mathrm{rea},V} = \varepsilon_V \alpha_2 \frac{4\pi}{\Lambda_{DC}^2}\,, \tag{2.54}$$

and the suppression factor ε_V can be estimated using our semiclassical model by following a procedure similar to the one described for the case of glueball emission. We find that ε_V has a behaviour similar to ε_Φ as a function of its variables, and a slightly larger absolute value, see Fig. 2.5.

2.B.2 Re-annihilation temperature

The temperature at which the re-annihilation cross section saturates and the relic abundance freezes out is determined by two competing processes: de-excitation and dissociation. The cross section saturates when the former dominates over the latter for all the bound states with $M_{\mathcal{Q}\mathcal{Q}^*} < 2M_\chi$. We will now try to argue that for $T > T_D$ there are states for which the dissociation rate is larger than the de-excitation one. Therefore, the most reasonable scenario is one in which the re-annihilation cross section saturates at $T_R \lesssim T_D$.

States with $M_{\mathcal{Q}\mathcal{Q}^*} > 2M_\chi - M_\Phi$ can be dissociated by glueballs with vanishing kinetic energy. Therefore, these states are the most easily dissociated since all the glueballs present in the Universe contribute to their breaking rate

$$\Gamma_{\mathrm{dis}} = n_\Phi \langle \sigma_{\mathrm{dis}} v \rangle\,, \tag{2.55}$$

where $\sigma_{\mathrm{dis}} \sim \Lambda_{DC}^{-2}$ and n_Φ is the number density of glueballs which, at $T > T_D$, is dominated by the population coming form the confinement of dark gluons: $n_\Phi \sim T^3$. The de-excitation rate can be estimated using the well known result for spontaneous emission[15]

$$\Gamma_{\mathcal{Q}\mathcal{Q}^*} \sim \alpha_2\, \Delta E^3\, |\langle R_f | \vec{r} | R_i \rangle|^2\,, \tag{2.56}$$

where ΔE is the difference of energy levels. A reasonable estimate for this rate can be given for transitions between these states and the ground level. In this case $\Delta E \sim \Lambda_{DC} + \alpha_{\mathrm{DC}}^2 M_{\mathcal{Q}}$, while the matrix element is a fraction of the Bohr radius, $r_b \sim 1/(\alpha_{\mathrm{DC}} M_{\mathcal{Q}})$. This estimate gives $\Gamma_{\mathcal{Q}\mathcal{Q}^*}$ smaller than Γ_{dis} and suggests that for $T > T_D$ re-annihilation cannot proceed through the formation of these states. At $T \sim T_D$ glueballs start to decay. Their number density decays exponentially and the dissociation process becomes soon inefficient. Therefore all the states can contribute to the re-annihilation process and the cross section saturates.

After the decay of the primordial glueballs, dissociation processes involving electroweak gauge bosons can play a role. However their cross section is suppressed by an electroweak factor and, moreover, their energy distribution is thermal. At $T \lesssim T_D$ one needs vector bosons in the tail of the Bose-Einstein distribution in order to have

[15] This rate corresponds to dipole transitions and is associated to the usual atomic selection rules. Higher multipole transitions can be considered, but we limit our discussion to the case of the dipole since we are interested only in an order-of-magnitude estimate.

enough energy to dissociate the bound states. As a result, the rate of this process is exponentially suppressed by a factor $\exp[-(2B_\chi - B_{\mathcal{Q}\mathcal{Q}^*})/T]$ and, even if it is efficient at T_D, it becomes soon inefficient.

For these reasons, we consider the case in which the reannihilation occurs at T_D as the most plausible. This is in agreement with what suggested in Ref. [32]. Due to the large uncertainties on the estimates of the rates, however (especially for what concerns $\Gamma_{\mathcal{Q}\mathcal{Q}^*}$, where neither ΔE nor the matrix element can be computed from first principles), we do not exclude the possibility that the dissociation processes are never efficient and re-annihilation takes place directly at Λ_{DC}.

2.C A model with hypercharge

In this article we focused on the minimal block V of Table 2.1 as a benchmark for our analysis. However, the $L \oplus \bar{L}$ model has many peculiarities and deserves a separate discussion. In particular, in this case the DM candidate has non-vanishing hypercharge and interacts at tree level with the Z boson.

Higher-dimensional operators

This model has a $U(1)_D$ accidental symmetry, comprising dark parity as a subgroup, under which the dark quarks L and $\bar{L}$ have charge ± 1. Differently from the other models, this symmetry is broken by higher-dimensional operators with classical dimension $[\mathcal{O}_{\rm dec}] = 5$ of the form

$$\mathcal{O}_{\rm dec} = \ell \mathcal{G}_{\mu\nu} \sigma^{\mu\nu} L \,.$$

In order to have a stable DM candidate and make the model viable, one can gauge the $U(1)_D$ in the ultraviolet and break it spontaneously to the dark parity subgroup by means of a scalar field. For instance, if a scalar ϕ with charge 2 acquires a vacuum expectation value the symmetry is broken according to the pattern:

$$U(1)_D \to \mathbb{Z}_2 .$$

At the scale of the spontaneous breaking only operators that are dark-parity even are generated, hence the gluequark is absolutely stable.

Z-boson mediated direct detection

Below the confinement scale, the spectrum comprises a composite Dirac fermion with SM quantum numbers $2_{1/2}$, whose EM neutral component is identified with the DM. The non-zero hypercharge induces a tree-level interaction with the Z boson which is strongly constrained by direct searches. The corresponding spin-independent elastic cross section on nuclei $\mathcal{N}$ is given by [93]:

$$\sigma = \frac{G_{\rm F}^2 M_{\mathcal{N}}^2}{8\pi} \Big(N - (1 - 4\sin^2\theta_W) Z \Big)^2 ,$$

where Z and N are the number of protons and neutrons in the nucleus $\mathcal{N}$ and $M_{\mathcal{N}}$ is its mass. This cross section is excluded by direct detection experiments for masses $M_\chi \lesssim 10^8\,\text{GeV}$ [94]. This bound rules out the model in the scenario $T_R = T_D$, corresponding to the left panel of Figure 2.4, but can be satisfied in the scenario $T_R = \Lambda_{DC}$.

In fact, the constraint from direct detection experiments can be also avoided by introducing a heavy singlet gluequark. In this case the presence of Yukawa couplings induces a splitting among the electromagnetically neutral Majorana fermions. The DM is the lightest among these fermions, so that tree-level elastic scattering mediated by the Z boson cannot exist due to its Majorana nature. Inelastic scatterings are kinematically forbidden if the splitting is large enough; this is easily realized for $M_{\text{N}} \lesssim y^2 \times 10^5\,\text{TeV}$, where y is the Yukawa coupling. This scenario is analogous to Higgsino DM in supersymmetry, see [22, 25] for an extensive discussion.

Accidentally stable mesons

If the model is not in the conformal window, it is possible to consider the light quark regime. In this case, the model is characterized by the presence of NGBs made of LL or $\bar{L}\bar{L}$ constituents which have $U(1)_D$ number ± 2 and therefore cannot decay. If the accidental $U(1)_D$ is gauged in the UV and spontaneously broken to dark parity, then dimension-5 operators can be generated which let the NGBs decay while keeping the gluequarks stable.

3 Chiral dark sector with SM interactions

3.1 Introduction

In this chapter we focus on confining, chiral dark gauge theories, in particular those with no fundamental dark scalar fields. Models of this kind with DM candidates appeared for example in Refs. [47, 48, 49]. In this class of theories the masses of all the dark states are generated dynamically, since no fermion mass term is allowed by gauge invariance. The same is not true in vectorlike theories, since in that case bare mass terms can be larger than the dynamical scale and determine the masses of some of the physical states, possibly including the DM candidate [30, 25, 2]. Chiral theories are more constrained in general, hence less simple to construct, than vectorlike theories. The cancellation of gauge anomalies, for example, is a non-trivial requirement that significantly restricts the possible models. Interesting studies in this direction include techniques for finding anomaly-free sets of fermions in theories with a $U(1)$ chiral factor [95, 96, 97], and a method to construct chiral theories starting from irreducible representations of a simple, anomaly-free gauge group [98]. Chiral theories are also notoriously difficult to simulate on the lattice [99, 100], and their IR behavior is still not known for simple gauge groups. In that case bilinear fermion condensates cannot be singlets under both the gauge and the Lorentz group. It has been speculated that the theory may 'tumble' into a Higgs phase with reduced gauge group [101] or even break spontaneously Lorentz invariance [102], although a reasonable possibility is that no bilinear fermion condensate forms at all at the non-perturbative level.

Lacking a clear theoretical understanding of chiral theories with simple groups, in this work we consider models where the dark gauge group is the product of a simple, vectorlike factor G_{DC} (dark color), which gets strong and confines at a scale Λ_{DC} larger than the EW scale, times a weak factor G_D. In the context of these theories, we will specifically investigate those where the dark quarks are charged under the SM gauge group $G_{SM} = SU(3)_c \times SU(2)_{EW} \times U(1)_Y$, while the SM fermions are neutral under $G_{DC} \times G_D$. The full gauge group $G_{DC} \times G_D \times G_{SM}$ is assumed to be chiral. To avoid large corrections to the electroweak precision observables, we will require that the dark quarks transform as vectorlike representations of $G_{DC} \times G_{SM}$. Depending on whether $G_{DC} \times G_D$ is chiral and on the vacuum alignment, the dark condensate can break G_D spontaneously and preserve G_{SM}. In absence of Yukawa couplings between the Higgs field and the dark quarks, this ensures negligibly small corrections to the electroweak precision observables, as in theories of vectorlike confinement [16]. Having dark quarks charged under the SM implies a further constraint though: since the theory is chiral and mass terms are not allowed, unification of SM gauge forces into a simple group G_{GUT}

is possible only if dark quarks come in complete representations of G_{GUT}. This has to be contrasted with vectorlike theories, where GUT partners completing the multiplets can have much higher masses. Another difference between vectorlike and chiral gauge theories will be discussed at length in this work and concerns the accidental stability of the DM candidate: while in vectorlike theories dark baryons are generically more stable than dark pions [22], the same is not true for chiral theories, where the operators responsible for the dark pion decay can easily have a very large dimension.

Chiral theories with a product gauge group $G_{DC} \times G_D \times G_{SM}$ can be classified according to the number of irreducible representations of Weyl fermions. For a non-abelian subgroup G_D, candidate theories can be constructed with just one or two representations. They will be studied in a forthcoming work. Here we focus on models with an abelian subgroup $G_D = U(1)_D$; in that case the minimum number of representations to have a chiral theory is 4. The three possible types of minimal theories are defined in Table 3.1, where R and r are (generally complex) irreducible representations of respectively G_{DC} and G_{SM}, and a is a rational number. The case with fermions transforming as singlets under G_{SM} ($r = 1$) and as fundamental representations of $G_{DC} = \mathrm{SU}(N_{DC})$ ($R = F$) was studied in Refs. [47, 48]. There the dark color gauge group confines in the infrared forming three dark pions, according to the pattern of global symmetry breaking $SU(2) \times SU(2) \to SU(2)_V$. The $U(1)_D$ is spontaneously broken and one of the dark pions is eaten to form a massive dark photon. The residual global symmetry is $\mathrm{U}(1)_{3V} \times \mathrm{U}(1)_V$, where $\mathrm{U}(1)_V$ is the dark baryon number and $\mathrm{U}(1)_{3V} \subset SU(2)_V$ is an additional vectorial factor. The two uneaten dark pions have $\mathrm{U}(1)_{3V}$ charge ± 2 and are thus accidentally stable, providing a viable DM candidate. Interactions with the Standard Model sector are achieved through a kinetic mixing between the $\mathrm{U}(1)_D$ gauge field and hypercharge [103].

The purpose of this work is to study the theories of Table 3.1 with non-trivial SM representations r. Compared to the analysis of Refs. [47, 48], these models are characterized by less suppressed interactions between the dark and SM sectors, and lead to experimental signatures that are more easily testable. In particular, even though the DM candidate is a singlet under the SM, it has charged partners that can be discovered at colliders.

The chapter is organized as follows. Section 3.2 makes an analysis of the minimal models of Tab. 3.1 and identifies those that are fully realistic. In these theories r is a fundamental of $\mathrm{SU}(2)_{EW}$ or a fundamental of $\mathrm{SU}(3)_c$. The rest of the chapter focuses on the model with $\mathrm{SU}(2)_{EW}$ doublets. Its Lagrangian and symmetries are discussed in Section 3.3, the spectrum and the lifetimes of the lowest-lying states are analyzed in Section 3.4, while its cosmological history is studied in Section 3.5. The discussion of the phenomenological constraints set by direct and indirect DM searches, and by collider data is postponed to Chapter 4. We present our summary and outlook in Section 3.6. Finally, the content of the Appendices is as follows: 3.A reports useful formulas on dark pions used in the text; 3.B gives a short description of the model with $\mathrm{SU}(3)_c$ triplets; 3.C includes a detailed analysis of the Boltzmann equations relevant for the evolution of the dark sector during freeze out; 3.D discusses some aspects of the phenomenology of dark

Type I

	G_{DC}	$\mathrm{U}(1)_D$	G_{SM}	$\mathrm{U}(1)_{3V}$	$\mathrm{U}(1)_V$
ψ_1	R	$+1$	r	$+1$	$+1$
ψ_2	R	-1	r	-1	$+1$
χ_1	$\bar{R}$	$-a$	$\bar{r}$	-1	-1
χ_2	$\bar{R}$	$+a$	$\bar{r}$	$+1$	-1

Type II

	G_{DC}	$\mathrm{U}(1)_D$	G_{SM}	$\mathrm{U}(1)_{3V}$	$\mathrm{U}(1)_V$
ψ_1	R	$+1$	r	$+1$	$+1$
ψ_2	R	-1	$\bar{r}$	-1	$+1$
χ_1	$\bar{R}$	$-a$	$\bar{r}$	-1	-1
χ_2	$\bar{R}$	$+a$	r	$+1$	-1

Type III

	G_{DC}	$\mathrm{U}(1)_D$	G_{SM}	$\mathrm{U}(1)_{3V}$	$\mathrm{U}(1)_V$
ψ_1	R	$+1$	r	$+1$	$+1$
ψ_2	R	$+a$	$\bar{r}$	-1	$+1$
χ_1	$\bar{R}$	$-a$	$\bar{r}$	-1	-1
χ_2	$\bar{R}$	-1	r	$+1$	-1

Table 3.1: The three minimal classes of chiral theories with 4 irreducible representations of the gauge group $G_{DC} \times \mathrm{U}(1)_D \times G_{SM}$. All fields are left-handed Weyl fermions. Charges under the accidental global $\mathrm{U}(1)_{3V} \times \mathrm{U}(1)_V$ are indicated in the last column, separated by a vertical line. The parameter a is an arbitrary rational number in the interval $[-1, 1)$ for Type II and II theories, and in the interval $[0, 1)$ for Type I theories.

photons.

3.2 Analysis of minimal models

The minimal models of Table 3.1 are all free of gauge anomalies except when r is an irreducible (non-trivial) representation of hypercharge, in which case the only anomaly-free choice is Type II. [1] They have fermion representations that are chiral under $G_{DC} \times \mathrm{U}(1)_D \times G_{SM}$ and vectorlike under $G_{DC} \times G_{SM}$. For R complex, representations under $G_{DC} \times \mathrm{U}(1)_D$ are chiral in Type I and II theories, and vectorlike in Type III. The physical domain of the parameter a can be restricted to the interval $[0, 1)$ for Type I and to the

[1] For $a = -1$ Type III theories with hypercharge are also anomaly free, since in this limit they are equivalent to Type II.

interval $[-1, 1)$ for Type II and III. [2] If R is real or pseudoreal, then Type II theories are overall vectorlike and therefore not interesting for our purposes; Type I and III instead become physically equivalent and remain chiral as long as r is complex. Similarly, if r is real or pseudoreal then Type III theories are overall vectorlike and not interesting; Type I and II instead become physically equivalent and remain chiral if R is complex.

The choices for the representations R and r can be restricted by requiring that the dark color group G_{DC} is asymptotically free (as needed to have confinement), and that the SM gauge couplings remain perturbative (with no Landau poles) until the Planck scale. The corresponding conditions are:

$$T(R)\dim(r) < \frac{11}{8} C_2(Adj) \tag{3.1}$$

$$T(r)\dim(R) \leqslant \frac{3}{8}\left(\log\frac{M_{Pl}}{\Lambda_{DC}}\right)^{-1}\left[\frac{2\pi}{\alpha_i(m_Z)} + b_i^{SM}\log\frac{M_{Pl}}{m_Z}\right], \qquad i = 1, 2, 3\,, \tag{3.2}$$

where Λ_{DC} is the dark confinement scale, while $T(\mathcal{R})$, $\dim(\mathcal{R})$ and $C_2(\mathcal{R})$ are respectively the Dynkin index, the dimension and the quadratic Casimir of a representation $\mathcal{R}$. For the dark color gauge group to confine, one needs also to require that the respective number of Weyl flavors (n_f) is below the lower end of the conformal window (n_f^c); this adds the following condition

$$n_f \equiv 4\dim(r) < n_f^c\,. \tag{3.3}$$

Focusing on the case of irreducible representations r, Eqs. (3.1) and (3.2) can be satisfied only if r is a fundamental of one of the SM simple group factors. Furthermore, the only possible dark color representations turn out to be:

- R = fundamental of $\mathrm{SU}(N_{DC})$ for $2 \leqslant N_{DC} \leqslant 6$
- R = fundamental of $\mathrm{SO}(N_{DC})$ for $4 \leqslant N_{DC} \leqslant 6$ ($N_{DC} = 4$ only if $\dim(r) \leqslant 2$)
- R = fundamental of $\mathrm{USp}(4)$ or $\mathrm{USp}(6)$.

In those cases where an estimate of n_f^c is available from lattice simulations, Eq. (3.3) is satisfied and does not impose further restrictions.

In absence of the weak $\mathrm{U}(1)_D \times G_{SM}$ gauging, the pattern of global symmetries of the theories listed above is constrained by the Vafa-Witten theorem, which ensures that the vectorial subgroup is linearly realized [104, 105]. Assuming maximal symmetry breaking [106, 107], one has the following three patterns and corresponding numbers of Nambu-Goldstone bosons (NGBs):

- $\mathrm{SU}(2\dim(r))_L \times \mathrm{SU}(2\dim(r))_R \times \mathrm{U}(1)_V \to \mathrm{SU}(2\dim(r))_V \times \mathrm{U}(1)_V$
  in $\mathrm{SU}(N_{DC} > 2)$ dark color theories with vectorlike representations
  # NGBs $= 4\dim^2(r) - 1$

[2] One can always redefine $a \to 1/a$ by rescaling the $\mathrm{U}(1)_D$ charge and relabeling $\psi_i \leftrightarrow \chi_i$. In Type I theories it is possible to further restrict a to $[0, 1)$ by relabeling $\chi_1 \leftrightarrow \chi_2$.

- $\mathrm{SU}(4\,\dim(r))_R \to \mathrm{SO}(4\,\dim(r))$
  in $\mathrm{SO}(N_{DC})$ dark color theories with real representations
  # NGBs $= (4\,\dim(r)-1)(2\,\dim(r)+1)$

- $\mathrm{SU}(4\,\dim(r))_R \to \mathrm{USp}(4\,\dim(r))$
  in USp(4), USp(6) and SU(2) dark color theories with pseudoreal representations
  # NGBs $= (4\,\dim(r)+1)(2\,\dim(r)-1)$.

The weak gauging reduces this global invariance to a subgroup and determines the vacuum alignment. [3] In Type I theories with R complex there exists no bilinear dark condensate that leaves $\mathrm{U}(1)_D$ unbroken, and (up to a field redefinition) the vacuum aligns in the SM-preserving direction with $\langle\psi_1\chi_1\rangle = \langle\psi_2\chi_2\rangle \neq 0$. In the other theories the vacuum also preserves G_{SM} and has the same orientation, at least for values of the dark coupling e_D smaller than a certain critical value e_D^c. Assuming $e_D < e_D^c$ and focusing on irreducible representations r, the residual global symmetry is

$$\mathrm{U}(1)_{3L} \times \mathrm{U}(1)_{3R} \times \mathrm{U}(1)_V \to \mathrm{U}(1)_{3V} \times \mathrm{U}(1)_V\,, \tag{3.4}$$

where $\mathrm{U}(1)_{3L}$ ($\mathrm{U}(1)_{3R}$) acts on the relative phase between ψ_1 and ψ_2 (χ_1 and χ_2), and the charges under the accidental vectorlike subgroup $\mathrm{U}(1)_{3V} \times \mathrm{U}(1)_V$ are shown in Tab. 3.1. Notice that while $\mathrm{U}(1)_{3V}$ is exact both at the classical and quantum level, the dark baryon number $\mathrm{U}(1)_V$ is anomalous with respect to $\mathrm{U}(1)_D$. The NGB implied by the symmetry breaking in Eq. (3.4) is eaten to make the dark photon massive, and there remain no massless NGBs.

The quantum numbers of all the NGBs under $G_{SM} \times \mathrm{U}(1)_{3V} \times \mathrm{U}(1)_V$ are summarized in Table 3.2. The lightest dark particles charged under $\mathrm{U}(1)_{3V} \times \mathrm{U}(1)_V$ are accidentally stable. In Type I theories with complex R, these are two dark pions (with charge ± 2 under $\mathrm{U}(1)_{3V}$) and the lightest dark baryon (with charge N_{DC} under $\mathrm{U}(1)_V$). The stable dark pions are neutral under the SM and thus potentially good DM candidates. If r is a doublet of $\mathrm{SU}(2)_{EW}$, then the lightest baryon can be SM singlet only for an even number of dark colors. Theories with $N_{DC} = 3, 5$ are thus excluded by the severe constraints that exist on the fraction of DM component with non-vanishing electromagnetic charge (see Sec. 4.3.3 and references therein). If r is a triplet of $\mathrm{SU}(3)_c$, the lightest dark baryon is a SM singlet for $N_{DC} = 3, 6$. Theories with $N_{DC} = 4, 5$ are problematic if not excluded by the current bounds on exotic matter (see Ref. [108]). Type II and III theories, as well as theories with real or pseudoreal dark color representations R, do not seem to lead to any additional realistic model. Indeed, if r is a doublet of $\mathrm{SU}(2)_{EW}$ then: Type II are physically equivalent to Type I; Type I with R (pseudo) real and Type III are vectorlike. If r is a triplet of $\mathrm{SU}(3)_c$, instead, Type I theories with R (pseudo) real, as well as Type II and III ones contain stable colored states that form exotic bound states at QCD confinement; they are therefore very constrained by data and most likely excluded. Finally, a particular example of Type II theories are those where r is an

[3] A thorough analysis of the vacuum alignment in theories with a weak chiral gauging will be reported in a forthcoming work [5].

	R complex				
	Type I	Type II	Type III	$\mathrm{U}(1)_{3V}$	$\mathrm{U}(1)_V$
$\psi_1\chi_1 + \psi_2\chi_2$	Adj	Adj	Adj	0	0
$\psi_1\chi_1 - \psi_2\chi_2$	1+Adj	1+Adj	1+Adj	0	0
$\psi_1\chi_2$	1+Adj	S+A	S+A	+2	0
$\psi_2\chi_1$	1+Adj	$\bar{\mathrm{S}}$+$\bar{\mathrm{A}}$	$\bar{\mathrm{S}}$+$\bar{\mathrm{A}}$	−2	0

	R real	R pseudoreal	$\mathrm{U}(1)_{3V}$	$\mathrm{U}(1)_V$
$\psi_1\psi_1$	S	A	+2	+2
$\psi_1\psi_2$	S	A	0	+2
$\psi_2\psi_2$	S	A	−2	+2
$\chi_1\chi_1$	$\bar{\mathrm{S}}$	$\bar{\mathrm{A}}$	+2	−2
$\chi_1\chi_2$	$\bar{\mathrm{S}}$	$\bar{\mathrm{A}}$	0	−2
$\chi_2\chi_2$	$\bar{\mathrm{S}}$	$\bar{\mathrm{A}}$	−2	−2

Table 3.2: Standard Model quantum numbers of the NGBs in the minimal theories of Table 3.1. We assume that r is a fundamental representation of one of the simple SM factors, and denote the corresponding singlet, adjoint, symmetric and antisymmetric representations respectively with 1, Adj, S and A. If the SM simple factor is $U(1)_Y$, then those NGBs transforming as the adjoint must be removed. Each NGB corresponds to a dark color-singlet fermion bilinear. Theories with R complex have their NGBs listed in the upper panel. The NGBs of theories with R real or pseudoreal are those listed in the Type I column of the upper panel plus those in the lower panel. The last two columns report the quantum numbers under the global $\mathrm{U}(1)_{3V} \times \mathrm{U}(1)_V$.

irreducible representation of hypercharge only. In such theory the accidentally stable pions have both $\mathrm{U}(1)_{3V}$ charge and hypercharge, and as such are not an acceptable DM candidate. The impossibility of gauging hypercharge in theories with irreducible r directly follows from the fact that the only anomaly-free, unbroken subgroup of the dark global invariance is $\mathrm{U}(1)_{3V}$ itself. This means that the accidentally stable NGBs have necessarily non-zero hypercharge.

In light of the above difficulty with hypercharge and in order to build models compatible with Grand Unification of the SM gauge couplings, it is interesting to analyze the case where the representation r is reducible. This possibility is severely constrained by the condition of Eq. (3.2) implied by the request of perturbativity of the SM gauge couplings. In practice, apart from adding SM singlets or doubling the matter content of minimal models, the only possibility is to have r equal to the direct sum of a doublet of $\mathrm{SU}(2)_{EW}$ plus a triplet of $\mathrm{SU}(3)_c$. This choice implies two additional anomaly-free vectorial $U(1)$ subgroups, which are unbroken by the dark condensate and can be chosen to gauge hypercharge. One such choice corresponds to a standard assignment of hypercharges for the weak doublet and color triplet fermions contained in a fundamental

of $\mathrm{SU}(5)_{GUT}$. One can thus consider a GUT chiral model where quantum numbers are assigned as in Type I of Tab. 3.1 with $r = 5$ of $\mathrm{SU}(5)_{GUT}$. Its main difficulty is given by the presence of two very light pseudo NGBs, that are subject to strong phenomenological and cosmological constraints. The existence of potentially massless NGBs is in fact a general issue in chiral gauge theories, where unwanted accidental symmetries cannot be lifted by mass terms or Yukawa couplings. In the theories of Tab. 3.1, if r is made of κ irreducible components, then one has $(2\kappa - 2)$ NGBs that are complete gauge singlets (i.e. neutral under both G_{SM} and $\mathrm{U}(1)_D$). Indeed, $(2\kappa - 2)$ is the number of axial abelian factors that are free from dark color anomalies and remain classically unbroken after turning on the weak gauging. For $\kappa = 2$, as in the case of the GUT model under discussion, one predicts two such NGBs. One of them has $\mathrm{SU}(3)_c$ anomalous interactions and receives a mass from the QCD dynamics, $\delta m_\phi^2 = m_\pi^2 f_\pi^2 / f_\phi^2$. A further contribution to the mass of both NGBs comes from GUT gauge interactions, which explicitly break the two axial $U(1)$ factors. This effect scales naively as $\delta m_\phi^2 \sim (\alpha_{GUT}/4\pi)\Lambda_{DC}^4 / M_{GUT}^2$. For $\Lambda_{DC} \lesssim 10^5\,\mathrm{GeV}$, the QCD contribution dominates, one NGB behaves as the QCD axion and the model is excluded by current constraints. Larger values of Λ_{DC} give the chance of evading the bounds on axions, but are challenging for cosmology, since the abundance of the stable (massive) NGBs is naively too large in presence of a standard cosmological history. While this model is potentially very interesting, assessing its relevance requires a dedicated analysis that we defer to a future work. Finally, we notice that a similar, though different, chiral GUT model was considered in Ref. [109]. There, the quantum number assignments are of Type II (Type III was also mentioned as a possibility), and a dark scalar field is added whose Yukawa couplings give an additional contribution to the NGBs masses. In order to let the dangerous dark pions decay, the authors use higher-dimensional operators assuming a low cutoff scale. As a consequence, the model has no DM candidate.

3.3 The model with $\mathrm{SU}(2)_{EW}$ doublets

The analysis of the previous section suggests that, if one restricts to irreducible representations r, the only chiral theories of Tab. 3.1 with realistic DM candidates are $\mathrm{SU}(N_{DC} > 2)$ Type I models with $\mathrm{SU}(2)_{EW}$ doublets or $\mathrm{SU}(3)_c$ triplets. In the following we will focus on the model with EW doublets and analyze in detail its phenomenology and cosmological history.

At the renormalizable level, the Lagrangian of the model can be written as

$$\mathcal{L} = \mathcal{L}_{SM} + \mathcal{L}_{DS} + \mathcal{L}_{mix}\,, \tag{3.5}$$

where $\mathcal{L}_{DS}$ describes the dark fermions and their minimal couplings, while

$$\mathcal{L}_{mix} = \frac{\varepsilon}{2} B^{\mu\nu} F^D_{\mu\nu} \tag{3.6}$$

is a mixing term between hypercharge and the dark photon. We assume that $\mathrm{SU}(N_{DC})$ confines at a scale Λ_{DC} higher than the electroweak scale, at which all the other inter-

actions are weak. We anticipate that, in order to obtain a viable DM candidate, Λ_{DC} will be of order $1-50\,\text{TeV}$.

The low-energy dynamics of the theory can be characterized in terms of its continuous and discrete global symmetries. Let us first consider the case $0 < a < 1$. In absence of the weak gauging, there is a global $\text{SU}(4)_L \otimes \text{SU}(4)_R \otimes \text{U}(1)_V$ symmetry, spontaneously broken to $\text{SU}(4)_V \otimes \text{U}(1)_V$. After turning on the weak gauging, the dark photon acquires a mass and the residual global symmetry is $\text{U}(1)_{3V} \times \text{U}(1)_V$. The $\text{U}(1)_V$ dark baryon number is actually anomalous with respect to $\text{U}(1)_D$, whereas $\text{U}(1)_{3V}$ is a genuine accidental symmetry. For $a \neq 1$, the model also possesses two approximate discrete symmetries with interesting phenomenological implications:

Dark Charge Conjugation The transformation

$$\mathcal{C}_D : \begin{cases} A_\mu^D \longrightarrow -A_\mu^D \\ \psi_1 \longleftrightarrow \psi_2 \\ \chi_1 \longleftrightarrow \chi_2 \end{cases} , \tag{3.7}$$

dubbed dark charge conjugation in the following, leaves $\mathcal{L}_{DS}$ invariant and is not broken by the dark condensate. It is explicitly violated by the mixing term $\mathcal{L}_{mix}$, as it cannot be extended to the full SM sector. In analogy with QED, one can state a generalized version of Furry's theorem: any Green function of $\mathcal{C}_D$-invariant operators with an odd number of dark photon fields vanishes identically. Two important consequences are:

- The decay of the dark photon to a $\mathcal{C}_D$-even state, such as any combination of SM particles, is forbidden for $\varepsilon = 0$. This implies that the dark photon is stable if its decays to dark sector particles are kinematically forbidden.
- For $\varepsilon = 0$, the mixing term between hypercharge and the dark photon is not radiatively generated. Hence, ε receives quantum corrections proportional to itself. A small or vanishing ε, depending on the UV dynamics, is therefore technically natural.

G-parity. In analogy with QCD, a generalized G-parity transformation acting only on dark sector fields can be defined as [110]:

$$\mathcal{G}_2 : \begin{cases} \psi \longrightarrow e^{i\pi T_2} \mathcal{C} \psi \\ G_\mu^a \lambda_a \longrightarrow -G_\mu^a \lambda_a^* \end{cases} , \tag{3.8}$$

where T_2 and λ^a are respectively $\text{SU}(2)_{EW}$ and $\text{SU}(N_{DC})$ generators, G_μ^b is the dark gluon field, and $\psi_i \leftrightarrow \chi_i$ under the charge conjugation $\mathcal{C}$. For $a \neq 1$, $\mathcal{G}_2$ is an exact symmetry in the absence of $\text{U}(1)_D$ gauge interactions. Under the combined action of $\mathcal{C}_D$ and $\mathcal{G}_2$, all the NGBs have a definite parity, and this will be useful to analyze their properties.

Accidental stability and higher-dimensional operators

The accidental $\mathrm{U}(1)_{3V}$ symmetry is an exact invariance at the renormalizable level. In order to estimate the lifetime of the lightest dark states with non-vanishing $\mathrm{U}(1)_{3V}$ charge, it is important to identify the lowest-dimensional operators that violate this symmetry. A simple analysis reveals that, for any given dimension, $\mathrm{U}(1)_{3V}$-violating operators can be built only for a discrete set of rational values of the parameter a. In particular, we find that:

- For $D = 5$, no $\mathrm{U}(1)_{3V}$-violating operator exists, for any value of a.
- For $D = 6$, the only possibility is $a = 0$. The operators are of the form:

$$\psi_1\psi_2\chi_i\chi_i \quad \text{or} \quad \chi_i\chi_i\chi_i\chi_j \ (\text{for } N_{DC} = 4) \qquad \forall\, i,j = 1,2\,. \tag{3.9}$$

- For $D = 7$, it is possible to build $\mathrm{U}(1)_{3V}$-violating operators only for $a = \pm 3$ and $a = \pm 1/3$. For example one has ($\forall\, j = 1,2$):

$$\begin{aligned} &\psi_1^\dagger i\bar{\not\partial}\psi_2\psi_2\chi_j \quad \text{and} \quad \psi_2^\dagger i\bar{\not\partial}\psi_1\psi_1\chi_j \qquad \text{for } a = \pm 3\,, \\ &\chi_1^\dagger i\bar{\not\partial}\chi_2\chi_2\psi_j \quad \text{and} \quad \chi_2^\dagger i\bar{\not\partial}\chi_1\chi_1\psi_j \qquad \text{for } a = \pm\frac{1}{3}\,. \end{aligned} \tag{3.10}$$

This shows that the accidental stability of the lightest NGBs charged under $\mathrm{U}(1)_{3V}$ is a robust prediction of our chiral theory, as $\mathrm{U}(1)_{3V}$-violating operators can have naturally very high dimension. This has to be compared with vectorlike theories, where accidental symmetries acting on NGBs are typically violated at the $D = 5$ level [22]. A similar analysis shows that in our theory $\mathrm{U}(1)_V$-violating operators first appear at the $D = 6$ level for $N_{DC} = 4$; in this case they have the form $\psi_i\psi_j\psi_k\psi_l$ or $\chi_i\chi_j\chi_k\chi_l$ ($\forall\, i,j,k,l = 1,2$).

The case a = 0

In the limit $a = 0$ the theory possesses an enhanced global symmetry at the renormalizable level that is left unbroken by the weak gauging:

$$\mathrm{U}(1)_{3L} \times \mathrm{SU}(2)_R \times \mathrm{U}(1)_V \to \mathrm{U}(1)_{3V} \times \mathrm{U}(1)_V\,, \tag{3.11}$$

where $\mathrm{SU}(2)_R$ acts on the χ fields. This pattern of symmetry breaking gives three exact NGBs: one of them is eaten by the dark photon, the other two are the SM-singlet NGBs, which become massless for $a \to 0$. They can acquire a mass only through $\mathrm{SU}(2)_R$-breaking operators. The first such operators appear at the $D = 6$ level, for example of the form $\psi_1\psi_2\chi_i\chi_j$. The corresponding NGB mass squared is of order

$$m^2 \sim \frac{\bar{g}^2}{16\pi^2}\frac{\Lambda_{DC}^4}{\Lambda_{UV}^2}\,, \tag{3.12}$$

where $\bar{g}^2/\Lambda_{UV}^2$ is the coefficient of the $D = 6$ operator. For $\Lambda_{UV}/\bar{g} \gtrsim 10^{16}\,\text{GeV}$ and $\Lambda_{DC} \sim 1-50\,\text{TeV}$, this implies a very light and long-lived pair of NGBs. Such light degrees of freedom are relativistic at the epoch of neutrino decoupling, and can give a sizable contribution to the number of additional relativistic species ΔN_{eff}. The relevance of this scenario will be discussed in Sec. 3.5.5.

3.4 Phenomenological profile

In this section we sketch the phenomenological profile of the model with $\text{SU}(2)_{EW}$ doublets, discussing its spectrum and the dynamics of its NGBs.

3.4.1 Dark Baryons

The spectrum of dark hadrons contains baryonic states, made of the antisymmetric product of N_{DC} dark quarks, with mass of order Λ_{DC}. They have $\text{U}(1)_V$ baryon number N_{DC} and the lightest among them are accidentally stable. They are organized in multiplets of the SU(4) flavour group. Due to Fermi statistics, their wave function is completely symmetric under the combined action of flavour and spin symmetries.

For $N_{DC} = 3$ the lightest baryons have spin 1/2 and flavour structure $\square\!\square$, corresponding to a 20 of the global SU(4), which decomposes into $2_{\pm 3} \oplus 2 \times 2_{\pm 1} \oplus 4_{\pm 1}$ of $\text{SU}(2)_{EW} \times \text{U}(1)_{3V}$. Since this contains no SM singlet, the lightest, accidentally stable baryons will have non-vanishing electromagnetic charge. As discussed in Sec. 3.5.1, their relic density is never small enough to satisfy the stringent constraints on the charged fraction of DM, and the model is thus excluded. Similar conclusions hold for any odd number of dark colors, in particular $N_{DC} = 5$.

For $N_{DC} = 4$ the lightest baryons have spin 0 and flavour structure $\begin{smallmatrix}\square\square\\\square\square\end{smallmatrix}$, corresponding to a $20'$ of the global SU(4), which decomposes into $1_{\pm 4} \oplus 1_{\pm 2} \oplus 2 \times 1_0 \oplus 3_{\pm 2} \oplus 3_0 \oplus 5_0$ of $\text{SU}(2)_{EW} \times \text{U}(1)_{3V}$. The SM singlet components neutral under $\text{U}(1)_{3V}$ are expected to be the lightest, accidentally stable baryons. They contribute a small fraction of the DM abundance and are electromagnetically neutral. Similar conclusions hold for any even number of dark colors. Taking into account the constraints from Landau poles, we conclude that models with $N_{DC} = 4, 6$ are viable and we will focus on them in the following.

3.4.2 Dark Pions and low-energy effective theory

At energies much lower than Λ_{DC}, the dynamics of the lightest states in the spectrum can be characterized by making use of Chiral Perturbation Theory (ChPT). The pattern of spontaneous symmetry breaking implies the existence of 15 pseudo NGBs in the adjoint of SU(4), one of which eaten by the dark photon. These can be classified according to the transformation properties of the associated fermionic currents:

- Two $\text{SU}(2)_{EW}$ triplets charged under $\text{U}(1)_D$, the $\mathbf{3}_\pm$.

	$\mathrm{SU}(2)_{EW}$	$\mathrm{U}(1)_V$	$\mathcal{C}_D$	$\mathcal{C}_D \cdot \mathcal{G}_2$
$3_\pm$	3	± 2	$3_\mp$	$-$
$3'_0$	3	0	$-$	$+$
3_0	3	0	$+$	$-$
$1_\pm$	1	± 2	$1_\mp$	$+$
γ_D	1	0	$-$	$\times$

Table 3.3: Transformation properties of the NGBs and of the dark photon under the symmetries of the model.

- Two $\mathrm{SU}(2)_{EW}$ triplets neutral under $\mathrm{U}(1)_D$, the $\mathbf{3_0}$ and the $\mathbf{3'_0}$, with dark conjugation charge equal to $+1$ and -1, respectively.
- Two SM singlets, the $\mathbf{1}_\pm$. These are the lightest particles charged under $\mathrm{U}(1)_V$, and will constitute our primary DM candidate.
- A global singlet, the $\mathbf{1_0}$, that is eaten to form the longitudinal polarization of the dark photon. With an appropriate choice of the gauge fixing, this can be removed from the spectrum.

A summary of the transformation properties of these particles under the relevant global and gauge symmetries is provided in Tab. 3.3.

We construct the effective chiral Lagrangian by adopting a standard non-linear representation for the NGB fields

$$\Sigma(x) = \exp\left(\frac{2i\pi^a(x)T^a}{f}\right), \tag{3.13}$$

and write the covariant derivative as

$$D_\mu\Sigma = \partial_\mu\Sigma - \frac{igW^a_\mu}{2}\left(T^a_{EW}\Sigma - \Sigma T^a_{EW}\right) - ie_D A^D_\mu\left(T_D\Sigma - a\Sigma T_D\right), \tag{3.14}$$

where $\mathrm{SU}(4)$ generators are normalized to $\mathrm{Tr}(T^aT^b) = \delta^{ab}/2$ and

$$T^a_{EW} = \begin{bmatrix}\sigma_a & 0\\ 0 & \sigma_a\end{bmatrix}, \qquad T_D = \begin{bmatrix}\mathbb{1} & 0\\ 0 & -\mathbb{1}\end{bmatrix}. \tag{3.15}$$

At lowest order in the derivative expansion there is only the NGB kinetic term

$$\mathcal{L}_0 = \frac{f^2}{4}\,\mathrm{Tr}\left[D_\mu\Sigma D^\mu\Sigma^\dagger\right], \tag{3.16}$$

together with the NGB potential generated by 1-loop radiative effects (see Sec. 3.4.4). The kinetic term, in particular, contains the lowest-order interactions of $3_\pm$ and $1_\pm$ with the dark photon (the other NGBs do not interact at this order with γ_D):

$$\mathcal{L}_0 \supset -ie_D(1+a)A^D_\mu(\pi_-\partial_\mu\pi_+ - \pi_+\partial_\mu\pi_-) + 4ae_D^2A^D_\mu A^D_\mu\pi_+\pi_-. \tag{3.17}$$

While the cubic term is that of scalar QED with charge $(1+a)$, the quartic term has a modified (unless $a=1$) coefficient. This comes as a consequence of the spontaneous breaking of $\mathrm{U}(1)_D$, and leads to a non-trivial dependence on a of the cross section for the process $1_+1_- \to \gamma_D\gamma_D$, which sets the DM abundance in our model. Another feature of $\mathcal{L}_0$ due to the chiral gauging is the appearance of vertices with three NGBs and one dark photon. They are proportional to $(1-a)$ and thus vanish in the vectorlike limit $a=1$. Their analog with the photon in the QCD chiral Lagrangian is forbidden by parity. Their expressions are reported in Appendix 3.A.

At $\mathcal{O}(p^4)$, the chiral Lagrangian reads

$$\begin{aligned}\mathcal{L}_1 =& C_1\ \mathrm{Tr}\big[D_\mu\Sigma D^\mu\Sigma^\dagger\big]\,\mathrm{Tr}\big[D_\nu\Sigma D^\nu\Sigma^\dagger\big] + C_2\ \mathrm{Tr}\big[D_\mu\Sigma D_\nu\Sigma^\dagger\big]\,\mathrm{Tr}\big[D^\mu\Sigma D^\nu\Sigma^\dagger\big] \\ &+ C_3\ \mathrm{Tr}\big[D_\mu\Sigma D_\mu\Sigma^\dagger D^\nu\Sigma D^\nu\Sigma^\dagger\big] + C_4\ \mathrm{Tr}\big[D_\mu\Sigma D_\nu\Sigma^\dagger D^\mu\Sigma D^\nu\Sigma^\dagger\big] \\ &+ C_5\ \mathrm{Tr}\big[W^L_{\mu\nu}D^\mu\Sigma D^\nu\Sigma^\dagger + W^R_{\mu\nu}D^\mu\Sigma^\dagger D^\nu\Sigma\big] + C_6\ \mathrm{Tr}\big[W^L_{\mu\nu}\Sigma W_R^{\mu\nu}\Sigma^\dagger\big]\,,\end{aligned} \tag{3.18}$$

where

$$\begin{aligned}W^L_{\mu\nu} &= T^a_{EW}W^a_{\mu\nu} + T_D F^D_{\mu\nu} \\ W^R_{\mu\nu} &= T^a_{EW}W^a_{\mu\nu} + a\,T_D F^D_{\mu\nu}\,.\end{aligned} \tag{3.19}$$

The size of the chiral coefficients is estimated to be $C_i \sim 1/(16\pi^2)$ from Naive Dimensional Analysis (NDA). [4] Working at $\mathcal{O}(p^4)$ one also has to include the Wess-Zumino-Witten term, which encodes the effects of anomalies. By explicit calculation, all squared anomalies (both $\mathrm{U}(1)_D^2$ and $\mathrm{SU}(2)_{EW}^2$ ones) turn out to vanish, while mixed ones under $\mathrm{SU}(2)_{EW}\times\mathrm{U}(1)_D$ do not. In particular, the axial current that interpolates the $3_0'$ has an anomaly

$$\langle 0|\,\partial^\mu J_\mu^{(3_0')i}\,|0\rangle = -\frac{g e_D(1+a)}{16\sqrt{2}\pi^2}\varepsilon^{\mu\nu\rho\sigma}W^i_{\mu\nu}F^D_{\rho\sigma}\,, \tag{3.20}$$

which can mediate the decay $3_0' \to W\gamma_D$ as discussed below.

3.4.3 Decay channels

As discussed in the previous section, the $1_\pm$ are accidentally stable at the renormalizable level and their decay is induced only by higher-dimensional operators. The other NGBs and the dark photon instead can decay through the following channels:

- **Dark Photon:** γ_D

  The dark photon lifetime is suppressed by a factor ε^2, as $\mathcal{C}_D$ makes γ_D stable in absence of the mixing term (3.6). As shown in the next section, this can have striking implications on the cosmological history of the model, leading to dark matter dilution if ε is small enough. The dominant decay channel is into SM

[4] The form of the last two terms in Eq. (3.18) is schematic, since terms with different physical field strengths will have different coefficients. Also, the appropriate powers of the couplings have been omitted in the NDA estimate of the chiral coefficients for simplicity.

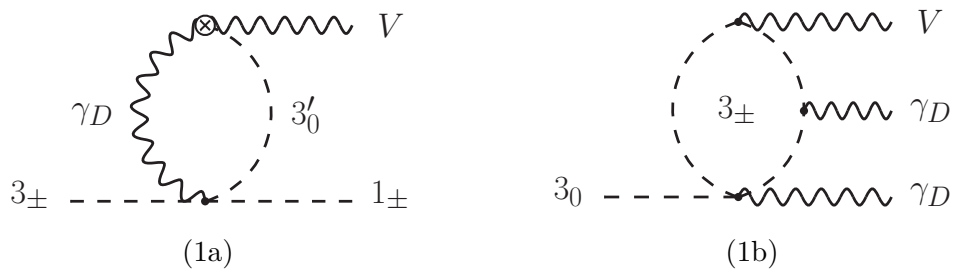

Figure 3.1: On the left (1a): Feynman diagram for the decay $3_\pm \to 1_\pm V$. The crossed vertex denotes the anomalous interaction. On the right (1b): One of the Feynman diagrams mediating the decay $3_0 \to \gamma_D \gamma_D V$.

fermions, $f\bar{f}$, but Zh and W^+W^- are also relevant if kinematically allowed. A detailed expression of the rate is given in Appendix 3.D, and has the form

$$\Gamma = C(m_i, g_i)\, \varepsilon^2 \alpha_D m_{\gamma_D}, \tag{3.21}$$

where $C(m_i, g_i)$ is an $\mathcal{O}(1)$ factor, accounting for the multiplicity of the final states, whose details depend on the masses and couplings.

- **Charged Triplets:** $3_\pm$

  Due to $\mathrm{U}(1)_{3V}$ invariance, the $3_\pm$ decays to final states that contain at least one $1_\pm$. The main channels are [5]

$$3_\pm \longrightarrow 1_\pm V \qquad \text{and} \qquad 3_\pm \longrightarrow 1_\pm \gamma_D \gamma_D V \qquad (V = W, Z, \gamma)\,. \tag{3.22}$$

  The first one is forbidden if $\mathcal{G}_2 \cdot \mathcal{C}_D$ is unbroken (see Tab. 3.3) and thus occurs only through a loop of dark photons with the anomalous $3_0' W \gamma_D$ vertex, see Fig. 3.1a. The second occurs through a tree-level diagram also featuring one anomalous vertex. The estimated rate is the same for both channels:

$$\Gamma \sim \frac{\alpha_W \alpha_D^2}{(16\pi^2)^3} (1-a^2)^2 \frac{m_{3_\pm}^5}{f^4}\,. \tag{3.23}$$

  Numerically, this implies

$$c\tau \sim 6.6 \left(\frac{500\,\mathrm{GeV}}{m_{3_\pm}}\right) \left(\frac{2\cdot 10^{-3}}{\alpha_D}\right)^2 \times 10^{-3}\,\mathrm{cm}\,, \tag{3.24}$$

  which does not give rise to displaced vertices at high-energy colliders for any value of e_D allowed by cosmology.

[5] The decay $3_\pm \to 1_\pm \gamma_D V$ is also allowed but its width is parametrically smaller than that of the other channels.

- **Neutral Triplet:** $3_0'$

  The decay modes of $3_0'$ are restricted by $\mathrm{SU}(2)_{EW}$ and $\mathcal{C}_D$ invariance. If kinematically allowed, the main channel is

  $$3_0' \longrightarrow V\ \gamma_D. \tag{3.25}$$

  This process proceeds through the anomaly and its rate is [6]

  $$\Gamma = \frac{\alpha_D \alpha_W N_c^2 (1+a)^2}{8\pi^3} \frac{m_3^3}{f^2}\, g\left(\frac{m_W^2}{m_3^2}, \frac{m_{\gamma_D}^2}{m_3^2}\right), \tag{3.26}$$

  where

  $$g(x,y) = \left[(1-x-y)^2 - xy\right]\sqrt{1-2(x+y)+(x-y)^2}\,. \tag{3.27}$$

  For small m_3 this channel is kinematically forbidden and $3_0'$ decays to $V\,\bar{f}f$ through the $\mathcal{C}_D$-violating mixing term (3.6). The decay rate receives a suppression of order $\varepsilon^2(\alpha_D/4\pi)$ with respect to Eq. (3.26), and the $3_0'$ can become long-lived on collider scales. In the limit of ε small, decays between different electroweak components also become important, though suppressed by phase space. For $\varepsilon \lesssim 3\times 10^{-6}\,(2m_3/m_1)^{3/2}\,(1\,\mathrm{TeV}/m_1)^{1/2}$, the electromagnetically-charged components $3_0'^{\pm}$ mostly decay into the neutral component $3_0'^0$ by emitting a soft pion: $3_0'^{\pm} \to 3_0'^0\pi^{\pm}$. The decay width for this de-excitation process is [14]:

  $$\Gamma_{\mathrm{EW}} \simeq \frac{2}{\pi} G_{\mathrm{F}}^2\, V_{ud}^2\, \Delta m^3\, f^2 \sqrt{1-\frac{m_\pi^2}{\Delta m^2}}, \tag{3.28}$$

  where $\Delta m \simeq 166\,\mathrm{MeV}$ is the mass splitting between the charged and neutral components (see Eq. (3.37)).

- **Neutral Triplet:** 3_0

  Invariance under $\mathrm{SU}(2)_{EW}$ and $\mathcal{C}_D$ also restricts the decays of 3_0. The main channel is

  $$3_0 \longrightarrow \gamma_D\gamma_D V\,, \tag{3.29}$$

  which proceeds through 1-loop diagrams with $\mathcal{O}(p^2)$ interactions, see Fig. 3.1b. Its amplitude is finite, consistently with the absence of a counterterm in the $\mathcal{O}(p^4)$ Lagrangian (3.18). The NDA estimate of the decay rate is therefore

  $$\Gamma \sim \frac{\alpha_D^2 \alpha_W (1-a)^2}{(16\pi^2)^2} \frac{m_3^3}{f^2}\,. \tag{3.30}$$

  When this channel is forbidden by kinematics, the two dark photons can be closed to form a loop and the V becomes virtual, so that the decay is to a SM pair ($f\bar{f}$, VV or Vh). The estimated width in this case is

  $$\Gamma \sim \frac{\alpha_D^2 \alpha_W^2}{(4\pi)^5} \frac{m_3^3}{f^2}. \tag{3.31}$$

[6] Here and in the following, m_3 denotes the mass of 3_0, which is equal to the mass of $3_0'$ at the 1-loop level.

For the benchmark point $m_1 = 2m_{\gamma_D}$, this translates numerically into

$$c\tau \sim 6.5 \left(\frac{500\,\text{GeV}}{m_3}\right)\left(\frac{2\cdot 10^{-3}}{\alpha_D}\right)^2 \times 10^{-5}\,\text{cm}\,, \tag{3.32}$$

implying that the decay can be still considered as "prompt" on collider scales.

3.4.4 Spectrum

When the weak $\mathrm{SU}(2)_{EW} \times \mathrm{U}(1)_D$ gauging is switched on, 1-loop radiative effects generate a potential, hence a mass term, for the NGBs. It is a peculiar feature of our model that all the states receive mass from the weak gauging (unless $a = 0$). Using the Weinberg sum rules and saturating them with the lowest-lying spin-1 resonances, the effective potential can be computed at leading order in $1/N_{DC}$ using a standard approach, see for example [111]. We find the mass terms

$$m_1^2 = 24\ln(2)a\frac{e_D^2}{16\pi^2}m_\rho^2 \tag{3.33}$$

$$m_3^2 = 12\ln(2)\frac{g^2}{16\pi^2}m_\rho^2 \tag{3.34}$$

$$m_{3^\pm}^2 = \left(24\ln(2)\frac{e_D^2}{16\pi^2} + 12\ln(2)\frac{g^2}{16\pi^2}\right)m_\rho^2\,, \tag{3.35}$$

where $m_\rho \simeq 4\pi f/\sqrt{N_{DC}}$ is the mass of the first vector resonance. For $a = 1$ Eq. (3.33) agrees with the charged-neutral pion mass difference in QCD, taking into account that the dark pions have $\mathrm{U}(1)_D$ charge $2e_D$ in this limit. [7] As regards the dark photon, inserting $\Sigma = \mathbb{1}$ in (3.16) yields

$$m_{\gamma_D}^2 = 2e_D^2(1-a)^2f^2 \sim \frac{N_{DC}}{8\pi^2}e_D^2(1-a)^2m_\rho^2\,. \tag{3.36}$$

At sub-leading order, the degeneracy between the electromagnetically charged and neutral components of the triplets is lifted by electroweak and custodial symmetry breaking. While the mass squared of the triplets are of $\mathcal{O}(g^2)$, the mass splitting arises at $\mathcal{O}(g^4)$. One should therefore take into account the NGB wavefunction renormalization, which also contributes at $\mathcal{O}(g^4)$ to the physical mass. Computing the NGB effective potential is thus not enough to fully capture the mass splitting. On the other hand, the loop integral relevant for the mass splitting is finite and converges at around the electroweak scale, i.e. much earlier than the onset of the dark strong dynamics. The same calculation valid for elementary scalars is therefore valid also in our case and gives [14]:

$$\Delta m|_{EW} = \frac{g}{4\pi}m_W\sin^2\frac{\theta_W}{2} = 166 \pm 1\,\text{MeV}\,. \tag{3.37}$$

[7] Notice however that there is a factor of 4 discrepancy with the result of Refs. [47, 48].

3.5 Cosmology

Depending on its spectrum, the model can undergo different thermal histories. In this section we will describe the cosmological evolution and compute the DM abundance predicted in the bulk of the theoretical parameter space, and then comment how the physics is modified in special limits of the parameters.

In this spirit we will first discuss the case where:

- The dark photon is lighter than the SM-singlet dark pions ($m_{\gamma_D} < m_1$) but has a mass larger than their freeze-out temperature ($m_{\gamma_D} > T_{\text{f.o}} \sim m_1/20$). This can be expressed as a condition on the parameter a, implying $0.26 \lesssim a \lesssim 0.93$ for $N_{DC} = 4$;
- Both $3_\pm$ and $3_0, 3_0'$ are heavier than $1_\pm$, and the mass splitting $\Delta m = m_3 - m_1$ is larger than the temperature relevant for the freeze-out of the singlets, *i.e.* $\Delta m \gtrsim m_1$. This condition corresponds to a dark coupling of order $\alpha_D \lesssim \alpha_2/4a$;
- The dark coupling α_D is sufficiently large that the singlets annihilate efficiently in dark photons at temperatures of order $T \sim m_1$, and triplets decay promptly to lighter states. This condition requires a dark coupling

$$\alpha_D \gtrsim 10^{-9} \frac{1}{(1+a)^2} \left(\frac{m_1}{\text{TeV}}\right)^{\frac{1}{2}}. \tag{3.38}$$

The decay width of the dark photon is controlled by an additional independent parameter: the ε coefficient. We shall first discuss the case in which the dark photon decays promptly at temperatures relevant for the computation of the dark matter relic density, $T \sim m_1$. This corresponds to requiring $\Gamma_{\gamma_D} > H(T = m_1)$, which can be expressed as a condition on ε:

$$\varepsilon \gtrsim 10^{-7} \left(\frac{a}{N_{DC}(1-a)^2}\right)^{\frac{1}{4}} \left(\frac{m_1}{\text{TeV}}\right)^{\frac{1}{2}}. \tag{3.39}$$

We will then consider the case where the dark photon decays after the freeze-out of dark matter but before Big Bang Nucleosynthesis (BBN), and study the possible entropy injection that it gives into the SM bath with the subsequent dilution of the DM relic abundance. Finally, we will comment on the case of cosmologically stable dark photons as a possible dark matter candidate. In the latter scenario, requiring the dark photon lifetime to be larger than 10^{25} s implies

$$\varepsilon \lesssim 10^{-24} \left(\frac{\text{GeV}}{m_{\gamma_D}}\right)^{\frac{1}{2}}. \tag{3.40}$$

3.5.1 Dark baryons

Dark baryons are produced at the confinement temperature and are accidentally stable. They are thus expected to be a dark matter component. Their relic abundance is set

by the freeze out of the process of annihilation into dark pions and other mesons. Since their mass is parametrically larger than the mass of the NGBs, baryons freeze out at temperatures where dark pions are still in chemical equilibrium with the SM thermal bath; therefore, assuming thermalization of the decay products, the computation of the dark pion relic abundance is unaffected by the baryons.

The baryon-antibaryon annihilation cross section is difficult to compute from first principles, but can be estimated as

$$\sigma_{B\bar{B}\to\text{mesons}} v = c\,\frac{4\pi}{m_\rho^2}\,, \tag{3.41}$$

where c is an $\mathcal{O}(1)$ proportionality factor. This estimate can be checked in the case of QCD by making use of nuclear physics data [112]. For anti-neutrons annihilating on a proton target, the data display the expected $1/v$ dependence and are well reproduced for $c \simeq 3$. Using Eq. (3.41) with $c = 3$ and comparing with the pion annihilation cross section (3.44), one finds that the energy density of dark baryons relative to dark pions is suppressed by a factor

$$\frac{\Omega_{DB}}{\Omega_{D\pi}} \simeq \frac{\langle\sigma_{\pi\pi\to\gamma_D\gamma_D} v\rangle}{\langle\sigma_{B\bar{B}\to\text{mesons}} v\rangle} \sim \frac{1}{3}\frac{e_D^2(1+a)^4}{24\ln(2)a}\,. \tag{3.42}$$

Therefore, the dark matter is expected to have two components, with dark pions giving the dominant contribution in the majority of the parameter space. For example, for $a = 1/2$ and $\alpha_D \leqslant 0.04$, the DM fraction made of dark baryons is of order 10% or smaller. Finally, requiring that dark baryons do not overclose the Universe sets an upper bound on the confinement scale $\Lambda_{DC} \lesssim 100\,\text{TeV}$, and correspondingly on the mass of the scalar triplets $m_3 \lesssim 10\,\text{TeV}$.

3.5.2 Short-lived dark photons

Let us first focus on the case in which dark photon decays are efficient at temperatures relevant for the computation of the relic abundance, i.e. when $\varepsilon \gtrsim 10^{-7}$.

For these values of the mixing parameter, the dark and visible sectors are in thermal and chemical equilibrium at temperatures larger than the pion mass scale, thanks to processes mediated by dark photons. As the Universe cools down, pions become non relativistic. If the splitting between EW triplet and singlet pions is larger than the temperatures relevant for the freeze out (as in the parameter space region under consideration), then the abundance of triplets is suppressed by an exponential Boltzmann factor and the dynamics can be described by considering singlets and dark photons only. [8]

The relevant process for the calculation of the DM relic abundance is the annihilation of dark pions, dominated by the dark photon channel $1_+1_- \to \gamma_D\gamma_D$. For dark photon

[8] If this is not the case, i.e. for $\alpha_D \gtrsim \alpha_2/4a$, then processes such as $1_+1_- \to 3_+3_-$ can give a non zero population of triplets. A complete analysis, in such a scenario, would require a careful study of the system of coupled Boltzmann equations for singlets and triplets.

prompt decays, the process is described by a standard Boltzmann equation for a single DM species ($Y_\pi = (n_{\pi_+} + n_{\pi_-})/s$, $x = m_1/T$):

$$\frac{\mathrm{d}Y_\pi}{\mathrm{d}x} = -\frac{1}{2x^2}\frac{s(m_1)}{H(m_1)}\langle\sigma_{\pi\pi\to\gamma_D\gamma_D}v\rangle\left(Y_\pi^2 - Y_{\pi,eq}^2\right) . \tag{3.43}$$

In the case of light dark photons, the thermally-averaged annihilation cross section is [9]

$$\langle\sigma_{\pi\pi\to\gamma_D\gamma_D}v\rangle = \frac{1}{8\pi}\frac{e_D^4(1+a)^4}{m_1^2}f(y) + \mathcal{O}(v^2), \qquad y = \frac{m_{\gamma_D}^2}{m_1^2}, \tag{3.44}$$

with

$$f(y) = \sqrt{1-y}\left[\frac{y^2}{(y-2)^2} + \frac{(y-2)^2}{y^2}(K-1)^2 + 2K^2 + 2K - 2\right], \quad K = \frac{4a}{(1+a)^2}. \tag{3.45}$$

The limit of scalar QED is recovered by first setting $K = 1$ in Eq. (3.45), and then letting $y \to 0$ to obtain a massless dark photon. [10] In the regime of light dark photons, the Sommerfeld enhancement factor can be important, especially at the low values of the velocity relevant for indirect detection and CMB constraints. However, for $0.26 \lesssim a \lesssim 0.93$ the dark photon and the dark matter have comparable masses and the Sommerfeld enhancement is negligible.

3.5.3 Long-lived dark photons

The cosmological history can evolve differently if the dark photon is metastable, i.e. has a lifetime longer than the inverse Hubble rate at $T \sim m_1$ and decays before the present era. According to Eq. (3.39), this happens for $10^{-24} \lesssim \varepsilon \lesssim 10^{-8}$.

In this case, the following effects can take place and change the DM abundance:

- The SM and dark sectors could become thermally decoupled at temperatures larger than the freeze-out temperature of the pions. The computation of the relic abundance of DM can be modified, especially if number-changing interactions in the dark sector are efficient.
- If dark photon annihilations into SM particles are out of equilibrium, then the evolution of the dark pion density with temperature is modified with respect to the standard freeze-out scenario, as previously noted in Ref. [76]. The abundance of dark photons can also be affected in this case.

[9] This formula differs from the corresponding result in Eq. (8) of Ref. [48].

[10] If one takes the limit $a \to 1$ by varying K and y together through their functional dependence on a, one finds a cross section different from that of scalar QED. This is because in this limit the contribution from the dark photon longitudinal polarization does not decouple. By virtue of the Goldstone Boson Equivalence Theorem (since the mass of the dark photon goes to zero for $a \to 1$), the latter can be computed in terms of the annihilation into 1_0's, which are part of the physical spectrum for $a = 1$. Once added to the contribution from the transverse dark photon polarizations, this result correctly reproduces the $a = 1$ limit of Eq. (3.44). Notice that computing correctly the annihilation cross section into 1_0's requires to include the contributions from both the four-pion derivative interactions from the Chiral Lagrangian and the radiatively-generated quartic potential.

- If sufficiently long-lived, dark photons can give rise to an early phase of matter domination. Their subsequent decay and entropy injection into the SM thermal bath suppress the abundance of DM relics.

We discuss each of these effects in the following.

Kinetic equilibrium

The SM and dark sectors are kept in thermal equilibrium by interactions involving the dark photon-hypercharge mixing or mediated by loops of NGB triplets.

After diagonalising the kinetic mixing of Eq. (3.6), one finds that electromagnetically-charged particles also have a coupling, of order εe, to the dark photon. The leading process controlling the kinetic equilibrium between dark and SM sectors is thus the elastic scattering, mediated by the dark photon, of a charged pion on SM particles. Its cross section is of order

$$\sigma \sim 2\pi\varepsilon^2 \frac{\alpha_{\rm em}\alpha_D}{T^2} \,. \tag{3.46}$$

Comparing the rate of this process with the Hubble rate, we see that for $\varepsilon \lesssim 10^{-7}$ it becomes inefficient at a temperature of order m_1, in the region relevant for the relic abundance computation.

When dark photon interactions become inefficient, those mediated by a loop of pion triplets between pion singlets and EW gauge bosons can still be effective in maintaining thermal equilibrium. The low-energy theory obtained by integrating out the triplets contains two operators that can give the leading contribution, depending on the value of the coupling e_D. The first has dimension 8 and involves two derivatives of the pions, the second has dimension 6 and breaks the NGB shift symmetry. Their coefficients are estimated to be:

$$\begin{aligned} \mathcal{O}_8 &\sim \frac{1}{f^2}\frac{1}{m_3^2}\frac{g_2^2}{16\pi^2}\,(\partial\pi)^2\left(W^i_{\mu\nu}\right)^2 \\ \mathcal{O}_6 &\sim \frac{m_\rho^2}{16\pi^2 f^2}\frac{1}{m_3^2}\frac{e_D^2 g_2^2}{16\pi^2}\,(\pi)^2\left(W^i_{\mu\nu}\right)^2 \,, \end{aligned} \tag{3.47}$$

where $m_\rho^2/(16\pi^2 f^2) \sim 1/N_{DC}$ in the large N_{DC} limit.

We find that these interactions are efficient in maintaining kinetic equilibrium during the pion freeze out in the majority of the relevant parameter space. There is only a small corner, corresponding to triplets with masses in the range $(500 - 1500)\,\text{GeV}$, where the kinetic decoupling occurs at a temperature of order $T_{kd} \sim (1 - 0.1)m_1$. In the following we will compute the DM abundance assuming that the temperature in the dark sector scales as the temperature in the visible sector. We thus neglect possible additional effects related to the kinetic decoupling in the region with $m_3 \lesssim 1500\,\text{GeV}$. While these effects can play a role during the freeze-out epoch, they are not expected to give qualitative changes in the dilution factor computed in Sec. 3.5.3.

Chemical equilibrium

At temperatures of order m_1 or smaller, the evolution of the dark sector is described by a system of two coupled Boltzmann equations for the two species $\pi_\pm$ and γ_D. As explained in more details in Appendix 3.C, for metastable dark photons and at temperatures higher than $T_{\rm decay}$ (where the latter is defined by the condition $\Gamma_{\gamma_D} \sim H(T_{\rm decay})$), these equations can be approximately written as

$$\begin{aligned}\frac{\mathrm{d}Y_\pi}{\mathrm{d}x} &= -\frac{1}{2x^2}\frac{s(m_1)}{H(m_1)}\langle\sigma_{\pi\pi\to\gamma_D\gamma_D}v\rangle\left(Y_\pi^2 - \frac{Y_{\pi,eq}^2}{Y_{\gamma_D,eq}^2}Y_{\gamma_D}^2\right)\,,\\ \frac{\mathrm{d}Y_{\gamma_D}}{\mathrm{d}x} &= \frac{1}{x^2}\frac{s(m_1)}{H(m_1)}\left[\frac{1}{2}\langle\sigma_{\pi\pi\to\gamma_D\gamma_D}v\rangle\left(Y_\pi^2 - \frac{Y_{\pi,eq}^2}{Y_{\gamma_D,eq}^2}Y_{\gamma_D}^2\right)\right.\\ &\qquad\left. - 2\langle\sigma_{\gamma_D\gamma_D\to SM}v\rangle\left(Y_{\gamma_D}^2 - Y_{\gamma_D,eq}^2\right)\right].\end{aligned} \tag{3.48}$$

If dark photon annihilations into SM particles are efficient to keep dark photons in chemical equilibrium until the freeze-out temperature, the abundance of dark pions follows the usual evolution. On the other hand, if $\sigma_{\gamma_D\gamma_D\to SM} \ll \sigma_{\pi\pi\to\gamma_D\gamma_D}$, then dark photons go out of chemical equilibrium before dark pions and have a much larger abundance. In this case the total density in the dark sector can be approximated as $Y_{\rm D,tot} \simeq Y_{\gamma_D}$ and taking the sum of the two equations in (3.48) we obtain, after an initial transient,

$$\begin{aligned}\frac{\mathrm{d}Y_\pi}{\mathrm{d}x} &= -\frac{1}{x^2}\frac{s(m_1)}{H(m_1)}\frac{1}{2}\langle\sigma_{\pi\pi\to\gamma_D\gamma_D}v\rangle\left(Y_\pi^2 - \frac{Y_{\pi,eq}^2}{Y_{\gamma_D,eq}^2}Y_{\gamma_D}^2\right)\\ \frac{\mathrm{d}Y_{\gamma_D}}{\mathrm{d}x} &= -2\frac{1}{x^2}\frac{s(m_1)}{H(m_1)}\langle\sigma_{\gamma_D\gamma_D\to SM}v\rangle\left(Y_{\gamma_D}^2 - Y_{\gamma_D,eq}^2\right)\,.\end{aligned} \tag{3.49}$$

From the first equation we see that the abundance of pions traces $(Y_{\pi,eq}/Y_{\gamma_D,eq})\,Y_{\gamma_D}$ once the dark photons are out of equilibrium and this modifies the freeze-out temperature for dark pions.

By solving the system (3.48) numerically we have verified that the approximation given by (3.49) is accurate. We find that the evolution of the dark pion and dark photon energy densities is modified with respect to the standard freeze out when $\sigma_{\gamma_D\gamma_D\to SM} \ll \sigma_{\pi\pi\to\gamma_D\gamma_D}$. However, in all the relevant parameter space, the asymptotic value for the DM relic abundance is within 50% of the naive estimate obtained from the simplified description of Eq. (3.43). A similar conclusion was reached in Ref. [76]. We refer the reader to Appendix 3.C for more details.

Dilution by entropy injection

If dark photons dominate the energy density of the Universe in some early phase of its evolution, they can modify the DM relic abundance by decaying and injecting entropy

in the SM bath. More in detail, the different evolution of the temperature during such early epoch of matter domination (EMD) translates into an effective dilution factor [75] (see also [2]),

$$\mathcal{F} \simeq \frac{4.8}{(g_*^{\rm SM}(T_{\rm EMD}))^{1/4}} \frac{\sqrt{M_{\rm Pl}\Gamma_{\gamma_D}}}{T_{\rm EMD}} \,, \tag{3.50}$$

that characterizes the prediction of the DM abundance today compared to the naive calculation. Here $T_{\rm EMD}$ has been defined as the temperature at the onset of the early matter domination era, while $g_*^{\rm SM}(T)$ is the number of SM relativistic degrees of freedom at the temperature T.

We computed $T_{\rm EMD}$ as the temperature at which the energy density of dark photons before their decay, ρ_{γ_D}, and the energy density of the SM radiation, ρ_{SM}, are equal. Since $\rho_{\gamma_D}(T) = Y_{\gamma_D}(T) s(T) m_{\gamma_D}$ and $\rho_{SM}(T) = (3/4) s(T) T$, one has

$$T_{\rm EMD} = \frac{4}{3} Y_{\gamma_D}(T_{\rm EMD})\, m_{\gamma_D} \,. \tag{3.51}$$

The dilution from dark photon decays was computed in previous studies in the context of models where γ_D annihilates into SM particles only through its kinetic mixing with hypercharge, see Refs. [76, 113, 77]. In that case, for $\varepsilon \lesssim 10^{-8}$ the dark photons have a chemical decoupling while they are still relativistic, and their abundance $Y_{\gamma_D}(T_{\rm EMD})$ is very large. In our model, even for very small ε, dark photons can annihilate into pairs of SM vector bosons through loops of NGB triplets, and undergo a standard freeze out at $T = T_{f.o.,\gamma_D}$. This gives a smaller abundance $Y_{\gamma_D}(T_{\rm EMD})$ hence a lower temperature $T_{\rm EMD}$. Using Eq. (3.51) and extracting $Y_{\gamma_D}(T_{\rm EMD})$ from an approximate analytic solution of the second equation in (3.49) gives

$$T_{\rm EMD} \simeq \frac{30}{\pi^2} \sqrt{\frac{4\pi^3 g_*^{\rm SM}(T_{f.o.,\gamma_D})}{45}} \frac{1}{g_*^{\rm SM}(T_{f.o.,\gamma_D})} \frac{1}{M_{\rm Pl}} \frac{x_{f.o.,\gamma_D}}{2\langle \sigma_{\gamma_D\gamma_D \to SM} v \rangle} \,, \tag{3.52}$$

which agrees well with the result obtained from a numerical integration of the system (3.48), and should be compared with the estimate in absence of dark photon annihilations:

$$(T_{\rm EMD})_{\rm naive} \simeq \zeta(3) \frac{30}{\pi^4} \frac{3}{g_*^{\rm SM}(T_{\rm EMD})}\, m_{\gamma_D} \,. \tag{3.53}$$

Figure 3.2 shows, for benchmark values of α_D and a, the isocurve in the (m_1, ε) plane that reproduces the observed DM abundance in our model (solid line) and in models where Eq. (3.53) applies (dashed line). While dilution is an important effect in the latter scenario, in our model it occurs for values of ε excluded by the bounds on the dark photon lifetime discussed below. The same conclusion holds in the majority of the interesting parameter space.

Bounds on the dark photon lifetime

The evolution of the Universe at temperatures below 1 MeV is accurately described by the standard cosmological model starting with BBN until the current epoch. Decays of long-lived particles during or after BBN can alter this picture and are generally excluded.

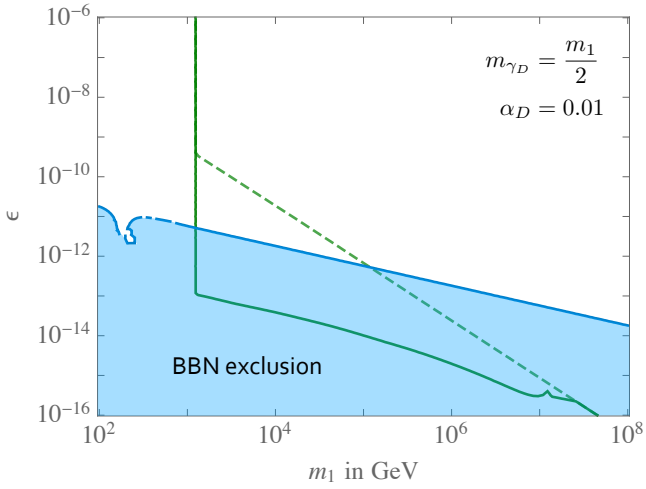

Figure 3.2: Isocurve of observed DM abundance (solid green line) and BBN bounds on the lifetime of the dark photon (shaded blue area) in the plane (m_1, ε). The dashed green curve is obtained by neglecting annihilations mediated by NGB triplets and using Eq. (3.53). The non-trivial dependence on ε is due to the dilution of the relic density caused by the early phase of matter domination. The plot assumes $\alpha_D = 0.01$ and $m_{\gamma_D} = m_1/2$.

Strong and robust constraints come in particular from observations of light elements abundances produced during BBN (see [157]) and from the CMB spectrum (see [158, 144]). To comply with these bounds, we require that metastable dark photons decay before BBN, i.e. we impose $T_{\rm decay} \gtrsim 10\,\text{MeV}$.

The decay temperature $T_{\rm decay}$ is computed by taking into account that the relation between time and temperature is modified with respect to the standard radiation-dominated case. In particular, the time interval comprised between the freeze-out and the decay of dark photons is:

$$t_{\rm decay} - t_{\rm f.o.,\gamma_D} \simeq \sqrt{\frac{90}{32\pi^3 g_{\rm f.o.}}} M_{\rm Pl} \left(\frac{r^{2/3}}{T^2_{\rm EMD}} - \frac{1}{T^2_{\rm f.o.,\gamma_D}} \right) + \sqrt{\frac{5}{\pi^3 g_{\rm EMD}}} \frac{M_{\rm Pl}}{T^2_{\rm EMD}} \times$$
$$\times \left[\frac{T^4_{\rm EMD}}{T^4_{\rm decay}} \left(\frac{\Gamma_{\gamma_D} M_{\rm Pl}}{\frac{5}{2} \left(\frac{4\pi^3}{45} g_{\rm EMD} \right)^{1/2} T^2_{\rm EMD} + \Gamma_{\gamma_D} M_{\rm Pl}} \right) - 1 \right], \tag{3.54}$$

where $g_{\rm f.o.} \equiv g_*^{\rm SM}(T_{\rm f.o.,\gamma_D})$, $g_{\rm EMD} \equiv g_*^{\rm SM}(T_{\rm EMD})$, $r \equiv g_{*S}^{\rm SM}(T_{\rm f.o.,\gamma_D})/g_{*S}^{\rm SM}(T_{\rm EMD})$, and $g_{*S}^{\rm SM}(T)$ is the effective number of 'entropic' relativistic degrees of freedom in the SM at the temperature T. This time interval corresponds, by definition of $T_{\rm decay}$, to the lifetime of the dark photon, i.e. $t_{\rm decay} - t_{\rm f.o.,\gamma_D} = \tau_{\gamma_D} = \Gamma^{-1}_{\gamma_D}$. From these identities and Eq. (3.54) it is possible to extract the value of $T_{\rm decay}$. The constraint $T_{\rm decay} \gtrsim 10\,\text{MeV}$

derived in this way excludes the blue region in the plot of Fig. 3.2. In practice, we find that all the relevant parameter space is excluded for $10^{-24} \lesssim \varepsilon \lesssim 10^{-12}$.

3.5.4 Cosmologically stable dark photons

In the limit of very small ε, i.e. for $\varepsilon \lesssim 10^{-24}$, the dark photons are cosmologically stable. Such small values of the mixing parameter are technically natural even though the dark sector comprises particles with SM charges, thanks to the dark charge conjugation symmetry (3.7). On the other hand, operators with two dark photons are not forbidden by $\mathcal{C}_D$ and will be generated at loop-level, inducing dark photon annihilations into SM particles. For instance, loops of NGB triplets mediate annihilations into pairs of W bosons with a cross section of order

$$\langle \sigma_{\gamma_D\gamma_D \to WW} v \rangle \sim \frac{1}{8\pi} \alpha_D^2 \alpha_2^2 \frac{m_{\gamma_D}^2}{m_3^4} \,. \tag{3.55}$$

These processes could set the abundance of dark photons to reproduce the observed DM one. The lower bound on triplets from collider searches derived in Sec. 4.5, $m_3 \gtrsim 300\,\text{GeV}$, implies however that the cross section of Eq. (3.55) is always too small if $m_{\gamma_D} < m_3$, and the energy density of dark photons would overclose the Universe. Conversely, for $m_{\gamma_D} > m_3$ the dark photon is no longer stable, as it can decay to triplets and W bosons.

3.5.5 Alternative choices of parameters and cosmological scenarios

So far we have described the cosmological evolution predicted in the bulk of the parameter space of our model. We now analyze some interesting limits where the thermal history is significantly different. These are obtained by varying the parameters α_D and a.

Varying α_D

As the strength of the dark coupling α_D increases, the abundances of dark pions and dark baryons become comparable, see Eq. (3.42). For $\alpha_D \gtrsim 0.4$ dark baryons become the dominant component of dark matter, with a dynamical scale of order $\Lambda_{DC} \sim 50 - 100\,\text{TeV}$.

Moreover, for couplings $\alpha_D \gtrsim \alpha_2$ the neutral triplets $3_0, 3_0'$ become lighter than the singlets and the dark photons. In this scenario the kinematics is reversed with respect to section 3.4.3. The dark photon decays to one $3_0'$ plus one electroweak boson V through the anomaly, while the triplet 3_0 can decay to SM particles at the two-loop order with a rate independent of ε. On the other hand, the $3_0'$ is metastable thanks to the $\mathcal{C}_D$ symmetry and can decay only through ε suppressed interactions. For very small or zero kinetic mixing, $\varepsilon \lesssim 10^{-24}$, the $3_0'$ is an interesting example of scalar triplet candidate of Minimal Dark Matter, with improved accidental stability and a dynamical mass. The dark matter would be multicomponent, with triplets $3_0'$, singlets $1_\pm$ and dark baryons,

each protected by a symmetry. For larger kinetic mixings, $\varepsilon > 10^{-24}$, the triplets are too short lived to be a DM candidate and the scenario is similar to the one described previously with now the $3_0'$ playing the role of metastable species.

In the case of small mass splitting $(m_3 - m_1)/m_1 \lesssim 0.1$, corresponding to dark couplings of order $\alpha_D \sim \alpha_2/2a$, co-annihilations could also play a role in determining the relic abundance. We do not attempt an analysis of these effects, leaving it to a future work.

Varying a

The other parameter that can be varied and has a large impact on the dynamics of the model is the chiral charge a. For $a > 0.9$ the dark photon becomes much lighter than the singlet, approaching the massless limit as $a \to 1$. For light dark photons, the dark sector interaction can become long-ranged and effects such as Sommerfeld enhancement and bound state formation in annihilation processes should be properly taken into account to have reliable predictions.

For sufficiently small a (e.g. $a \lesssim 0.26$ for $N_{DC} = 4$), the dark photon becomes heavier than the NGB singlet. The latter will thus annihilate into SM particles either through virtual dark photon exchange, with an ε-suppressed cross section, or though loops of triplets. In the model with SM-neutral dark fermions of Ref. [47], only the first process is possible and reproducing the correct DM abundance requires low values of the dynamical scale Λ_{DC} for small ε. In our model, on the other hand, annihilations mediated by dark photons turn out to be inefficient for $\varepsilon \lesssim 10^{-2}$, and in this limit the DM annihilates into W bosons through the operators of Eq. (3.47) induced by loops of triplets. At the same time, the dynamical scale cannot be too small in light of the collider bounds on NGB triplets discussed in Sec. 4.5. Enforcing these bounds and requiring the correct DM abundance implies a lower bound on the mass of the singlets $m_1 \gtrsim 130\,\text{GeV}$. For $\varepsilon \lesssim 10^{-24}$ and dark photon masses in the range $m_1 < m_{\gamma_D} < 2m_1$ (corresponding to $0.10 \lesssim a \lesssim 0.26$ for $N_{DC} = 4$), the dark photon is cosmologically stable and can annihilate efficiently into NGB singlets. Its energy density is thus small enough not to overclose the Universe (compare with Sec. 3.5.4), and gives an additional subdominant contribution to the DM abundance.

Finally, in the limit $a \to 0$, the NGB singlets become very light and are a component of dark radiation, rather than dark matter.

The case $a = 0$

As explained in section 3.3, for $a = 0$ the model has an enhanced global symmetry. The $1_\pm$'s become exact Nambu-Goldstone bosons (up to the effect of higher-dimensional operators), with only shift-symmetric interactions, and are massless. The analysis is qualitatively similar to the one performed in Ref. [48] for the model with SM-neutral fermions, with some qualifications.

The thermal abundance of dark baryons must account for all of the dark matter, and this fixes the dynamical scale to $\Lambda_{DC} \sim 50 - 100$ TeV. The massless singlets $1_\pm$, on the

other hand, behave as a component of dark radiation. Their abundance can be expressed in terms of an effective number of neutrinos:

$$\Delta N_{eff} = \frac{8}{7}\left(\frac{g_*^{SM}(1\,\mathrm{MeV})}{g_*^{SM}(T_{dec})}\right)^{\frac{4}{3}}, \tag{3.56}$$

where T_{dec} is the temperature at which the SM bath and dark radiation thermally decouple from each other. The number of SM degrees of freedom saturates at $(g_*^{SM})_{\max} = 106.75$ for large enough decoupling temperatures, implying $\Delta N_{eff} \gtrsim 0.05$.

There are two categories of processes that can keep the $1_\pm$ in thermal equilibrium: elastic scatterings mediated by dark photons – with a cross section suppressed by ε – and processes mediated by loops of triplets through the effective operators (3.47). The second class of interactions breaks the correlation between the cross section for DM direct detection and the number of relativistic degrees of freedom described in Ref. [48]. Moreover, it implies an upper bound on the decoupling temperature, valid also in the limit of ε small:

$$T_{dec} < 2.5\left(\frac{\Lambda_{DC}}{\mathrm{TeV}}\right)^{\frac{8}{7}}\ \mathrm{GeV}. \tag{3.57}$$

This differs from model of Ref. [48], where the decoupling temperature can be arbitrarily high depending on ε.

For dynamical scales $\Lambda_{DC} \sim 50-100\,\mathrm{TeV}$, the upper bound (3.57) is not strong enough to further constrain ΔN_{eff}. Furthermore, the observational bound $\Delta N_{eff} < 0.3$ [114] leaves unconstrained a wide region of the parameter space, corresponding to $\alpha_D \geqslant 10^{-8}$, and $\varepsilon \leqslant 10^{-3}$. In any point of such region, ΔN_{eff} falls in the interesting range that will be probed by future CMB experiments, see for example [115]. Complementary observables can be dark photon searches and direct detection signals from scattering of dark baryons on nucleons, depending on α_D and ε [48].

Finally, we notice that in this model the dark radiation and the dark baryon component of dark matter are tightly coupled due to dark meson-dark baryon interactions. This effect can have important implications on structure formation, suppressing structures on small scales and potentially alleviating the σ_8 and H_0 problem [116, 117], see also [118, 119]. We leave a detailed analysis of this scenario to the future.

3.6 Discussion and outlook

We have analyzed a class of dark sector theories characterized by a chiral $G_{DC} \times \mathrm{U}(1)_D \times G_{SM}$ gauge group where the vector-like factor G_{DC} confines at energies higher than the EW scale, while $\mathrm{U}(1)_D$ remains weak and is spontaneously broken. We assumed that the SM fermions are neutral under $G_{DC} \times \mathrm{U}(1)_D$ and that the dark fermions transform as non-trivial vector-like representations of the SM gauge group G_{SM}. The minimal models of this kind are listed in Tab. 3.1. They have four dark fermion multiplets and contain an accidental $\mathrm{U}(1)_{3V} \times \mathrm{U}(1)_V$ invariance that makes some of the NGBs and the lightest dark baryon cosmologically stable. Among minimal theories with SM irreducible

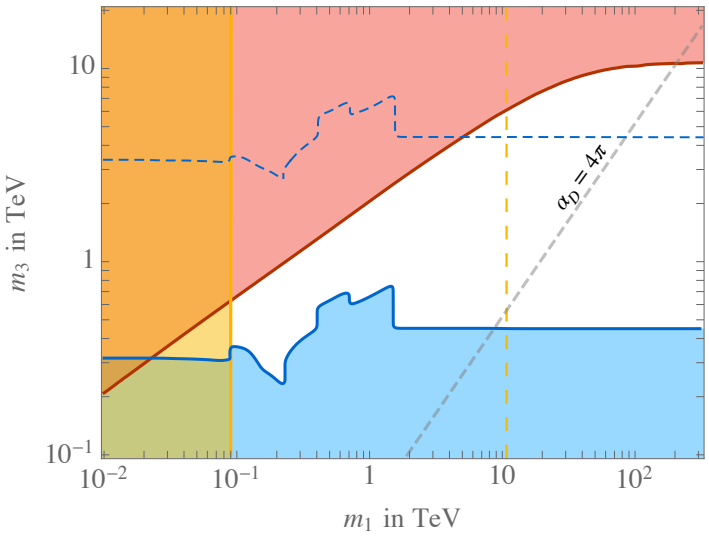

Figure 3.3: Isocurve of thermal relic density corresponding to the observed DM abundance (red curve), in the theory with EW doublets with $a = 1/2$ and $N_{DC} = 4$. Colored regions are excluded by current data from LHC searches (blue area), observations of gamma rays from dwarf spheroidal galaxies (yellow area) and by requiring that dark particles do not overclose the Universe (red area). The dashed blue curve shows the expected exclusion reach of a 100 TeV FCC with $20\,\text{ab}^{-1}$, while the dashed yellow curve shows the sensitivity of the CTA observatory from observations of the Galactic Center, assuming an Einasto DM profile. Our assumption of a weakly-coupled $\text{U}(1)_D$ gauge factor breaks down naively for points on the right of the dashed gray line. The plot assumes $\varepsilon = 10^{-6}$, which corresponds to prompt dark photon decays at high-energy colliders.

representations, we found that only those with $\text{SU}(2)_{EW}$ doublets or $\text{SU}(3)_c$ triplets are realistic. In these theories the DM abundance is reproduced by a pair of NGBs, the $\pi^\pm$, that are charged under $\text{U}(1)_{3V}$ but neutral under the SM, with a subdominant component in the form of dark baryons. We focused on the model with EW doublets, which predicts four additional EW triplets in the NGB spectrum besides the $\pi^\pm$. In this Chapter of the thesis we analyzed its cosmological history, while the constraints set by direct and indirect DM searches, as well as by collider data, will be discussed in Chapter 4.

Our results are summarized by the plots of Figs. 3.3, 3.4 and 3.5, where we display the thermal abundance prediction and the phenomenological bounds to be discussed in next Chapter. These show the allowed parameter space in the singlet-triplet mass plane for values of the kinetic mixing parameter equal to 10^{-6} (Fig. 3.3), 10^{-8} (Fig. 3.4) and 10^{-10} (Fig. 3.5). These benchmark values are chosen as representative of the three

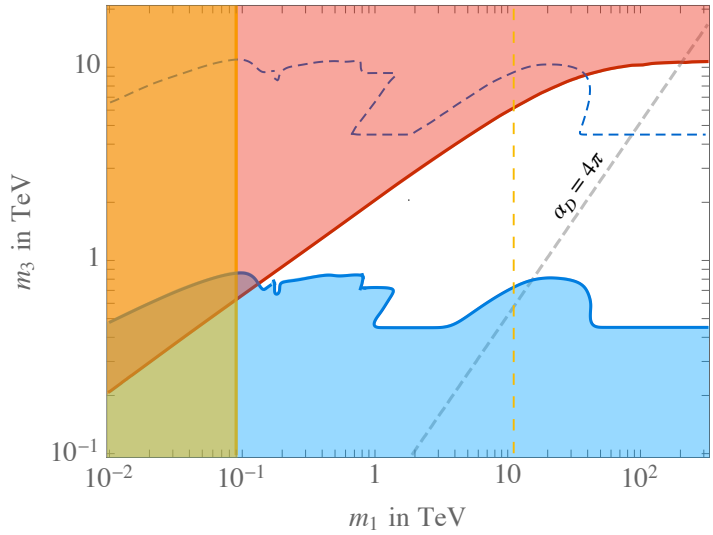

Figure 3.4: Same as Fig. 3.3 for $\varepsilon = 10^{-8}$, which corresponds to displaced dark photon decays at high-energy colliders.

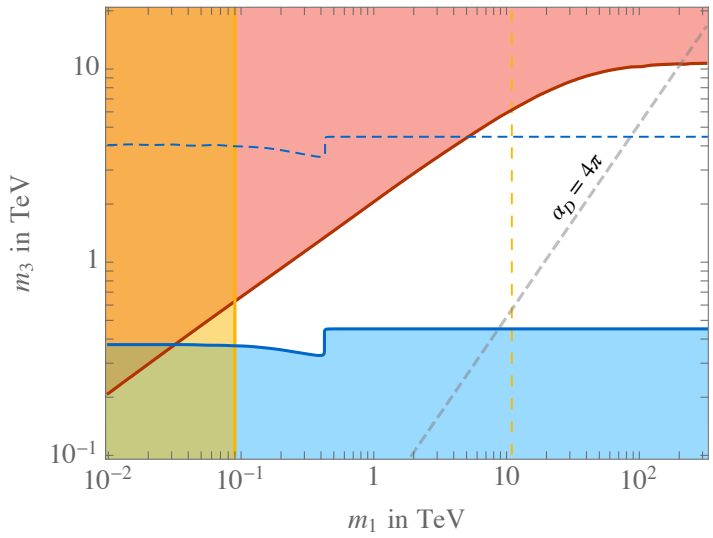

Figure 3.5: Same as Fig. 3.3 for $\varepsilon = 10^{-10}$, which corresponds to dark photons decaying outside the detector at high-energy colliders.

possible scenarios that characterize the production of the lightest dark states at high-energy colliders, i.e. those where dark photons decay promptly, with displaced vertices or outside the detector respectively. The white region is allowed by current data, while the remaining parameter space is excluded at 95% probability by collider searches (blue region), observations of gamma rays from dwarf spheroidal galaxies (yellow region), and by requiring that the thermal abundance of dark pions and baryons does not exceed the observed DM density (red region). One can further restrict the parameter space to the region where $\mathrm{U}(1)_D$ is weakly coupled at the dark confinement scale. Naively, these points lie on the left of the dashed gray line shown in the plots. The resulting parameter space has a finite extension and has been already probed significantly by the current experimental data. Notice, in particular, that the mass of the triplets cannot be much larger than $\sim 10\,\mathrm{TeV}$, otherwise dark sector particles would overclose the Universe. It is thus relevant to ask whether all of the physically sensible parameter space can be tested at future high-energy colliders or by future astrophysical observations. The dashed blue curves in the plots show the expected reach of a proton-proton FCC operating at a 100 TeV center-of-mass energy with $20\,\mathrm{ab}^{-1}$ of integrated luminosity, and have been obtained by performing a naive rescaling of the expected LHC exclusions with the Collider Reach$^\beta$ tool [120]. Similarly, the yellow dashed lines show the projected sensitivity of the CTA observatory from the observation of the Galactic Center [121]. Although points with the highest values of m_3 and an inverted hierarchy will remain inaccessible, most of the parameter space can be probed both by a 100 TeV collider and by future observations of the Galactic Center by CTA. The joint observation of a signal by the two classes of experiments will allow a detailed test of the model thanks to the correlated prediction of the particles' masses, dark matter annihilation cross section and collider production cross section. We expect that a similar or stronger conclusion can be drawn for the model with $\mathrm{SU}(3)_c$ triplets.

The existence of SM-charged partners of the DM is the key prediction that distinguishes our theories from the chiral model of Refs. [47, 48], where dark fermions are SM singlets. Both kinds of theories, on the other hand, lead to a similar DM phenomenology in terms of one SM-singlet scalar field (the DM candidate $\pi^\pm$), plus a massive dark photon. These are the lowest lying states in the spectrum of new particles in a large portion of our parameter space, and in fact characterize the low-energy limit of a larger class of DM theories studied in the literature. It is interesting to analyze how much of the results we obtained on the phenomenology of the DM relies on the properties of these infrared degrees of freedom, and which are instead the aspects distinctive of our UV completion.

The most general effective lagrangian which describes one scalar field $\pi^\pm$ (the DM candidate) plus a massive spin-1 field (the dark photon), and which is invariant under a global $\mathrm{U}(1)_{3V}$, has the following form:

$$\begin{aligned}\mathcal{L}_{eff} = &-\frac{1}{4}F^2_{\mu\nu,D} + \frac{1}{2}m^2_{\gamma_D}A^2_{\mu,D} + \varepsilon\, F_{\mu\nu,D}B^{\mu\nu} + \partial_\mu\pi^+\partial^\mu\pi^- - m_1^2\pi^+\pi^- \\ &+ ia_3 e_D A^D_\mu(\pi^-\partial^\mu\pi^+ - \pi^+\partial^\mu\pi^-) + a_4 e_D^2 A^2_{\mu,D}\pi^+\pi^- + \dots\,,\end{aligned} \tag{3.58}$$

where a_3, a_4 are arbitrary dimensionless coefficients and the dots stand for higher-dimensional operators. For generic values of a_3 and a_4, this theory becomes strongly coupled at the scale

$$\Lambda_S \sim \frac{4\pi}{e_D} \frac{m_{\gamma_D}}{\sqrt{|a_4 - a_3^2|}} \,. \tag{3.59}$$

The easiest way to see this is by introducing the Stueckelberg field corresponding to the longitudinal polarization of the dark photon by means of the field redefinition $A_\mu^D \to A_\mu^D - \partial_\mu \pi^0/(e_D f)$. The new basis makes the U(1) gauge invariance of the theory manifest, and at the same time uncovers the terms responsible for the strong coupling scale, namely the derivative interactions between π^0 and $\pi^\pm$. For the special choice $a_4 = a_3^2$ these terms can be redefined away by a local phase shift of $\pi^\pm$, and the theory becomes UV complete. This is very much analogous to the case of the electroweak chiral lagrangian plus a Higgs boson, which becomes UV complete for values of the Higgs couplings $c_V = c_{2V} = 1$ (see for example Ref. [122]). A relative strength $a_4/a_3^2 = 1$ between quartic and cubic couplings is in fact what scalar QED would predict. Indeed, the limit of scalar QED can be recovered by fixing $a_4 = a_3^2$ and letting $m_{\gamma_D} \to 0$.

The theory described by Eq. (3.58) with $a_4 = a_3^2$ and vanishing higher-dimensional operators has been analyzed in the literature as an example of dynamics with a scalar DM candidate plus a dark photon, see for example Ref. [113]. In that case the mass ratio m_{γ_D}/m_1 is an arbitrary parameter. For $m_{\gamma_D} < 2m_1$ and sufficiently small ε, the theory goes through an early phase of matter domination, which in turn leads to a dilution of the DM relic density. The models studied in this work and in Refs. [47, 48] lead to different values for the coefficients of Eq. (3.58). They predict

$$a_3 = 1 + a \,, \quad a_4 = 4a \,, \quad m_{\gamma_D} = \sqrt{2}(1-a) e_D f \,. \tag{3.60}$$

In this family of points of the parameter space the effective theory has an approximate enhanced global $\mathrm{SU}(2)_L \times \mathrm{SU}(2)_R$ symmetry, broken down spontaneously to $\mathrm{SU}(2)_V$ at the scale f. This symmetry is broken explicitly by the $\pi^\pm$ mass term and by the gauging. The $\pi^\pm$ can be thus thought of as two additional (pseudo) NGBs, together with π^0. The value of m_1 is still arbitrary from the low-energy viewpoint, i.e. it depends on the UV completion of Eq. (3.58). For example, it remains a free parameter if the UV theory is a linear sigma model with fundamental scalar fields. Hence, while the relation among a_3, a_4 and m_{γ_D} is a consequence of the global symmetries of the low-energy theory and of their weak chiral gauging, the prediction $m_1 \sim e_D f$ is specific to UV theories – such as those analyzed in this work and in Refs. [47, 48] – where $\pi^{\pm,0}$ are bound states of new strongly-coupled dynamics at the scale f, and where the only spurion is the gauge coupling e_D. The fact that the DM and the dark photon have comparable masses (unless $a \to 1$) has specific implications in the cosmological evolution and in the DM phenomenology. For example, it implies that effects due to Sommerfeld enhancement and bound-state formations are negligible in determining the DM relic density. Another prediction specific to our UV completion is the role of higher-dimensional operators, such as $A_{\mu,D}^2 W_{\rho\sigma}^2$ and $\pi^2 W_{\mu\nu}^2$, generated by loops of triplets. They are the main interactions between the dark and SM sectors for small ε, and in this case play a key role in the

cosmological evolution. For example, as discussed in Sec. 3.5.3, they keep the dark sector in thermal equilibrium with the SM bath until low temperatures. If, on the other hand, the UV dark dynamics interacts with the SM only through the kinetic mixing, like in the model of Refs. [47, 48], then the dark and SM sectors might be thermally decoupled throughout their entire cosmological histories. Predicting the DM thermal abundance in this case requires knowing the ratio of entropies set during the reheating epoch. The dim-6 operator $A^2_{\mu,D}W^2_{\rho\sigma}$ is also crucial to ensure efficient annihilations of the dark photons into SM particles. As discussed in Secs. 3.5.3 and 3.5.3, this process plays an important role during the freeze out and controls the amount of dilution induced by long-lived dark photons (see Fig. 3.2).

These considerations make clear the importance of having a UV complete description of the dynamics rather than just an effective theory. Crucial aspects of the cosmological evolution might not be captured by the lowest-lying degrees of freedom. On one hand, this is true because the cosmological relevance of a given process depends on its rate, which can be large despite a small cross section if the number density is large enough. This is the case of dark photon annihilation into SM vector bosons in our theory. On the other hand, heavy degrees of freedom can contribute to the DM density if they are stable and have a thermal abundance. Dark baryons are an example in our case. A top-down approach in the search for a DM theory is thus justified and has its own advantages over strategies based on effective models. Obviously, the landscape of UV theories is larger and much more difficult to explore than that of low-energy ones. We tried such path by taking as a guidance the following two criteria: the theory should generate dynamically all the new scales, including the mass of the DM candidate, and the stability of the latter should be explained by an accidental symmetry. This led us to consider strongly-coupled chiral gauge theories, which represent an incredibly rich playground but, at the same time, are subject to highly non-trivial theoretical constraints. The models analyzed in this work are interesting and particularly attractive since they lead to correlated predictions for experiments at high-energy colliders and for astrophysical observations.

This work leaves some open questions, mainly mentioned along the chapter. The most pressing regards the feasibility of a chiral model with SM interactions compatible with the Grand Unification of SM gauge interactions hinted by the present data. Moreover, many of the alternative scenarios described is section 3.5.5 have some phenomenologically interesting features that would deserve further investigations.

3.A Useful formulas for dark pions

In this Appendix we collect two useful results on dark pions.

The first concerns the vertices with three NGBs and one dark photon that appear in the chiral Lagrangian. They have the following expression:

$$\begin{aligned}\mathcal{L}_0 \supset \frac{e_D(a-1)}{f}\Big[& gA^D_\mu \varepsilon_{abc}\big(s_+\pi^a_- + s_-\pi^a_+\big)\pi'^b W^\mu_c - \frac{ig}{\sqrt{2}}A^D_\mu W^\mu_a\big(\pi^a_+\pi^b_- - \pi^a_-\pi^b_+\big)\pi^b \\ & + \frac{1}{3}A^D_\mu\partial_\mu\Big(\pi'^a(\pi^a_+ s_- + \pi^a_- s_+)\Big) + \frac{i}{3\sqrt{2}}A^D_\mu\varepsilon_{abc}\partial_\mu(\pi^a_+\pi^b_-\pi^c) \\ & - A^D_\mu\partial^\mu\pi'_a(\pi_+ s^a_- + \pi_- s^a_+) + \frac{i}{3\sqrt{2}}A^D_\mu\varepsilon_{abc}\pi^a_+\pi^b_-\partial_\mu\pi^c\Big],\end{aligned} \tag{3.61}$$

where $\mathrm{SU}(2)_{EW}$ indices are denoted by lower case Latin letters (a, b, c) and, only for this formula, $s_\pm$, $\pi^a_\pm$, π^a and π'^a denote respectively the $1_\pm$, $3_\pm$, 3_0 and $3'_0$.

The second result are the (tree-level) spin- and color-averaged partonic cross sections for Drell-Yan production of pairs of dark pions. We find (here superscripts indicate the electromagnetic charges and π denotes any of the NGBs)

$$\hat\sigma_{u_i\bar d_j\to\pi^+\pi^0} = \hat\sigma_{\bar u_i d_j\to\pi^-\pi^0} = \frac{g^4}{576\pi}\frac{|V_{ij}|^2}{\sqrt{\hat s}(\hat s - m_W^2)^2}(\hat s - 4M^2)^{\frac{3}{2}}, \tag{3.62}$$

$$\begin{aligned}\hat\sigma_{u_i\bar u_j\to\pi^+\pi^-} = \frac{g^4}{144\pi}\frac{(\hat s-4M^2)^{\frac{3}{2}}}{\sqrt{\hat s}}\Bigg[& \frac{1}{8}\frac{1}{(\hat s - m_Z^2)^2} + \frac{4}{9}\sin^4\theta_W\left(\frac{1}{\hat s - m_Z^2} - \frac{1}{\hat s}\right)^2 \\ & + \frac{1}{12}\sin^2\theta_W\frac{1}{\hat s - m_Z^2}\left(\frac{1}{\hat s} - \frac{1}{\hat s - m_Z^2}\right)\Bigg],\end{aligned} \tag{3.63}$$

$$\begin{aligned}\hat\sigma_{d_i\bar d_j\to\pi^+\pi^-} = \frac{g^4}{144\pi}\frac{(\hat s-4M^2)^{\frac{3}{2}}}{\sqrt{\hat s}}\Bigg[& \frac{1}{8}\frac{1}{(\hat s - m_Z^2)^2} + \frac{1}{9}\sin^4\theta_W\left(\frac{1}{\hat s - m_Z^2} - \frac{1}{\hat s}\right)^2 \\ & + \frac{1}{24}\sin^2\theta_W\frac{1}{\hat s - m_Z^2}\left(\frac{1}{\hat s} - \frac{1}{\hat s - m_Z^2}\right)\Bigg],\end{aligned} \tag{3.64}$$

in agreement with the results of Ref. [14]. Here M denotes the mass of the particle that is being produced, which can be either a $\mathrm{U}(1)_{3V}$-charged or neutral triplet. For $\theta_W = 0$ the first cross section reduces to the sum of the other two, as expected by $\mathrm{SU}(2)_{EW}$ invariance.

3.B Model with $\mathrm{SU}(3)_c$ triplets

The other viable minimal model identified by the analysis of section 3.2 is a Type I theory with SM color triplets (hence r in Tab. 3.1 is a fundamental of $\mathrm{SU}(3)_c$). From a qualitative viewpoint, the analysis of this model closely parallels the one carried out in

the main text for the model with electroweak doublets, since the SM strong interactions are perturbative at energies of the order of the dark confinement scales we are interested in. The approximate global symmetry breaking pattern gets enlarged to

$$\mathrm{SU}(6)_L \otimes \mathrm{SU}(6)_R \otimes \mathrm{U}(1)_V \to \mathrm{SU}(6)_V \otimes \mathrm{U}(1)_V \,, \tag{3.65}$$

so there are 35 pseudo-NGBs, one of which is eaten by the dark photon. They can be classified as:

- Two color singlets, charged under $\mathrm{U}(1)_D$, the $\mathbf{1}^{\pm}$. These have exactly the same properties as the corresponding states in the model with electroweak doublets, and thus constitute stable dark matter candidates.
- Two neutral octets charged under $\mathrm{SU}(3)_c$ only, the $\mathbf{8_0}, \mathbf{8'_0}$. These are the analog of the $3_0, 3'_0$.
- Two charged octets, the $\mathbf{8}^{\pm}$, charged under $\mathrm{SU}(3)_c$ and $\mathrm{U}(1)_D$. These are the analog of the $3^{\pm}$.

The phenomenology is very similar to the electroweak case. Dark matter is still made of SM singlets and the calculation of the relic abundance is unmodified. Heavier pseudo-NGBs now transform as SM color octects (i.e. still in the adjoint of the SM group), and the constraints from colliders are expected to be more severe. We leave the analysis of this model to a future work.

3.C Boltzmann equations for long-lived dark photons

A complete description of the evolution of the dark sector during the freeze-out epoch would include, in principle, all number-changing processes involving dark photons and SM-singlet dark pions. Since the underlying theory is strongly coupled, every effective interaction allowed by the symmetries is expected to be generated at some level. This leads to a complicated system of coupled Boltzmann equations with many processes. It is possible to obtain a simplified yet accurate description by identifying the leading effects and focus our attention on them. We can distinguish the following classes of leading processes: [11]

- Pion annihilations into two dark photons, with cross section given by Eq. (3.44);
- Dark photon decays, suppressed by an ε insertion due to $\mathcal{C}_D$ protection;
- Dark photon annihilations into EW gauge bosons, mediated by a loop of triplet pions. This process is allowed by $\mathcal{C}_D$ and has a cross section given by Eq. (3.55);

[11] Processes with dark photon absorption and conversion, such as $\gamma_D \psi_{\mathrm{SM}} \longrightarrow V \psi'_{\mathrm{SM}}$, where V is a standard model gauge boson, can be safely neglected. Their rate is suppressed by ε^2 due to $\mathcal{C}_D$ and turns out to be negligible when ε is small enough to have long-lived dark photons.

- Pion scatterings with initial or final state radiation: $\pi^\pm\pi^\pm \to \pi^\pm\pi^\pm\gamma_D$ or $\pi^\pm\gamma_D \to \pi^\pm\gamma_D\gamma_D$, with thermally-averaged cross sections $\langle\sigma_{\pi\pi\to\pi\pi\gamma_D} v\rangle \sim \langle\sigma_{\pi\gamma_D\to\pi\gamma_D\gamma_D} v\rangle \sim \alpha_D^3 T^4 e^{-m_{\gamma_D}/T}/m_1^6$. This estimate relies on the assumption that $m_{\gamma_D} \sim m_1$. [12]

Assuming that the kinetic decoupling of the SM and dark sectors occurs at sufficiently small temperatures and that entropy is conserved, [13] the set of Boltzmann equations is thus given by ($x = m_1/T$):

$$\begin{aligned}
\frac{\mathrm{d}Y_\pi}{\mathrm{d}x} &= -\frac{1}{x^2}\frac{s(m)}{H(m)}\frac{1}{2}\langle\sigma_{\pi\pi\to\gamma_D\gamma_D} v\rangle \left(Y_\pi^2 - \frac{Y_{\pi,eq}^2}{Y_{\gamma_D,eq}^2} Y_{\gamma_D}^2\right) , \\
\frac{\mathrm{d}Y_{\gamma_D}}{\mathrm{d}x} &= \frac{1}{x^2}\frac{s(m)}{H(m)}\left[\frac{1}{2}\langle\sigma_{\pi\pi\to\gamma_D\gamma_D} v\rangle \left(Y_\pi^2 - \frac{Y_{\pi,eq}^2}{Y_{\gamma_D,eq}^2} Y_{\gamma_D}^2\right)\right. \\
&\qquad + \frac{1}{4}\langle\sigma_{\pi\pi\to\pi\pi\gamma_D} v\rangle Y_\pi^2 \left(1 - \frac{Y_{\gamma_D}}{Y_{\gamma_D,eq}}\right) \\
&\qquad + \frac{1}{2}\langle\sigma_{\pi\gamma_D\to\pi\gamma_D\gamma_D} v\rangle Y_\pi Y_{\gamma_D} \left(1 - \frac{Y_{\gamma_D}}{Y_{\gamma_D,eq}}\right) \\
&\qquad \left. - 2\langle\sigma_{\gamma_D\gamma_D\to SM} v\rangle \left(Y_{\gamma_D}^2 - Y_{\gamma_D,eq}^2\right)\right] \\
&\quad - x\frac{1}{H(m)}\Gamma_{\gamma_D\to SM}\left(Y_{\gamma_D} - Y_{\gamma_D,eq}\right) .
\end{aligned} \tag{3.66}$$

We have checked numerically, by performing the corresponding thermal average and including the kinematic cut to emit a massive particle, that $2 \to 3$ processes are subleading and give a relative corrections of order 10^{-3} or smaller. The last term in Eq. (3.66), corresponding to the decay of dark photons, is the only one that grows with x. It can be neglected as long as the dark photon energy density is subleading in the energy budget of the Universe and $x\,\Gamma_{\gamma_D\to SM} \ll H(m)$. We discuss the effect of the dark photon decays in section 3.5.3. Neglecting these terms, we are left with the simplified system of Eq. (3.48), which describes the out-of-equilibrium evolution of two species. Its numerical solution is shown in Figs. 3.6 and 3.7 for a benchmark point with $m_1 = 100\,\mathrm{GeV}$ and $m_3 = 700\,\mathrm{GeV}$. For this choice, $\sigma_{\gamma_D\gamma_D\to SM} \ll \sigma_{\pi\pi\to\gamma_D\gamma_D}$ and dark photons are out of equilibrium during freeze out, see Fig. 3.7. The dark pion abundance tracks $(Y_{\pi,eq}/Y_{\gamma_D,eq})\,Y_{\gamma_D}$ and is much larger than the value predicted by a standard evolution until freeze out occurs, see Fig. 3.6. Despite the different thermal evolutions and freeze-out temperatures, the

[12] For $m_{\gamma_D} \ll m_1$, instead, $2 \to 3$ processes are no longer Boltzmann suppressed and can be efficient, keeping dark photons in chemical equilibrium until much lower temperatures – similarly to what happens to CMB photons after recombination.

[13] This is a good approximation as long as the entropy from the dark photon decay products is negligible, that is, as long as the dark photons' energy density is subleading in the energy budget of the Universe. If dark photons dominate the energy density, they can give rise to a dilution of cold relics due to entropy injection, as described in Sec. 3.5.3.

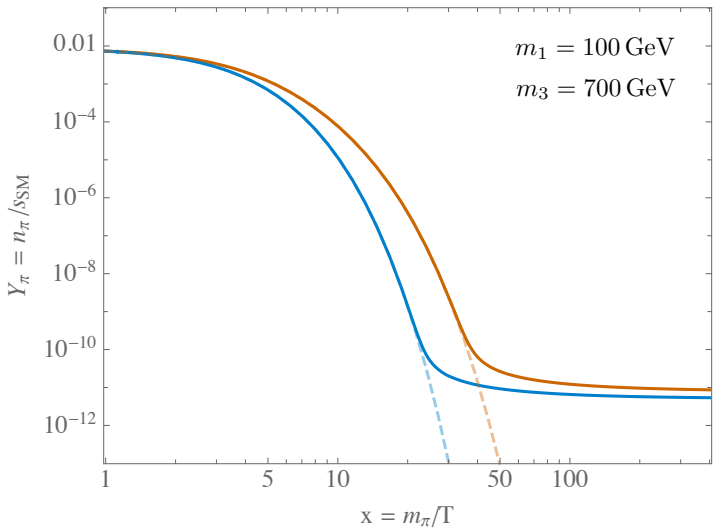

Figure 3.6: Thermal evolution of the dark pion abundance obtained by solving numerically the system (3.66) with $a = 1/2$ and $N_{DC} = 4$. The numerical solution for $\varepsilon \lesssim 10^{-8}$ (solid orange line) traces the combination $(Y^2_{\pi,eq}/Y^2_{\gamma_D,eq})\, Y^2_{\gamma_D}$ (dashed orange line) until the freeze out. For comparison, we also show the thermal abundance of dark pions for $\varepsilon > 10^{-8}$ (solid blue line), corresponding to the ordinary freeze-out evolution of Eq. (3.43), and its thermal equilibrium density $Y_{\pi,eq}$ (dashed blue line).

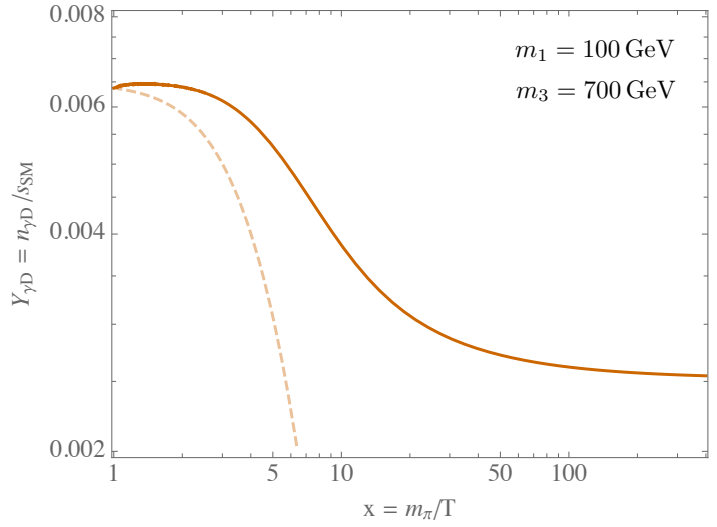

Figure 3.7: Thermal evolution of the dark photon abundance obtained by solving numerically the system (3.66) with $a = 1/2$ and $N_{\rm DC} = 4$. The solid orange line is the numerical solution for $\varepsilon \lesssim 10^{-8}$, while the dashed orange line corresponds to the thermal equilibrium density $Y_{\gamma_D,eq}$.

asymptotic abundances differ by less than 30% compared to the standard case in all the relevant parameter space.

3.D The Dark Photon

In this Appendix we summarise some useful properties of the dark photon, providing formulas valid to all orders in ε and also at resonance $m_{\gamma_D} = m_Z$. These equations confirm and extend the computations of Refs. [123, 124, 125], where similar results were provided to first order in ε and away from resonance. We start from a lagrangian written in terms of the ordinary SM gauge bosons $\hat{W}^3_\mu, \hat{B}_\mu$ and a massive $\hat{Z}'$ with a kinetic mixing term with the hypercharge gauge boson:

$$\begin{aligned}\mathcal{L} = &-\frac{1}{4}\hat{W}^3_{\mu\nu}\hat{W}^{\mu\nu,3} - \frac{1}{4}\hat{B}_{\mu\nu}\hat{B}^{\mu\nu} - \frac{1}{4}\hat{A}_{\mu\nu,D}\hat{A}^{\mu\nu}_D - \frac{\varepsilon}{2}\hat{A}_{\mu\nu,D}\hat{B}^{\mu\nu} \\ &+ \frac{1}{2}c_W^2\hat{m}_Z^2\,\hat{W}^3_\mu\hat{W}^{\mu,3} + \frac{1}{2}s_W^2\hat{m}_Z^2\,\hat{B}_\mu\hat{B}^\mu - c_W s_W\hat{m}_Z^2\,\hat{W}^3_\mu\hat{B}^\mu + \frac{1}{2}\hat{m}^2_{\gamma_D}\,\hat{A}_{\mu,D}\hat{A}^\mu_D\,.\end{aligned} \tag{3.67}$$

All the symbols with a hat (such as $\hat{B}_\mu$) refer to fields and parameters in the interacting basis of Eq. (3.67). Symbols without a hat will refer to the same quantities in the mass eigenbasis. The mass and kinetic mixing can be diagonalized to all orders in ε through the field redefinition

$$\begin{pmatrix}\hat{W}^{\mu,3}\\ \hat{B}^\mu\\ \hat{A}^\mu_D\end{pmatrix} = \begin{pmatrix}s_W & c_W c_\xi & -c_W s_\xi\\ c_W & -s_W c_\xi - \dfrac{\varepsilon}{\sqrt{1-\varepsilon^2}}s_\xi & s_W s_\xi - \dfrac{\varepsilon}{\sqrt{1-\varepsilon^2}}c_\xi\\ 0 & \dfrac{1}{\sqrt{1-\varepsilon^2}}s_\xi & \dfrac{1}{\sqrt{1-\varepsilon^2}}c_\xi\end{pmatrix}\begin{pmatrix}A^\mu\\ Z^\mu\\ A^\mu_D\end{pmatrix}, \tag{3.68}$$

where c, s are shorthands for cosines and sines, the subscript W identifies the weak mixing angle θ_W, and ξ refers to a new mixing angle defined by the relation:

$$\tan(2\xi) = \frac{2\hat{m}_Z^2\,\varepsilon\sqrt{1-\varepsilon^2}s_W}{\hat{m}_Z^2 - \hat{m}^2_{\gamma_D} - \varepsilon^2\hat{m}_Z^2(1+s_W^2)}\,. \tag{3.69}$$

We are left with a diagonal mass matrix with:

$$\begin{aligned} m_\gamma &= 0\\ \frac{m_Z^2}{2} &= \frac{\hat{m}_Z^2}{2}c_\xi^2 + \frac{\varepsilon c_\xi s_\xi s_W\hat{m}_Z^2}{\sqrt{1-\varepsilon^2}} + \frac{1}{2}\frac{\hat{m}^2_{\gamma_D}s_\xi^2 + \hat{m}_Z^2\varepsilon^2 s_W^2 s_\xi^2}{1-\varepsilon^2}\\ \frac{m^2_{\gamma_D}}{2} &= \frac{\hat{m}_Z^2}{2}s_\xi^2 - \frac{\varepsilon c_\xi s_\xi s_W\hat{m}_Z^2}{\sqrt{1-\varepsilon^2}} + \frac{1}{2}\frac{\hat{m}^2_{\gamma_D}c_\xi^2 + \hat{m}_Z^2\varepsilon^2 s_W^2 c_\xi^2}{1-\varepsilon^2}\,.\end{aligned} \tag{3.70}$$

It is useful to express the currents to which the physical vector bosons are coupled in terms of the currents for the original photon, Z and dark photon fields:

$$\begin{pmatrix} J^\mu_A \\ J^\mu_Z \\ J^\mu_{A_D} \end{pmatrix} = \begin{pmatrix} 1 & 0 & 0 \\ -\frac{\varepsilon}{\sqrt{1-\varepsilon^2}} c_W s_\xi & c_\xi + \frac{\varepsilon}{\sqrt{1-\varepsilon^2}} s_W s_\xi & \frac{1}{\sqrt{1-\varepsilon^2}} s_\xi \\ -\frac{\varepsilon}{\sqrt{1-\varepsilon^2}} c_W c_\xi & -s_\xi + \frac{\varepsilon}{\sqrt{1-\varepsilon^2}} s_W c_\xi & \frac{1}{\sqrt{1-\varepsilon^2}} c_\xi \end{pmatrix} \begin{pmatrix} J^\mu_{\hat{A}} \\ J^\mu_{\hat{Z}} \\ J^\mu_{\hat{A}_D} \end{pmatrix}. \tag{3.71}$$

Decays

By virtue of its coupling to the SM sector, the dark photon is unstable and decays to SM particles. Restricting to two-particle final states, that are more important than other ones due to phase space suppression, the possible channels are

$$\gamma_D \to f\,\bar{f}, \qquad \gamma_D \to Zh, \qquad \gamma_D \to W^+ W^-, \tag{3.72}$$

where f can be any SM fermion. The decays to fermions dominate the total width and are mediated by the following interactions

$$\mathcal{L} \supset A_{\mu,D} \sum g_{L,i} \bar{\psi}_{L,i} \partial^\mu \psi_{L,i} + A_{\mu,D} \sum g_{R,i} \bar{\psi}_{R,i} \partial^\mu \psi_{R,i}\,, \tag{3.73}$$

where $g_{L/R}$ can be extracted to all orders in ε from Eq. (3.71):

$$g_i = (T_{3L} + Y) \frac{\varepsilon c_W c_\xi}{\sqrt{1-\varepsilon^2}} - \frac{T_{3L} c_W - Y s_W}{c_W s_W} \left(\frac{\varepsilon s_W c_\xi}{\sqrt{1-\varepsilon^2}} - s_\xi \right). \tag{3.74}$$

At leading order in ε, this formula reduces to the expressions reported in Ref. [124], up to a factor of c_W that is reabsorbed in the definition of ε. The tree-level decay width is given by [124]:

$$\Gamma_{\gamma_D \to f\bar{f}} = \frac{\alpha_{em} \varepsilon^2 N_c}{6\pi m_{\gamma_D}} \sqrt{1 - \frac{4m_f^2}{m_{\gamma_D}^2}} \left(m_{\gamma_D}^2 \left(g_L^2 + g_R^2 \right) - m_f^2 \left(-6 g_L g_R + g_L^2 + g_R^2 \right) \right). \tag{3.75}$$

This expression is a good approximation above the $b\bar{b}$ threshold, below which QCD corrections must be taken into account. As regards the second channel of Eq. (3.72), the kinetic mixing induces a coupling of the form

$$\mathcal{L} \supset c_{hZ\gamma_D} h Z^D_\mu Z^\mu, \tag{3.76}$$

where

$$c_{hZ\gamma_D} = \frac{2m_Z^2}{v} \left(c_\xi + \frac{\varepsilon s_W s_\xi}{\sqrt{1-\varepsilon^2}} \right) \left(-s_\xi + \frac{\varepsilon s_W c_\xi}{\sqrt{1-\varepsilon^2}} \right). \tag{3.77}$$

The corresponding decay rate is

$$\begin{aligned} \Gamma_{\gamma_D \to Zh} = c_{hZ\gamma_D}^2 & \frac{\left(m_{\gamma_D}^2 - m_h^2 - m_z^2 \right)^2 + 12 m_{\gamma_D} m_Z^2 - 4 m_Z^2 m_h^2}{192\pi m_{\gamma_D}^5 m_Z^2} \\ & \times \sqrt{\left(m_{\gamma_D}^2 - m_h^2 - m_z^2 \right)^2 - 4 m_Z^2 m_h^2}\,. \end{aligned} \tag{3.78}$$

The couplings mediating the third channel in Eq. (3.72) are of the form

$$\begin{aligned}\mathcal{L} \supset i\frac{c_W s_\xi}{s_W}\Big[&\partial_\mu Z_\nu^D \left(W_\mu^+ W_\nu^- - W_\nu^+ W_\mu^-\right) \\ &+ Z_\nu^D \left(-W_\mu^+ \partial_\nu W_\mu^- + W_\mu^- \partial_\nu W_\mu^+ + W_\mu^+ \partial_\mu W_\nu^- - W_\mu^- \partial_\mu W_\nu^+\right)\Big],\end{aligned} \tag{3.79}$$

and the rate is [126]

$$\Gamma_{\gamma_D \to W^+W^-} = \frac{\alpha s_\xi^2 c_W^2\, m_{\gamma_D}}{48 s_W^2}\, \frac{m_{\gamma_D}^4 + 20 m_{\gamma_D}^2 m_W^2 + 12 m_W^4}{m_W^4} \left(1 - 4\frac{m_W^2}{m_{\gamma_D}^2}\right)^{\frac{3}{2}}. \tag{3.80}$$

4 Phenomenology

In this chapter we turn to the discussion of the phenomenology of particle physics models of dark matter. In the first section we present an analysis on how to constrain the lifetime of dark matter particles for generic models and for a wide range of masses, using the observation of the 21 cm global signal, published in Ref. [4].

We then proceed to an analysis of the specific phenomenological signatures for the models of gluequark and chiral dark matter introduced in the preceeding chapters. Indirect searches offer the most stringent constraints on models of gluequark dark matter. Direct detection seems out of reach for the minimal models of gluequarks while it can be a useful complementary probe in models of chiral dark matter, depending on the value of the kinetic mixing parameter. Finally, collider searches are very promising for models of chiral dark matter with Standard Model interactions. Even if the dark matter candidate is a SM singlet, charged partners can be efficiently produced at colliders and can be tested with a wide variety of search strategies.

4.1 Constraints on the lifetime of dark matter from the 21 cm global signal

The observation of the cosmic 21-cm spectrum can serve as a probe for Dark Matter properties. In this section we discuss how the knowledge of the signal amplitude at a given redshift allows one to put conservative bounds on the DM decay rate which are independent of astrophysical parameters. These limits are valid for the vast majority of DM models, those without extra intergalactic medium cooling or additional background radiation. Using the experimental results reported by the EDGES collaboration, we derive bounds that are stronger than the ones derived from other CMB observations and competitive with the ones from indirect detection. Related work has appeared in Refs. [127, 128].

4.1.1 The 21 cm cosmological signal

The 21-cm line is associated with the transition between the spin singlet and triplet hyperfine states of neutral hydrogen. It provides a powerful probe of the high redshift Universe when, after recombination ($z \simeq 1000$) and prior to reionization ($z \lesssim 10$), the baryon content of the Universe is mostly in the form of neutral hydrogen and helium. The relative abundance of the two hyperfine levels can be parametrized in terms of the spin temperature, $T_{\rm S}$, as: $n_1/n_0 \equiv g_1/g_0 \exp(-\Delta E/T_{\rm S})$ where $g_{1,0}$ are the multiplicities of the two states and $\Delta E = 0.068\,{\rm K} = 2\pi/21\,{\rm cm}$ is the hyperfine splitting. The signal

can be seen as an absorption or emission feature in contrast to the low-energy tail of the CMB spectrum, according to whether the spin temperature is larger or smaller than the CMB temperature at the relevant cosmic time.

Accounting for cosmological redshift, the 21 cm signal from the cosmic intergalactic medium (IGM) can be observed in the frequency band $\nu = 1420/(1+z)\,\mathrm{MHz}$. The global sky averaged signal, observed as a function of the frequency, provides a map of the IGM average spin temperature as a function of time, tracing the cosmic history of neutral hydrogen. Working in the Rayleigh-Jeans limit, where the intensity of radiation is proportional to the temperature of the corresponding source, the amplitude of the signal can be parametrized by the brightness temperature offset [129, 130]:

$$\delta T_b(z) = 27\, x_{\mathrm{HI}} \left(1 - \frac{T_{\mathrm{CMB}}(z)}{T_{\mathrm{S}}(z)}\right) \left(\frac{\Omega_{\mathrm{b}} h^2}{0.023}\right) \left(\frac{\Omega_{\mathrm{m}} h^2}{0.15}\right)^{-1/2} \sqrt{\frac{1+z}{10}}\,\mathrm{mK}\,, \tag{4.1}$$

where x_{HI} is the fraction of neutral hydrogen, very close to 1 before reionization, $T_{\mathrm{CMB}}(z) = 2.73\,(1+z)$ K is the CMB temperature at redshift z and $T_{\mathrm{S}}(z)$ is the spin temperature previously defined.

The spin temperature is set by three competing processes: scattering with CMB photons, collisional coupling of the IGM and interactions with Lyman-α photons from the first stars [129]. The first one tends to couple T_{S} and T_{CMB}, while the other two, if efficient, couple T_{S} with the kinetic temperature of the gas, T_{gas}. The gas temperature traces the CMB temperature until Compton scattering becomes inefficient ($z \sim 200$) and the gas starts to cool adiabatically (*i.e.* $T_{gas} \propto (1+z)^2$). The shape of the global 21-cm cosmic signal is determined by the interplay of these three different processes and by the evolution of the gas temperature. In particular, the presence of an absorption signal is related to the time at which the first stars form and start to recouple the spin temperature to the kinetic temperature of the gas. The IGM can be heated by various astrophysical mechanism among which shock heating and heating from UV and X-rays photons [129]. Dark Matter (DM) annihilations or decays can be an additional source of gas heating which can suppress or erase the absorption signal expected in the 21 cm spectrum. These mechanisms are sensitive to a number of astrophysical parameters and the observation of the global 21 cm cosmic signal is not expected to be sufficient to disentangle the effect of DM from the uncertainty on these parameters [131, 132, 133]. Only a statistical study of the spatial fluctuations of the 21 cm cosmic signal will be able to break the degeneracy.

However, we point out that the observation of an absorption line in the global 21 cm spectrum, at a given redshift, allows one to put conservative constraints on the decay of DM particles which are independent of the astrophysical parameters. Whereas the signal shape and position depend on those parameters, the amplitude of an absorption signal at a given redshift is constrained by the condition $T_{\mathrm{S}}(z) \geqslant T_{\mathrm{gas}}(z)$. Since the astrophysical sources can only heat the IGM, a lower bound on $T_{\mathrm{gas}}(z)$ can be obtained by assuming that its evolution is determined by Compton scattering and adiabatic cooling alone. This results in a conservative bound on the amplitude of the absorption signal as a function of redshift. The presence of DM decays or annihilations can inject energy in

the IGM, heating the gas and resulting in a reduced amplitude of the signal; therefore, the observation of a signal of definite amplitude at a given redshift implies an upper bound on the amount of energy injected in the IGM by DM interactions. The idea to put conservative bounds on energy injection due to annihilation of DM particles has been proposed in [134] (see section 4.1.3 for more details).

Discussion of the assumptions

The EDGES collaboration reported a detection of an absorption signal in the 21 cm spectrum at redshift $z \approx 17$ with amplitude

$$\delta T_{\rm EDGES} = -500^{+200}_{-500}\ {\rm mK}\,, \tag{4.2}$$

with uncertainties at 99% confidence [135].

The discrepancy between the value of the amplitude predicted by standard cosmology ($\delta T_b \gtrsim -200\,{\rm mK}$) and the one observed by EDGES has been at the center of many speculations in the recent literature. Many proposals have been put forward to give a physical explanation of the anomaly: modified cosmological evolution, excess of radiation in the tail of the CMB spectrum or DM-baryon scattering [135, 136, 137, 138, 139, 140].

However, even if the EDGES observation provides evidence for an absorption signal at more than 5σ, the statistical significance of the measurement is not enough to rule out conventional cosmology at the 5σ level. We believe that this result provides a strong evidence for the existence of a signal but it is still not enough to unequivocally establish the need of new physics beyond the standard cosmological scenario.

Therefore, we do not include non-standard sources of cooling of the IGM, excess radiation in the tail of the CMB spectrum or consider the possibility of a modified cosmological evolution. We assume that only standard astrophysical processes are at work and we use the conservative assumption that the signal has an amplitude larger than -100 mK (-50 mK), to derive bounds on the DM lifetime.

Given this assumption, the validity of our results is limited to models that do not provide an enhanced absorption signal. The majority of the DM models present in the literature fulfill this assumption[1].

4.1.2 Bounds on Dark Matter decays

Decays of DM particles inject energy in the Universe at a rate given by:

$$\left(\frac{dE}{dV dt}\right)_{\rm injected} = f_{\rm DM}\rho_{\rm DM,0}\,\tau_{\rm DM}^{-1}(1+z)^3\,, \tag{4.3}$$

where $f_{\rm DM}$ is the fraction of DM that can decay, $\rho_{\rm DM,0}$ is the DM energy density today and $\tau_{\rm DM}$ is the DM lifetime. The injected energy can either be absorbed by the IGM

[1] For a discussion of the features necessary to give an enhanced absorption signal see for instance [141, 142].

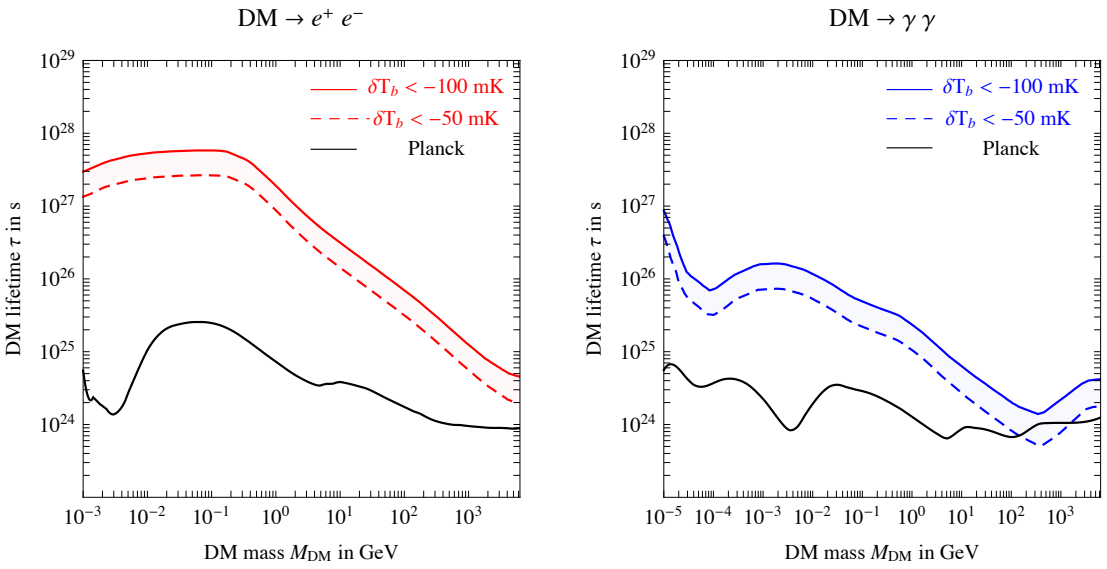

Figure 4.1: *Bounds on DM lifetime assuming decays into electrons (left panel) or photons (right panel). The solid (dashed) red line is obtained requiring that the amplitude of the 21cm absorption signal, including DM decays, satisfies* $\delta T_b < -100\,(-50)\,\mathrm{mK}$ *and assuming a single component DM, i.e. taking* $f_{\rm DM} = 1$*. For comparison we report the bounds derived from observations of the CMB power spectrum* [143, 144].

(through ionization and excitation of hydrogen atoms or heating of the gas) or free-stream until today. The reionization history of the Universe is modified only by the fraction of injected energy that is deposited in the IGM. The energy deposition rate per unit volume is given by:

$$\left(\frac{dE}{dV\,dt}\right)_{\rm deposited} \equiv f(z, M_{\rm DM}) \left(\frac{dE}{dV\,dt}\right)_{\rm injected}, \tag{4.4}$$

where we have defined the energy deposition efficiency $f(z, M_{\rm DM})$. The $f(z, M_{\rm DM})$ functions also depend on the decay channel, however we omit this dependence for the sake of notation.

In the presence of this energy injection the evolution of the hydrogen ionization fraction, $x_e \equiv n_e/n_b$, and the gas temperature, $T_{\rm gas}$, is governed by the following equations[145, 146, 147]:

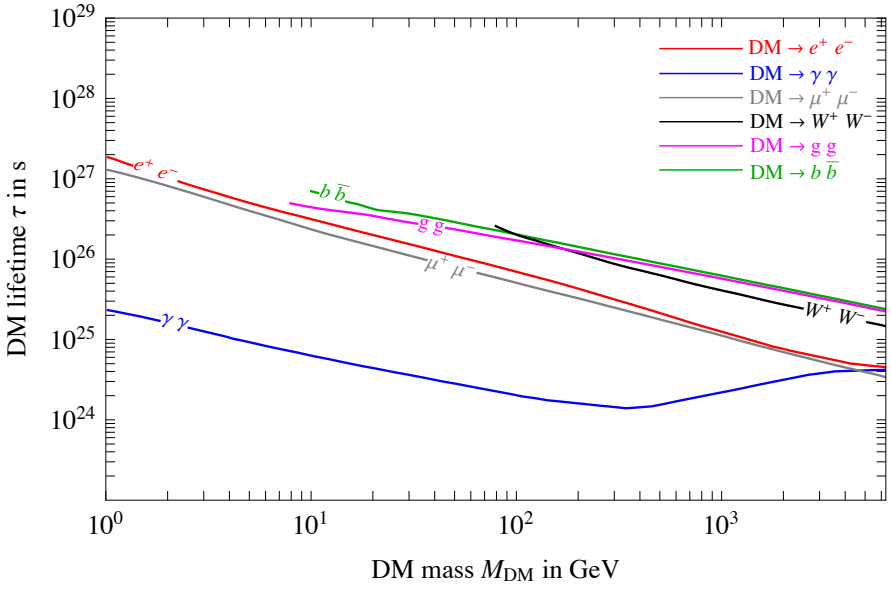

Figure 4.2: *Bounds on DM decaying with a* 100% *branching fraction in different channels. We require* $\delta T_b < -100\,\mathrm{mK}$ *and assume a single component DM,* i.e. $f_{\rm DM} = 1$.

$$\frac{dx_e}{dz} = \frac{\mathcal{P}_2}{(1+z)H(z)}\Big[\alpha_{\rm H}\, n_{\rm H}\, x_e^2\, C - \beta_{\rm H}\, e^{-E_\alpha/T_{\rm CMB}}(1-x_e)\Big] \tag{4.5a}$$
$$- \frac{1}{(1+z)H(z)}\frac{1-x_e}{3n_{\rm H}}\left(\frac{\mathcal{P}_2}{E_0} + \frac{1-\mathcal{P}_2}{E_\alpha}\right)\left(\frac{dE}{dV\,dt}\right)_{\rm deposited}$$
$$\frac{dT_{\rm gas}}{dz} = \frac{1}{1+z}\Big[2T_{\rm gas} - \gamma_{\rm C}\,(T_{\rm CMB}(z) - T_{\rm gas})\Big] + \tag{4.5b}$$
$$- \frac{1}{(1+z)H(z)}\frac{1+2x_e}{3n_{\rm H}}\frac{2}{3\,(1+x_e+f_{\rm He})}\left(\frac{dE}{dV\,dt}\right)_{\rm deposited}.$$

The standard cosmological evolution is encoded in the first line of each equation where $\alpha_{\rm H}$ is the case-B recombination coefficient [148], $\beta_{\rm H}$ the photoionization coefficient, $C \equiv \langle n_e^2\rangle/\langle n_e\rangle^2$ the clumping factor, $E_0 = 13.6\,\mathrm{eV}$ the ground state binding energy of the hydrogen and $E_\alpha = 3/4E_0$ the energy associated with the Lyman-α transition. The Peebles $\mathcal{P}_2$ coefficient gives the probability for a hydrogen atom in the $n = 2$ state to decay in the ground state before being ionized [145]:

$$\mathcal{P}_2 = \frac{1 + K_{\rm H}\Lambda_{\rm H} n_{\rm H}(1-x_e)}{1 + K_{\rm H}\,(\Lambda_{\rm H} + \beta_{\rm H})\,n_{\rm H}(1-x_e)}\,, \tag{4.6}$$

where $\Lambda_{\rm H} \simeq 5.5 \times 10^{-15}\,\mathrm{eV}^2$ is the decay rate for the $2s$ state and $K_H = \pi^2/(E_\alpha^3 H(z))$. The effect of Compton scattering between CMB photons and free electrons is encoded

in the dimensionless coefficient γ_C:

$$\gamma_C = \frac{8\sigma_{\rm T} a_R T_{\rm CMB}^4}{3Hm_e} \frac{x_e}{1+x_e+f_{\rm He}}\,, \tag{4.7}$$

where $\sigma_T \simeq 1.7\times10^3\,{\rm GeV}^{-2}$ is the cross section for Thomson scattering, $a_R \simeq 0.66$ is the radiation constant, m_e the electron mass and $f_{\rm He} \equiv n_{\rm He}/n_b \simeq 0.22$ the number fraction of Helium.

The second line in equations (4.5a)-(4.5b) encodes the effect of energy injection due to DM decays. We followed the "SSCK" prescription, in which a fraction $(1-x_e)/3$ of the deposited energy goes into ionization while a fraction $(1+2x_e)/3n_{\rm H}$ heats the plasma [149, 150]. In the analysis we used the energy deposition functions computed in [151] and assumed a unit value for both $f_{\rm DM}$ and the clumping factor C [149, 152]. The mass dependence of the bounds only enters through the energy deposition functions $f(z, M_{\rm DM})$.

Solving eq.(4.5) and assuming $T_{\rm S} = T_{\rm gas}$ we derive the maximum amplitude for the signal at $z = 17.2$. Requiring that the 21 cm spectrum presents an absorption feature with $\delta T_b < -100\,{\rm mK}$ or $\delta T_b < -50\,{\rm mK}$, as suggested by the EDGES observation, we get the bounds reported in Fig. 4.1 and Fig. 4.2. For DM in the mass range $1\,{\rm MeV} - 10\,{\rm TeV}$ decaying into e^+e^-, our bounds constrain $\tau_{\rm DM} > 10^{25}\,{\rm s}$. This constraint is significantly stronger than the one derived from observations of the CMB power spectrum [143, 144] and competitive with those coming from indirect searches [153, 154]. For the decay channel into photons the bounds become less stringent but still stronger than the ones from CMB. In Fig. 4.2 we report a compilation of bounds in the mass range $1\,{\rm GeV} - 10\,{\rm TeV}$ for different decay channels. For each channel, we use the secondary electron and photon energy spectra provided in [155, 156].

4.1.3 Comparison with the case of DM annihilations

Bounds on DM annihilation coming from the 21 cm line observation have been derived in [134] and are reproduced in Fig. 4.3. In Fig. 4.4 we reproduce the constraints on dark matter annihilation obtained by the Planck collaboration from the measurement of the CMB power spectrum [114].

In the case of DM annihilation the energy deposition rate is given by:

$$\left(\frac{dE}{dV\,dt}\right)_{\rm deposited} = B(z)\, f_{\rm DM}^2 f\left(z, M_{\rm DM}\right) \rho_{\rm DM,0}^2 \frac{\langle\sigma v\rangle}{M_{\rm DM}} (1+z)^6\,. \tag{4.8}$$

We note that for DM annihilations this rate depends on the small-scale inhomogeneities of the matter distribution through the cosmological boost factor $B(z)$. This introduces astrophysical uncertainties (related to our poor knowledge of the halo mass function, DM density profile, etc.) in the bounds on DM annihilations derived using the 21 cm line observation. Conversely, the energy injection rate (4.3) does not depend on the small-scale matter distribution; therefore bounds on the DM lifetime do not contain such astrophysical uncertainties.

Moreover, in the case of DM decays the energy injection scales as $(1+z)^3$ while in the case of DM annihilation it scales as $(1+z)^6$. Therefore, bounds derived observing the 21 cm line (sensitive to processes happening around $z \sim 20$) can improve the ones derived from CMB observables (sensible to processes happening around $z \sim 1000$) much more for DM decays than for annihilations.

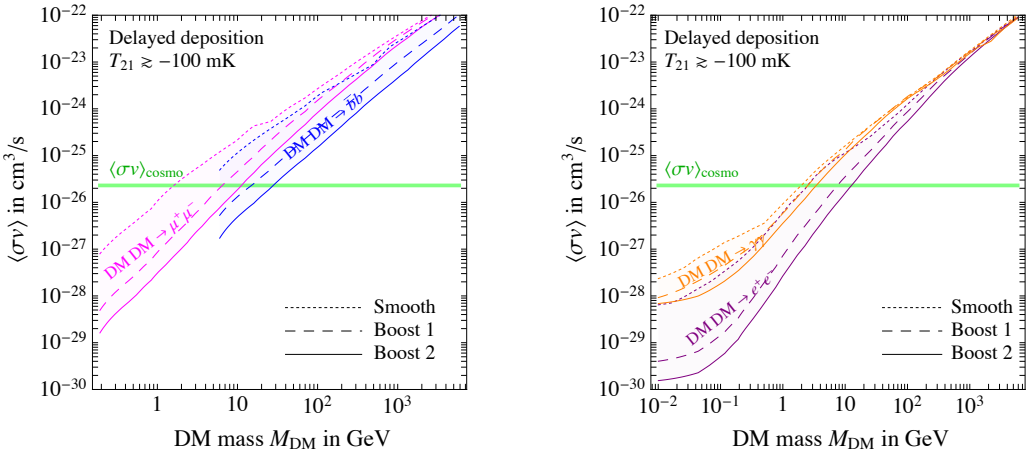

Figure 4.3: *Bounds on DM annihilation cross section into muons and b quarks (left panel) or electrons and photons (right panel) obtained requiring that the amplitude of the 21cm absorption signal, including DM decays, satisfies* $\delta T_b < -100$ mK *and assuming a single component DM, i.e. taking* $f_{\rm DM} = 1$.. *The solid (dashed) lines correspond to different boost factors. Reproduced from* [134].

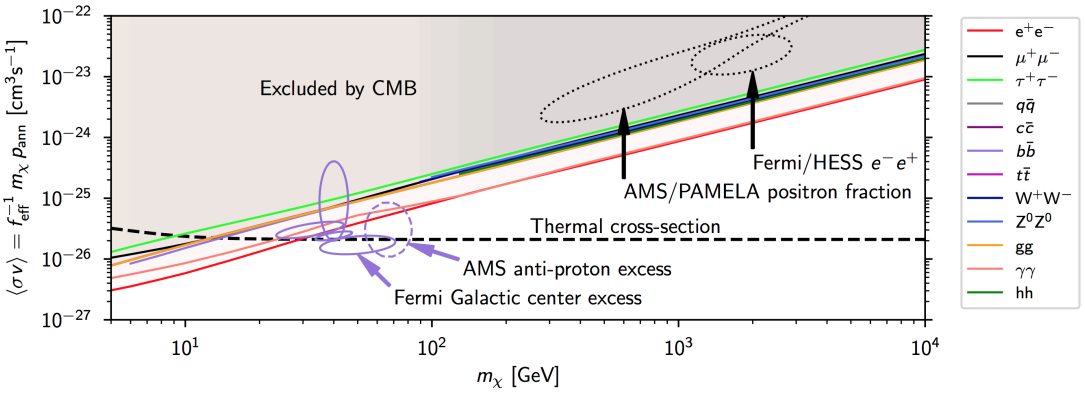

Figure 4.4: *Constraints on the DM mass and annihilation cross section reproduced from the Planck 2018 release [114]. The solid straight lines correspond to different annihilation channels as described in the legend.*

4.2 Indirect searches

Residual annihilations or decays of relic particles can produce cosmic rays and energetic photon signals, tested by indirect detection experiments. Moreover, additional long-lived particles from the dark sector can give rise to astrophysical and cosmological signals. We discuss the constraints derived from this class of observations on the models of Chapter 2 and 3.

4.2.1 Cosmologically long-lived particles

The evolution of the Universe at temperatures below 1 MeV is accurately described by the standard cosmological model starting with Big Bang Nucleosynthesis (BBN) until the current epoch. Decays of long-lived particles during or after BBN can alter this picture and are generally excluded. Strong and robust constraints come in particular from observations of light elements abundances produced during BBN (see [157]) and from the CMB spectrum (see [158, 144]). To comply with these bounds, we require that metastable particles decay before BBN, i.e. we impose $T_{\rm decay} \gtrsim 10\,\text{MeV}$.

In the models of gluequark dark matter this constraint excludes glueballs with a lifetime larger than 1 s, excluding the high-mass thermal region of the V model as shown in Fig. 2.4. However, we note that this bound could be potentially relaxed if glueballs decay through dimension-6 operators in models with Yukawa couplings or through higher loop radiative corrections.

In the model of chiral dark matter the role of cosmologically long-lived particle can be played by the dark photon, if the kinetic mixing parameter ε is sufficiently small. The limit and its phenomenological consequences for the thermal history are discussed in Section 3.5.3.

4.2.2 Gluequark Annihilation and Decay

Models with adjoint fermions of the confining gauge group can give rise to large annihilation signals in the heavy quark regime, *i.e.* when the bare mass of the constituent fermions $M_{\mathcal{Q}}$ is larger then the confinement scale Λ_{DC}. We thus focus on this case in the following discussion on gluequark annihilations.

As discussed in section 2.3.3 (and more extensively in Appendix 2.B), the annihilation can be either direct ($\chi\chi \to n\Phi/\text{SM}$) or mediated by the formation of a $\mathcal{Q}\mathcal{Q}^*$ bound state that subsequently decays ($\chi\chi \to \mathcal{Q}\mathcal{Q}^* \to n\Phi/\text{SM}$). In the former case the annihilation cross section is perturbative (see eq.(2.41)) and, given the relatively high mass of the gluequark, it does not lead to any interesting indirect detection signatures. The latter case, instead, because of the enhanced annihilation cross section, could lead to an interesting phenomenology and it is worth further study.

As discussed in section 2.3.3 and in Appendix 2.B, for angular momenta $\ell \gg 1$ the recombination cross section is of order $\sigma_{\rm rea} \simeq \varepsilon\, 4\pi/\Lambda_{DC}^2$. However, given the small velocities relevant for indirect searches ($v_{\rm rel} \sim 10^{-6}\sqrt{\text{TeV}/M_{\mathcal{Q}}}$ at the CMB epoch and $v_{\rm rel} \sim 10^{-3}$ in our galaxy), the angular momentum of the colliding particles $\ell \sim M_{\mathcal{Q}} v_{\rm rel}/\Lambda_{DC}$

is of order unity in a large region of the parameter space. In this case only s-wave processes take place and $\sigma_{\rm rea} v_{\rm rel}$ rather than $\sigma_{\rm rea}$ is constant. In this regime the value of the cross section is very uncertain, and we chose to estimate it in terms of two benchmark scenarios (see Appendix 2.B.1):

$$\langle \sigma_{\rm ann} v_{\rm rel} \rangle \sim \begin{cases} \dfrac{1}{\Lambda_{DC}^2} \\ \pi R_B^2 \approx \dfrac{\pi}{(\alpha_{\rm DC}^2 M_{\mathcal{Q}}^2)} \,. \end{cases} \tag{4.9}$$

Once formed, the $\mathcal{Q}\mathcal{Q}^*$ bound states de-excite and in general decay into dark gluons, SM gauge bosons or SM fermions. The branching ratios can be derived in terms of the perturbative annihilation cross section of dark quarks into the corresponding final states, see eq.(2.41). In the region of interest $\alpha_{\rm DC} > \alpha_2$ and one finds

$$\mathrm{BR}(GG) \sim 1 + \mathcal{O}\left(\frac{\alpha_2}{\alpha_{\rm DC}}\right), \qquad \mathrm{BR}(WW/\Psi\Psi) \sim \frac{\alpha_2^2}{\alpha_{\rm DC}^2}, \qquad \mathrm{BR}(ZG) \sim \frac{\alpha_2}{\alpha_{\rm DC}}\,, \tag{4.10}$$

where G denotes a dark gluon. For the specific case of the V model, the tree-level decay into SM fermions and ZG is forbidden (the χ_0 has vanishing coupling to the Z) and use of eq.(2.41) thus gives

$$\langle \sigma v_{\rm rel} \rangle_{\chi_0\chi_0 \to WW} \sim \langle \sigma_{\rm ann} v_{\rm rel} \rangle \times \frac{6}{27} \frac{\alpha^2}{\alpha_{\rm DC}^2}\,, \tag{4.11}$$

where the last factor is from the branching ratio of QQ into WW.

Similarly to residual annihilations, decays of the gluequark could give rise to indirect signals. The χ^0 decays mostly to $h\nu$ plus glueballs in the heavy quark regime, and to $h\nu$ or $h\nu + \varphi$ in the light quark regime (see eqs.(2.4),(2.9)). Both glueballs and NGBs in turn decay into SM particles and ultimately the gluequark decay leads to the production of light SM species which can be observed experimentally. Bounds can be avoided, on the other hand, if some mechanism is at work that makes the χ^0 absolutely stable or gives it a much longer lifetime than the one estimated in eq. (2.4) and (2.9).

Figure 4.5 summarizes the constraints in the plane $(\Lambda_{DC}, M_{\mathcal{Q}})$ that arise from experiments probing DM decay and annihilation. The red exclusion regions from DM annihilation have been derived for the two benchmark values of $\langle \sigma_{\rm ann} v_{\rm rel} \rangle$ in eq. (4.9), while the blue ones from DM decay were obtained by setting $\Lambda_{UV}/g_{UV} = \bar{M}_{\rm Pl} = 2.4 \times 10^{18}\,\mathrm{GeV}$ and $f_\chi = 3\Lambda_{DC}/(4\pi)$ when evaluating $\tau_{\rm DM}$ from eqs. (2.4),(2.9). Experimental bounds are given in terms of the DM mass M_χ; in order to translate them into the $(\Lambda_{DC}, M_{\mathcal{Q}})$ plane we set $M_\chi = M_{\mathcal{Q}}$ in the heavy quark regime and $M_\chi = \Lambda_{DC}$ in the light quark regime.

The constraints from DM annihilation are characterized by a large theoretical uncertainty, as one can easily see by comparing the left and right panels in the figure. Resolving such uncertainty would require a precise determination of the recombination cross section, which does not seem an easy task in general due to its non-perturbative

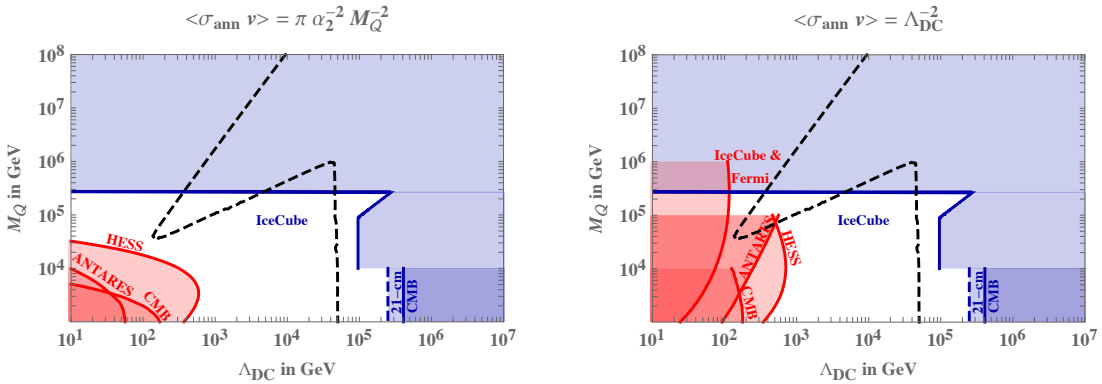

Figure 4.5: *Exclusion limits from experimental searches sensitive to the DM annihilation (red regions) and decay (blue regions). The limits from DM annihilation respectively in the left and right panels have been obtained by adopting the two benchmarks of eq. (4.9), while limits from DM decay were derived by setting* $\Lambda_{UV}/g_{UV} = \bar{M}_{\rm Pl} = 2.4\times10^{18}$ *GeV and* $f_\chi = 3\Lambda_{DC}/(4\pi)$ *in eqs. (2.4),(2.9).*

nature. Also the exclusion curve from DM decay has a sizable theoretical uncertainty, which largely comes from the unknown relation between M_χ and Λ_{DC} in the light quark regime (needed to translate the experimental bounds into the $(\Lambda_{DC}, M_{\mathcal{Q}})$ plane), and from the absence of a calculation of the gluequark decay constant (which controls the size of the DM decay rate and for which we were only able to give an order-of-magnitude estimate). In this case, however, dedicated lattice simulations could determine these quantities and thus drastically reduce the theoretical error on the blue exclusion curves.

The results of Fig. 4.5 stem from three classes of experiments, which are discussed in the following.

Cosmic Rays Experiments

Given the large gluequark mass needed to reproduce the DM relic density in the heavy quark regime, the strongest indirect detection bounds on DM annihilation come from the ANTARES neutrino telescope [159], HESS [160] and the multi-messenger analysis made by the Fermi gamma-ray telescope and IceCube [161]. The bounds can be roughly summarized as follows[2]:

$$\begin{aligned} \langle\sigma_{\rm ann} v_{\rm rel}\rangle &\lesssim 10^{-7}\,{\rm GeV}^{-2} \quad \text{(from ANTARES, HESS)} \\ \langle\sigma_{\rm ann} v_{\rm rel}\rangle &\lesssim 10^{-5}\,{\rm GeV}^{-2} \quad \text{(from Fermi-IceCube)}\,. \end{aligned} \tag{4.12}$$

Indirect searches also place bounds on the lifetime of heavy DM candidates. In the high-mass range, IceCube provides the most stringent bounds [162]. For $M_\chi = (10^5 -$

[2]Here and in eqs. (4.15),(4.17) we omit for simplicity the mild dependence that the bounds have on the DM mass. The exclusion curves of Fig. 4.5 have been obtained by using the exact expressions without performing such approximation.

10^7) GeV, they are roughly given by

$$\tau(\chi^0) \gtrsim 10^{26} \left(\frac{M_\chi}{100\,\text{TeV}}\right)^{3/2} \text{s}\,. \tag{4.13}$$

CMB power spectrum

The energy released by gluequark annihilations and decays around the epoch of recombination modifies the CMB power spectrum. This, similarly to indirect detection experiments, constrains the lifetime and the annihilation rate of the DM. The annihilation cross section is constrained to be smaller than [143]

$$\langle \sigma_{\text{ann}} v_{\text{rel}} \rangle \lesssim 10^{-8} \left(\frac{M_\chi}{100\,\text{GeV}}\right) \text{GeV}^{-2}\,, \tag{4.14}$$

while the limits on the DM lifetime are [144]

$$\tau\left(\chi^0\right) \gtrsim 10^{24}\,\text{s}\,. \tag{4.15}$$

These bounds are slightly less stringent than the ones coming from indirect detection, but have the advantage to be free from astrophysical uncertainties. They are provided for DM masses up to 10 TeV, but are expected to be approximately mass-independent for masses above this value. The CMB bounds shown in Fig. 4.5 have been obtained under this assumption.

21 cm line

While CMB is sensitive to sources of energy injection at the epoch of recombination, the cosmic 21-cm spectrum is sensitive to sources of energy injection during the dark ages. As discussed in section 4.1, the recent observation of an absorption feature in this spectrum, if confirmed and in agreement with standard cosmology, can be used to put bounds on both the lifetime and the DM annihilation cross section. The limit on dark matter annihilation derived by neglecting astrophysical heating sources is of order [134, 128]:

$$\langle \sigma_{\text{ann}} v_{\text{rel}} \rangle \lesssim 10^{-5} \left(\frac{M_\chi}{10\,\text{TeV}}\right) \text{GeV}^{-2}, \tag{4.16}$$

while the one on the DM lifetime is [127, 128, 4]

$$\tau\left(\chi^0\right) \gtrsim 10^{25}\,\text{s}. \tag{4.17}$$

The latter is independent of astrophysical uncertainties on the distribution of DM.

As for the case of the CMB, these bounds are provided up to $M_\chi = 10\,\text{TeV}$ and to obtain Fig. 4.5 we assumed that they are constant at higher masses. Differently from the previous case, however, this assumption is not completely justified and further studies are needed to provide solid bounds in the high-mass range.

4.2.3 Chiral dark matter annihilation signals

In the chiral dark matter scenario, the dominant dark matter candidate for $\alpha_D \lesssim 0.4$ is a singlet dark pion with an ordinary thermal relic abundance set by annihilations in dark photons, which decay to SM particles through the kinetic mixing.

Observations of the positron and antiproton flux rates by AMS-02 can provide strong limits on DM annihilations in the parameter space of our model. However, these constraints are subject to large uncertainties associated with cosmic ray propagation and the estimate of astrophysical backgrounds, and for this reason we will not use them in the following.

The observation of gamma ray signals from clean DM-dominated environments, such as dwarf spheroidal galaxies, can also set stringent bounds provided that DM annihilations produce a large flux of photons. In our case, the dark matter mostly consists of SM-singlet dark pions that annihilate into dark photons. The dark photons decay in flight to SM final states. We do not attempt here a detailed analysis and a computation of the produced photon spectrum. We use the bounds of Ref. [163] on dark matter annihilations to short-lived mediators with mass $m_{\rm mediator} \sim m_{\rm DM}$, obtained from the recast of the FERMI-LAT results of Ref. [164]. Since dark photons decay to hadronic final states with a large branching ratio [165], we make use of the bounds that assume fully hadronic decays of the mediators. In most of the parameter space of our model, the dark pion and the dark photon have comparable mass and effects from Sommerfeld enhancement and bound state formation are negligible (see however the discussion in Sec. 3.5.5). With this assumption, we find that the measured flux of gamma rays from dwarf spheroidal galaxies of Ref. [164] excludes masses $m_1 \lesssim 100\,\text{GeV}$. [3] This limit is expected to improve in the future thanks to the discoveries of new dSphs galaxies from LSST combined with continued Fermi-LAT observations [166], reaching masses $m_1 \lesssim 400\,\text{GeV}$.

For completeness we have also analyzed the CMB limits on dark matter annihilation from the 2018 Planck release [114], that are less stringent but have independent uncertainties. We find that these data exclude masses $m_1 \lesssim 10\,\text{GeV}$.

In the future, the Cherenkov Telescope Array (CTA) observatory will start probing thermal dark matter in the TeV mass range through observations of the Galactic Center. Assuming an Einasto dark matter profile, the expected sensitivity [121] for thermal dark matter candidates is in the range $400\,\text{GeV} \lesssim m_1 \lesssim 10\,\text{TeV}$. CTA will thus be able to probe a large part of the parameter space relevant for the dark matter models presented in this work.

[3] This result is valid both if dark pions have a thermal abundance (hence they do not reproduce the observed DM density in generic points of the parameter space), and if they have the observed DM abundance (hence in general they are not thermal relics). In the latter case, an additional portion of the parameter space can be excluded.

4.3 Direct detection searches

4.3.1 Gluequark

From the point of view of DM direct detection experiments, where the momentum exchanged is less than 100 KeV, the gluequark behaves as an elementary particle with the same electroweak quantum numbers as the constituent quark. The main difference from elementary candidates with same quantum numbers is that the relic abundance is not controlled by the electroweak interaction, leading to a different thermal region.

For a triplet of SU(2) the spin-independent cross-section is $\sigma_{\rm SI} = 1.0 \times 10^{-45}\,{\rm cm}^2$, which is below the neutrino floor for masses $M_\chi > 15$ TeV. For an SU(2) doublet tree-level Z-mediated interactions induce a spin-independent cross section on nucleons $\sigma_{\rm SI} \approx 10^{-40}\,{\rm cm}^2$, which is ruled out for $M_\chi \lesssim 10^8\,{\rm GeV}$ [94]. Dark quark masses large enough to make the doublet model viable can be obtained only in the scenario where $T_R = \Lambda_{DC}$, while the scenario with $T_R = T_D$ is ruled out (see Appendix 2.C for more details).

4.3.2 Chiral DM

The elastic scattering of dark matter particles on nuclei gives rise to recoil signals that are being looked for in dedicated high-precision experiments. For values of ε large enough, the main contribution to the elastic cross section comes from the tree-level exchange of the Z and the dark photon. This is spin independent in the non-relativistic limit and strongly constrained by conventional direct-detection experiments. We performed a calculation valid for arbitrary values of ε and of the vector boson masses[4]. We find that, once the non-relativistic limit is taken, the spin-independent cross section per nucleon has a very simple form:

$$\sigma_{\pi N}^{\rm S.I.} = \varepsilon^2 \frac{\mu_{\pi N}^2}{\pi} \frac{Q_D^2 e^2 \cos^2\theta_W}{m_{\gamma_D}^4} \left(\frac{Z}{A}\right)^2 + \mathcal{O}\left(\frac{|\vec{p}|^2}{m_{Z,\gamma_D}^2}\right), \tag{4.18}$$

where $Q_D = (1+a)e_D$ for dark pions, θ_W is the weak mixing angle, Z, A are respectively the atomic and mass number of the target nuclei, e is the electromagnetic coupling, and $\mu_{\pi N}$ is the reduced mass of the dark matter-nucleon system. Up to higher-order corrections in the momentum expansion, dark matter particles interact only with protons (i.e. the contribution from scattering off neutrons vanishes), and the result scales as ε^2. Our formula is valid for generic models where the dark matter is a Dirac fermion or a complex scalar that couples with charge Q_D to kinetically-mixed dark photons or Z' bosons[5]. It agrees with the result of Ref. [48] and with previous literature on dark photons, see for example Refs. [123, 167, 125]. We checked the correctness of Eq. (4.18) by performing the calculation in two different ways: first, by diagonalising the kinetic and

[4] Our result is valid also in the case of mass resonance $m_Z = m_{\gamma_D}$. We assume that the on-shell dark photon mass is larger than the typical momentum exchanged.

[5] Notice that the spontaneous breaking of $\mathrm{U}(1)_D$, which is a direct coinsequence of its being chiral, leads to modified quartic interactions which are however not relevant for the tree-level cross section.

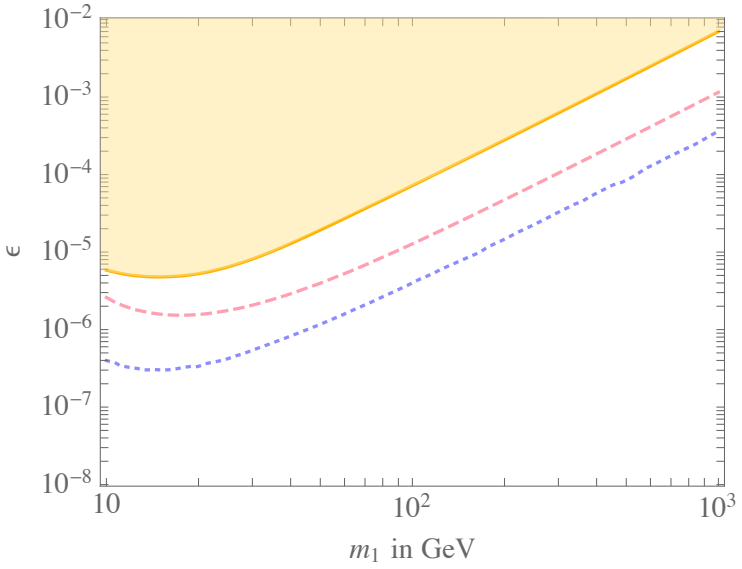

Figure 4.6: Direct detection bounds on the kinetic mixing parameter ε as a function of the dark matter mass m_1. We set $a = 1/2$ and fixed α_D such that the thermal relic abundance of dark pions reproduces the correct DM density. The solid yellow line corresponds to the spin-independent bound set by Xenon1T, while the pink dashed and purple dotted lines are respectively the projected sensitivity of the LZ experiment and the neutrino floor.

mass terms and deriving the modified couplings reported in Appendix 3.D; second, by working in the non-diagonal basis and computing the propagators including gauge-boson mixing. Both methods agree and give the simple result of Eq. (4.18).

An additional contribution to the elastic scattering of dark pions off nuclei comes from effective operators generated by loops of NGB triplets. Those of Eq. (3.47), for example, arise at the 1-loop level and mediate the DM scattering through 1-loop diagrams. Other operators like $\pi^\dagger i\overleftrightarrow{\partial}_\mu \pi J^\mu_{SM}$, where J^μ_{SM} is a SM quark or Higgs current, are generated at two loops and mediate the DM scattering at tree level. Using the analysis of Ref. [168], we estimate that the effect of any of these operators in our model is too small to be detected and does not lead to any bound.

We thus focus on the scattering of dark pions mediated by the Z and the dark photon, and use Eq. (4.18) to derive the constrains from direct-detection experiments in the (ε, m_1) plane. For the mass range of interest, the strongest bounds currently come from Xenon1T [94], while PandaX-II [169] and LUX [170] give comparable though weaker limits. We show the corresponding exclusion curve in Fig. 4.6, together with the projected sensitivity of the future LZ experiment [171] and the neutrino floor curve. We focus on dark pion masses up to 1 TeV, as already for $m_1 \sim 10$ TeV dark baryons contribute significantly to the relic density and deriving an accurate bound would require knowing precisely their fraction. Notice also that the data of Ref. [94] extend up to 1 TeV, though

a linear extrapolation to higher masses can be done in presence of a single component of dark matter.

4.3.3 Limits on charged relics

The theories of chiral dark matter of Chapter 3 with odd N_{DC} contain dark baryons with weak isospin equal to 1/2 and 3/2 and with zero hypercharge, thus carrying half-integer (i.e. non-vanishing) electromagnetic charge. Due to their accidental stability, the dark baryons form an electrically-charged subdominant component of the thermal relic abundance. We denote this charged dark matter component as cDM in the rest of this paragraph.

Even though the cDM fraction can be parametrically suppressed, this scenario is subject to very stringent constraints. The analysis of Refs. [172, 173] makes use of CMB data to derive limits on the fraction of charged relics, but assumes that the Compton scattering of these particles is negligible. While this is a good approximation in the case of milli-charged dark matter, it is not so in our theories, where the cDM-baryon scattering is efficient. Therefore, the bounds of Refs. [172, 173] cannot be applied in our scenario. On the other hand, cosmic rays with order-one charge can produce ionization signals that can be detected by experiments looking for ionizing particles. Bounds on charged stable particles with $q \sim |e|$ are subject to uncertainties in the mass window $(10^5 - 10^{11})\,\text{GeV}$, due to the large impact that supernovae shock waves can have on their galactic and momentum distribution (see for instance Refs. [174] and [175]). In our theories, however, dark baryons are thermal relics and there is an upper bound on their mass of order $10^5\,\text{GeV}$. For these values of masses, uncertainties should be under control. The analysis of Ref. [175] constraints the mass fraction of charged relics to be extremely small: $\Omega_{\text{cDM}} \lesssim (10^{-10} - 10^{-14})\,\Omega_{\text{DM}}$, depending on the experiment and on the mass. Combining this result with the collider bounds of sec. 4.5 excludes the whole parameter space of interest for models of chiral dark matter with odd N_{DC}.

4.4 Collider searches for gluequark models

Models of gluequark dark matter with fermions in the adjoint representation of a confining dark gauge group feature a rich spectrum of states which, in principle, one would like to study at colliders.

The lightest states in the spectrum, with mass given by eq.(2.8), are the NGBs from the $\text{SU}(N_F) \to \text{SO}(N_F)$ global symmetry breaking in the light quark regime. In the case of the V model, the five NGBs form a multiplet with weak isospin 2, and one expects $m_\varphi \gtrsim \Lambda_{DC}/5$. The phenomenology of a quintuplet of NGBs was studied recently in Ref. [28]. These states are pair produced at hadron collider in Drell-Yan processes through their electroweak interactions, and decay to pairs of electroweak gauge bosons through the anomalous coupling

$$\frac{2N_{DC}}{\sqrt{3}}\frac{\alpha_2^2}{4\pi}\frac{\varphi_{ab}}{f}W^a_{\mu\nu}\tilde{W}^{b\,\mu\nu}\,. \tag{4.19}$$

A promising discovery channel studied by Ref. [28] is $pp \to \varphi^0\varphi^\pm \to 3\gamma W^\pm$; the doubly charged states decay into same-sign W pairs and are somewhat more challenging to see experimentally. The LHC has an exclusion reach up to TeV masses, while a 100 TeV collider would test the light quark scenario approximately up to 5 TeV. In this regime colliders could start probing the thermal region.

The lightest states in the heavy quark regime are the glueballs. They couple to the SM only through higher-dimensional operators, and are rather elusive at colliders. In models without Yukawa couplings, where interactions with the SM occur through dimension-8 operators, the production cross section via vector boson fusion (VBF) or in association with a SM vector boson is too small to observe a signal in current or future colliders (for example, the VBF cross section at a 100 TeV collider is of order $\sigma(pp \to \Phi + jj) \lesssim 10^{-9}\,\text{fb}$ for $M_{\mathcal{Q}}/\Lambda_{DC} = 10$ and $M_\Phi > 500\,\text{GeV}$). In models with Yukawa couplings, such as the one described in section 2.C, the glueballs mix with the Higgs boson through the dimension six portal

$$\mathcal{L} \supset cN_{DC}\frac{y^2}{16\,\pi^2}\frac{g_{\text{DC}}^2}{\Lambda_{\text{UV}}^2}\mathcal{G}_{\mu\nu}^2|H|^2 \tag{4.20}$$

and production via gluon-fusion becomes also possible. While this leads to larger cross sections, the corresponding rate is too small to see a signal at the LHC and even high-intensity experiments like SHiP can only probe light glueballs in a region of parameter space that is already excluded by EW precision tests [25]. The single glueball production cross section at a 100 TeV hadronic collider is shown in figure 4.7, for glueballs heavier than 70 GeV. Lighter glueballs can be pair produced in the decay of on-shell Higgs bosons and their possible detection at future colliders has been studied for instance in Ref. [176].

Mesons can give interesting signatures in both light and heavy quark regimes. Bound states made of a pair of dark quarks, QQ, can be singly produced through their EW interactions. While the production of spin-0 mesons is suppressed since they couple to pairs of EW gauge bosons, spin-1 resonances mix with the SM gauge bosons of equal quantum numbers and can be produced via Drell-Yan processes. In the narrow width approximation the cross section for resonant production can be conveniently written in terms of the decay partial widths as

$$\sigma(pp \to QQ) = \frac{(2J_{QQ}+1)D_{QQ}}{sM_{QQ}}\sum_{\mathcal{P}} C_{\mathcal{P}\mathcal{P}}\Gamma(QQ \to \mathcal{P}\mathcal{P})\,, \tag{4.21}$$

where D_{QQ} is the dimension of the representation, J_{QQ} the spin, $\mathcal{P}$ the parton producing the resonance and $C_{\mathcal{P}\mathcal{P}}$ are the dimension-less parton luminosities.

In the heavy quark regime the QQ bound state is perturbative and its decay width can be computed by modelling its potential with a Coulomb plus a linear term. For $\alpha_{\text{DC}}M_{\mathcal{Q}} > \Lambda_{DC}$ the decay width of the lowest-lying s-wave bound states scales as

$$\Gamma(QQ \to \mathcal{P}\mathcal{P}) \sim D_{QQ}\alpha_{SM}^2\alpha_{\text{DC}}^3 M_{\mathcal{Q}}\,, \tag{4.22}$$

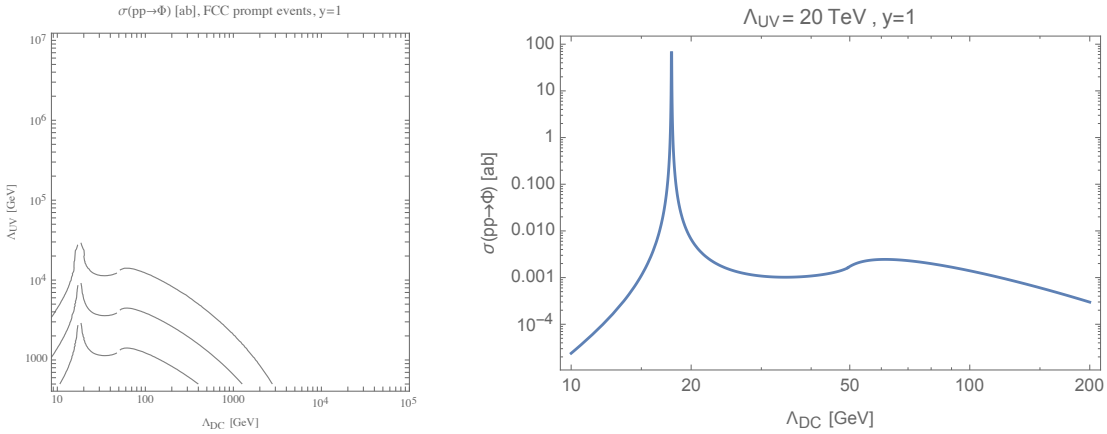

Figure 4.7: *Single glueball production cross section though gluon fusion in models with dimension 6 portal, equation* (4.20)*. Left: isocurves corresponding to a cross section of* 0.01*,* 1 *and* 100 ab *at a* 100 TeV *collider. Right: Single glueball production cross section at a* 100 TeV *collider as a function of the confinement scale for a fixed UV scale of* 20 TeV*, related to the mass of the heavy fermions with Yukawa interactions.*

.

where $\alpha_{\rm DC}^3$ originates from the non-relativistic Coulombian wave-function. When $\alpha_{\rm DC} M_{\mathcal{Q}} < \Lambda_{DC}$, the effect of the linear term in the potential becomes important and eq.(4.22) gets modified; since confinement enhances the value of the wave function at the origin, the width becomes larger in this regime. Using the Coulombian approximation thus provides conservative bounds. Explicit formulas for the rates are found in [25]. For example, in the V model the decay width of the s-wave spin-1 QQ resonance (isospin 1 in light of the Majorana nature of V) into a left-handed fermion doublet is

$$\Gamma^{(n)}\left(QQ^{J=1}_{I=1} \to f\bar{f}\right) = (N_{\rm DC}^5 - N_{\rm DC}^3)\frac{\alpha_2^2\alpha_{\rm DC}^3}{24n^3} M_{\mathcal{Q}}\,, \tag{4.23}$$

where n refers to the radial quantum number. The tiny energy splitting between levels is irrelevant at colliders and the total rate is dominated by the lowest-lying Coulombian ones. The branching ratio into pairs of leptons is about 7% and the strongest bounds currently arise from searches of spin-1 resonances at the LHC decaying into electrons and muons. We show the limits in the left plot of Fig. 4.8 and find that the LHC excludes masses up to $2 - 3.5\,$TeV depending on the ratio $M_{\mathcal{Q}}/\Lambda_{DC}$ (or equivalently on the value of $\alpha_{\rm DC}(M_{\mathcal{Q}})$).

In the light quark regime the lightest spin-1 state is the ρ meson with mass $M_\rho \sim \Lambda_{DC}$.

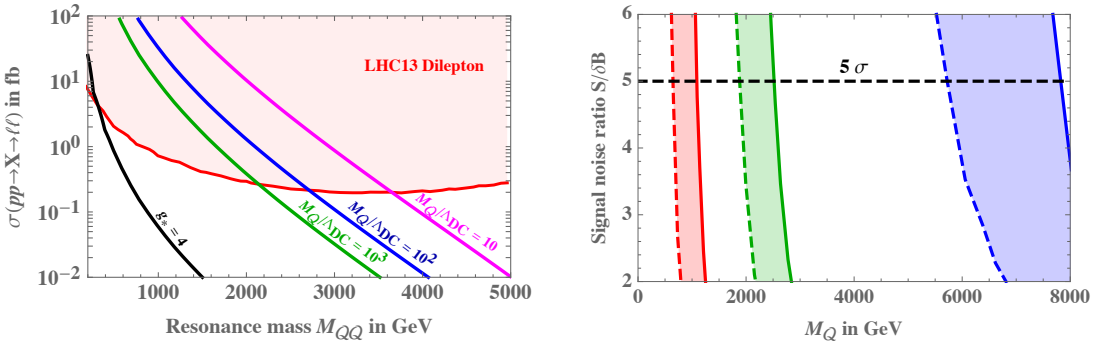

Figure 4.8: *Left: ATLAS bounds on the cross section for the direct production of a spin-1 QQ resonance decaying into muons and electrons [177]. Right: Estimated reach on gluequark pair production obtained by recasting the limits of Ref. [178] from disappearing tracks searches at the HL-LHC (red), the HE-LHC (green) and a* 100 TeV *collider (blue). The solid (dashed) lines assume a* 20% *(*500%*) uncertainty on the background estimate.*

.

The widths scale as [179]

$$\begin{aligned} \Gamma(\rho \to \varphi\varphi) &\sim \frac{g_*^2}{8\pi} M_\rho \\ \Gamma(\rho \to f\bar{f}) &\sim \alpha_{SM}^2 \left(\frac{4\pi}{g_*^2}\right) M_\rho \,, \end{aligned} \tag{4.24}$$

where g_* characterizes the interaction strength among bound states. For moderately large g_*, as suggested by large-N_{DC} counting $g_* \sim 4\pi/\sqrt{N_{DC}}$, the decay into light NGBs dominates while final states with leptons are suppressed. It thus follows a weaker bound than in the heavy quark regime, as illustrated in Fig. 4.8 for $g_* = 4$.

Gluequarks can also be pair produced at colliders through their EW interactions. In the heavy quark regime the energy threshold is much higher than the confinement scale and quarks are produced in free pairs. Because dark quarks are in the adjoint representation of dark color, when they get separated by a distance of $O(1/\Lambda_{DC})$ they hadronize producing color singlets that fly through the detector. On the contrary, dark quarks in the fundamental representation would not be able to escape, leading to quirks/hidden valley phenomenology [180, 181, 25]. The phenomenology of the open production is then identical to the one of an elementary electroweak multiplet except that the cross-section is enhanced by the multiplicity of the dark color adjoint representation, i.e. $N_{\rm DC}^2 - 1$ for SU($N_{\rm DC}$). Such an enhancement factor is not present for gluequark pair production near threshold in the light quark regime. In general, an electroweak triplet can be searched for in monojet and monophoton signals or disappearing tracks, the latter being more constraining. We derived the reach of the high-luminosity LHC (HL-LHC), the high-energy LHC (HE-LHC) and the proposed 100 TeV collider by recasting the results

of Ref. [178] for the V model in the heavy quark regime, see the right plot of Fig. 4.8. We find that the HL-LHC could discover gluequark triplets up to $\sim 600\,\text{GeV}$ while a $100\,\text{TeV}$ collider could reach $\sim 7\,\text{TeV}$. Such bounds are typically weaker than the ones from the production of QQ spin-1 resonances decaying to leptons.

4.5 Collider searches for models of chiral dark matter

The dark sector of the chiral dark matter model of Chapter 3 can be probed at high-energy colliders through SM gauge interactions in a way that is complementary to direct and astrophysical searches. Unlike kinetic mixing, whose effects strongly depend on the value of ε, a gauge portal to the SM does not introduce any unknown couplings, therefore providing sharper predictions. For values of the dark confinement scale under consideration, the production of the lightest SM-charged particles in the model is within the reach of the LHC or of one of its future extensions. In the rest of this section, we will be concerned with the analysis of the constraints arising from existing collider data and comment on the expected sensitivity at a Future Circular Collider (FCC). Given the rich phenomenology predicted by our model at colliders, our study should be considered as an exploratory one, to be completed in a future work. See Refs. [28, 29] for related studies.

4.5.1 Production and decays of NGB triplets

In the model with $\text{SU}(2)_{EW}$ doublets, the most promising process to probe the dark sector at colliders seems to be pair production of the NGB triplets; singlets couple either through ε or via non-renormalizable operators, and their direct production cross section is correspondingly suppressed. Triplets can be pair produced either via a Drell-Yan process or resonantly through the decay of a spin-1 dark meson. Since $m_\rho \sim 7\, m_\pi$ in our model, the latter contribution is subdominant and will be neglected in the following. For Drell-Yan production, the spin and color-averaged partonic cross sections at leading order are given in Eqs. (3.62)-(3.64) of Appendix 3.A. The corresponding hadronic cross sections have been obtained by convoluting those expressions with the 2014 MMHT parton distribution functions (PDFs) [182], and the result is shown in Fig. 4.9. Once produced, the triplets are generally unstable and decay as shown in Tab. 4.1, where for illustration purposes we set $m_1 = 2m_{\gamma_D}$. Broadly speaking, one can distinguish two main regions of parameter space exhibiting different phenomenologies: if $m_3 > m_{\gamma_D}$, then (all) the neutral triplets decay by emitting dark photons, otherwise they decay to SM particles. We shall refer to these as the normal and inverted hierarchies respectively. While the singlets always escape detection and are recorded as missing energy, the signature of the dark photons produced in the final state depends on their lifetime, which is a function of ε. In the case of an inverted hierarchy, the $3_0'$ is also long lived for small ε. One can thus distinguish four kinds of possible experimental signatures characterizing the final state:

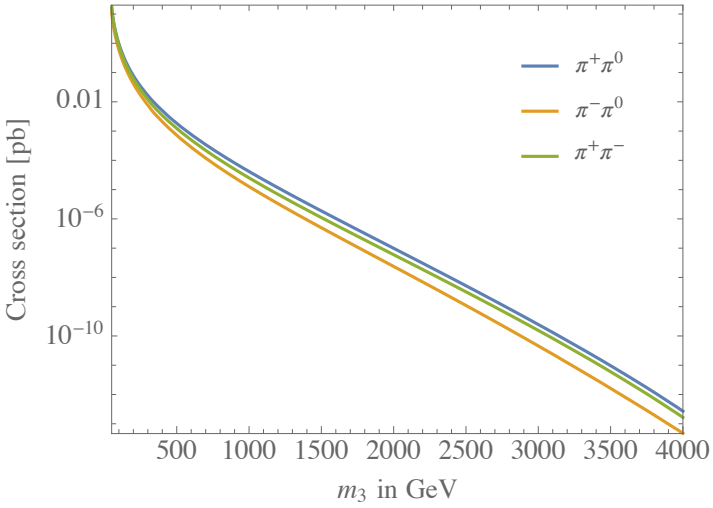

Figure 4.9: Leading-order cross section for $\pi^+\pi^0$ (blue), $\pi^-\pi^0$ (orange) and $\pi^+\pi^-$ (green) pair production at the 13 TeV LHC, where $\pi^{\pm,0}$ denotes any of the NGB triplets with electromagnetic charge indicated by the superscript.

- **Missing Energy:** For very small ε the dark photons decay outside the detector and, together with the NGB singlets, give rise to missing energy in collider events. The signatures in this case are similar to those of Supersymmetric models (where decaying charginos play the role of the triplets), and SUSY searches can be exploited to derive bounds on our scenario.

- **Displaced vertices:** In a large portion of parameter space, for small ε, the γ_D and $3_0'$ can decay inside the detector far from the interaction point. Due to the extremely low background, events with such displaced vertices lead to the strongest constraints in the region of the parameter space where they apply.

- **Disappearing tracks:** For $\varepsilon \lesssim 3 \times 10^{-6}(2m_3/m_1)^{3/2}(1\,\text{TeV}/m_1)^{1/2}$ and in the case of an inverted hierarchy, the electromagnetically-charged components of $3_0'$ mostly decay into the neutral one by emitting a soft pion. The latter goes undetected at high-energy colliders and the decaying particle manifests itself as a disappearing track. The same signature characterizes minimal DM models.

- **Prompt resonant decays:** For large ε, dark photons decay promptly in the detector and can be reconstructed as peaks in the invariant mass spectrum of jet or lepton/anti-lepton pairs. A similar resonant signature comes from the decays of 3_0's in the case of inverted hierarchy. Traditional searches for Z' resonances can be exploited in this case to set constraints on our model.

$m_3 < m_{\gamma_D} = m_1/2$	$m_3 < 2m_{\gamma_D} = m_1$	$m_3 > 2m_{\gamma_D} = m_1$	$m_3 > \sqrt{3}m_1$
$3_\pm \longrightarrow 1_\pm\, V$	$3_\pm \longrightarrow 1_\pm\, V$	$3_\pm \longrightarrow 1_\pm\, V$	$3_\pm \longrightarrow 1_\pm\, V\,(\gamma_D\gamma_D)$
$3_0 \longrightarrow \bar{f}f/VV/Vh$	$3_0 \longrightarrow \bar{f}f/VV/Vh$	$3_0 \longrightarrow V\ \gamma_D\,\gamma_D$	$3_0 \longrightarrow V\ \gamma_D\,\gamma_D$
$3_0' \longrightarrow V\,\bar{f}f$	$3_0' \longrightarrow V\,\gamma_D$	$3_0' \longrightarrow V\,\gamma_D$	$3_0' \longrightarrow V\,\gamma_D$
$3_0'^{\pm} \longrightarrow 3_0'^{0}\pi^\pm$			

Table 4.1: Main triplet decay modes in the various kinematic regimes, assuming $m_1 = 2m_{\gamma_D}$. Here V can be any electroweak gauge boson, depending on the electromagnetic charge of the initial triplet, h is the Higgs boson, while $\bar{f}f$ denotes a pair of SM fermions. In the case of inverted hierarchy, decays among different components of the $3_0'$ become important for ε small, when the rate of $3_0' \to V\,\bar{f}f$ is suppressed.

In order to illustrate the relative importance of these signatures in testing our model, we anticipate the results of the analysis performed in the next section and show in Fig. 4.10 the bounds in the (ε, m_3) plane for fixed ratios of the masses. We find that displaced decays can give the strongest bounds, followed by prompt resonant decays. The limits set by each of the different experimental signatures are in fact similar in strength, despite the different strategies and backgrounds involved. This can be understood as the result of the strong dependence of the production cross section on the triplet mass, mostly due to the scaling of the proton PDFs. The bounds we obtain are not far from the value of m_3 at which the number of signal events becomes of order unity, i.e. from the strongest obtainable bound. For this reason, although our analysis makes use of many simplifying approximations, we believe that its results give a good estimate of the actual constraints.

4.5.2 Bounds

In this section we derive the bounds on the triplet mass from each of the signatures discussed above, using data from ATLAS and CMS. For both dark photon and triplet decays, the final yields of leptons and hadrons are of the same order of magnitude but, except for displaced vertices, hadronic events have always a much higher background. For this reason, when analyzing missing energy events and searches for promptly-decaying resonances we shall concentrate on final states containing electrons or muons.

The 3_0 decays promptly into a pair of SM particles if $m_3 < 2m_{\gamma_D}$, while the dark photon will do so for large ε. Thus, both particles may be observed as resonances in the mass spectrum of the final products. Traditional Z' searches provide almost model-independent bounds on the production cross section times the branching ratio. It is then simple to recast these bounds into constraints on our model by inverting the triplet production cross section computed in the previous section. [6] Figure 4.11 shows the constraints set in the (m_1, m_3) plane by the searches performed by the CMS collaboration into leptonic channels [183, 185]. A similar search performed by ATLAS

[6] Although the limits from Z' searches are strictly valid for spin-1 resonances only, we shall apply them

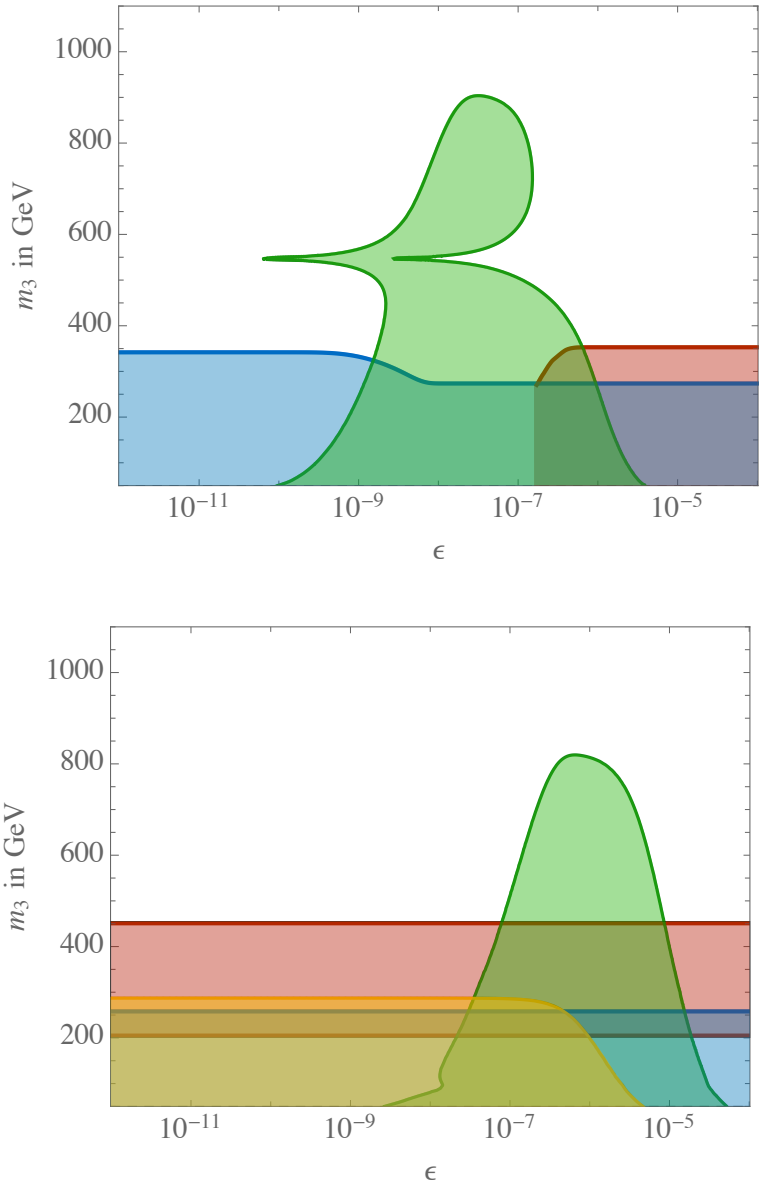

Figure 4.10: Exclusions from four different kinds of collider searches as a function of ε: missing energy events (blue region), displaced decays (green region), resonant decays to jet or lepton pairs (red region), and disappearing tracks (yellow region). The top panel assumes $m_3 = 3\,m_1$ (normal hierarchy), while in the bottom panel $m_3 = m_1/3$ (inverted hierarchy). Both plots are done setting $m_1 = 2\,m_{\gamma_D}$. The sharp cut-off of the bound from resonant decays at $\varepsilon \sim 2 \times 10^{-7}$ in the top panel is due to a lower bound on the dark photon mass imposed in the experimental analysis of Ref. [183]. The bound from disappearing tracks has been derived from the analysis of Ref. [184].

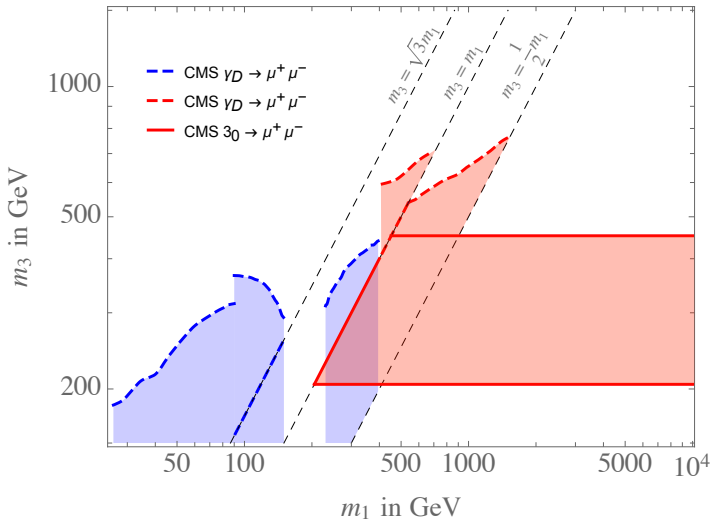

Figure 4.11: Bounds from the Z' searches of Refs. [183, 185] for $m_1 = 2m_{\gamma_D}$ (corresponding to $a \simeq 1/2$ at $N_{DC} = 4$). The plane is divided into different kinematic regions (see Tab. 4.1) by the gray thin dashed lines, inside which each constraint is valid. While exclusions denoted by continuous lines correspond to the decays of the 3_0 and are valid for arbitrary values of ε, dashed curves refer to γ_D decays and only apply for $\varepsilon \gtrsim 10^{-7}$, i.e. when dark photons decay promptly.

in Ref. [186] sets slightly weaker bounds. Depending on the ratio m_1/m_3, the bounds come from the decays of the γ_D (if ε is large), the 3_0 or both. If the decaying particle is a dark photon, its mass scales proportionally to that of the singlet, and this explains why the bounds grow quickly with m_1 (the background decreases with the mass of the decaying particle). The bounds from the decays of 3_0, instead, are horizontal lines in the (m_1, m_3) plane. Although the same analysis can be carried out with jets as final states, the corresponding bounds are weaker by at least one order of magnitude, because the slightly higher branching ratios are not able to compensate for the larger background (see for example Refs. [187, 188, 189]).

Recasting the bounds from missing energy searches at the LHC is not as simple as for resonant decays. This signature is common to many supersymmetric scenarios, and the data are usually interpreted as limits on the masses and couplings of the various SUSY particles, in a way that depends explicitly on the details of the model. To give an estimate of the bounds on our model, it is then simpler to take a step back and compare the total number of observed events with the theoretical prediction. [7] The number of

also to the scalar 3_0.

[7] A more refined analysis should take into account the distribution of the number of events with respect to the relevant kinematic variables, such as the transverse missing energy. This requires detailed

signal events is schematically modelled as

$$N_s(m_1, m_3, \varepsilon) = \mathscr{L} \sum_i \sigma_{pp\to(\pi\pi)_i}(m_1, m_3) BR((\pi\pi)_i \to f) P(m_1, \varepsilon)\, \delta_{eff}, \tag{4.25}$$

where $\mathscr{L}$ is the integrated luminosity and the sum runs over $(\pi\pi)_i = 3_0 3_0, 3'_0 3'_0, 3_+ 3_-$ with all possible combinations of electromagnetic charges. The branching ratios $BR((\pi\pi)_i \to f)$ are given in Tab. 4.2 for the final states f of interest in the case of a normal hierarchy. The factor $P(m_{\gamma_D}, \varepsilon)$ corresponds to the probability that the decay of the γ_D or $3'_0$ hap-

Production mode	Primary decay products	Final decay products	B.R.
$3_0^0\, 3_0^\pm$	$4\gamma_D\, Z\, W^\pm$	$4\gamma_D\, \ell_1^+\, \ell_1^-\, \ell_2^\pm\, \overset{(-)}{\nu}_2$	1.7%
$3_0^0\, 3_0^\pm$	$4\gamma_D\, \gamma\, W^\pm$	$4\gamma_D\, \ell^\pm\, \overset{(-)}{\nu}\, \gamma$	6.4%
$3_0^+\, 3_0^-$	$4\gamma_D\, W^- W^+$	$4\gamma_D\, \ell_1^-\, \nu_1\, \ell_2^+\, \nu_2$	3.2%
$3_0'^0\, 3_0'^\pm$	$2\gamma_D\, Z\, W^\pm$	$2\gamma_D\, \ell_1^+\, \ell_1^-\, \ell_2^\pm\, \overset{(-)}{\nu}_2$	1.7%
$3_0'^0\, 3_0'^\pm$	$2\gamma_D\, \gamma\, W^\pm$	$2\gamma_D\, \gamma\, \ell^\pm\, \overset{(-)}{\nu}$	6.4%
$3_0'^+\, 3_0'^-$	$2\gamma_D\, W^- W^+$	$4\gamma_D\, \ell_1^-\, \bar{\nu}_1\, \ell_2^+\, \nu_2$	3.2%
$3_\pm^0\, 3_\mp^\pm$	$1_+1_-\, Z\, W^\pm\, (2/4\gamma_D)$	$1_+1_-\, \ell_1^+\, \ell_1^-\, \ell_2^\pm\, \overset{(-)}{\nu}_2\, (2/4\gamma_D)$	1.7%
$3_\pm^0\, 3_\mp^\pm$	$1_+1_-\, \gamma\, W^\pm\, (2/4\gamma_D)$	$1_+1_-\, \gamma\, \ell^\pm\, \overset{(-)}{\nu}\, (2/4\gamma_D)$	6.4%
$3_\pm^+\, 3_\mp^-$	$1_+1_-\, W^-\, W^+\, (2/4\gamma_D)$	$1_+1_-\, \ell_1^-\, \bar{\nu}_1\, \ell_2^+\, \nu_2\, (2/4\gamma_D)$	3.2%

Table 4.2: Branching ratios into leptonic final states for each pair of triplets produced via Drell-Yan processes, assuming a normal hierarchy. Upper (lower) indices indicate the electromagnetic ($\mathrm{U}(1)_{3V}$) charge of each particle. Leptons appearing in the third column can belong to any of the three SM families, while the values in the fourth column report the branching ratios into fully leptonic final states and include the branching ratio of taus into lighter leptons.

pens outside the detector, while δ_{eff} is a reconstruction efficiency. Within a Bayesian framework, we set a 95% probability limit on the maximum number of signal events compatible with the data, and then translate it into a bound in the (m_1, m_3) plane using Eq. (4.25). We assume a Poissonian distribution for the number of events, and model the background by using a log-normal distribution. The mass of the triplets must be larger than half the Z mass to pass the constraints on the Z width from LEP. In practice, the particular value of this upper limit is irrelevant because the likelihood is exponentially suppressed for (much) lower values of N_s. We have thus assumed a flat prior on N_s and set $\delta_{eff} = 0.35$ to reproduce the bounds of Ref. [190] on the mass of supersymmetric particles. Using the data from Refs. [190, 191], we obtain the 95% probability bounds on the number of signal events shown in Tab. 4.3 in the channels with two or three leptons. Lepton plus photon searches and searches for hadronic final states have larger backgrounds and give less stringent bounds, see for example Ref. [192] and Ref. [193].

numerical simulations and, given the large number of final states, is beyond the scope of this paper. We leave such analysis to a future study.

Channel	N_b	N_{obs}	$N_s^{\max}$
3 leptons with OSSF pair $(+j)$	69 ± 5.5	81	31.5
2 leptons (OSDF) $(+j)$	172 ± 17.5	170	41.0
2 leptons (OSSF) $(+j)$	269 ± 17	267	45.5

Table 4.3: 95% probability bounds on the number of signal events, $N_s^{\max}$, from the missing energy searches of Refs. [190, 191] performed with $139\,\text{fb}^{-1}$ of integrated luminosity collected at the 13 TeV LHC. The number of background (N_b) and observed (N_{obs}) events is reported in the second and third columns respectively. Leptons are either electrons or muons, and the acronyms stand for opposite sign same flavour (OSSF) and opposite sign different flavour (OSDF). The $+j$ in brackets refers to the possible inclusion of one jet, since initial-state radiation might be present.

Figure 4.12 shows our recast in the plane (m_1, m_3) of the limit from three-lepton events of Tab. 4.3, both for large and small values of ε. Let us first consider the limit obtained assuming that ε is sufficiently small to let the dark photons decay outside the detector (red dashed line of Fig. 4.12). When $m_1 \ll m_3$, all four triplets are produced in the same amount and they all decay to missing energy, contributing to the bound. As m_1 increases, the charged triplets become heavier and their production cross section is suppressed, so they gradually become irrelevant. Furthermore, while the decays of 3_0 always give rise to missing energy (either through dark photons or through neutrinos), when $m_3 < m_{\gamma_D}$ the $3_0'$ cannot decay into dark photons and thus also stops contributing. [8] The effective multiplicity of triplets therefore changes from 4 to 1 along the m_1 axis, implying the two asymptotes in the plot. When ε is large and dark photons decay inside the detector, the only missing energy can come from singlets or neutrinos. Thus only charged triplets contribute for low m_1, until the 3_0 switches from dark-photon final states to leptons and neutrinos (see Tab. 4.1). This corresponds to an effective change of multiplicity from 2 to 1, as shown by the blue curve in the plot.

Finally, it is possible to use the same approach to investigate the case where the dark photons or the $3_0'$ decay inside the detector but far from the interaction point. Their signature in this case is that of two visible tracks originating from a displaced vertex. Such displaced decays occur in a range of values of ε that depends on m_1 and m_3 (and only for an inverted hierarchy in the case of the $3_0'$). Since a single displaced vertex from any of the $2-4$ dark photons produced in each collision is enough to yield a measurable signal, the reach in ε is slightly larger than the naive expectation, but still confined to a relatively narrow window of values. We made use of the searches for displaced dileptons and jets performed by the ATLAS collaboration in Refs. [194, 195, 196, 197]. Searches performed by CMS lead to similar or slightly stronger results but they rely on tighter event selections or trigger requirements that are not necessarily satisfied by

[8] Decays $3_0' \to V\bar{f}f$ can give missing energy in the form of neutrinos, but in those cases the final state usually contains too many jets or leptons to pass the selection of Refs. [190, 191].

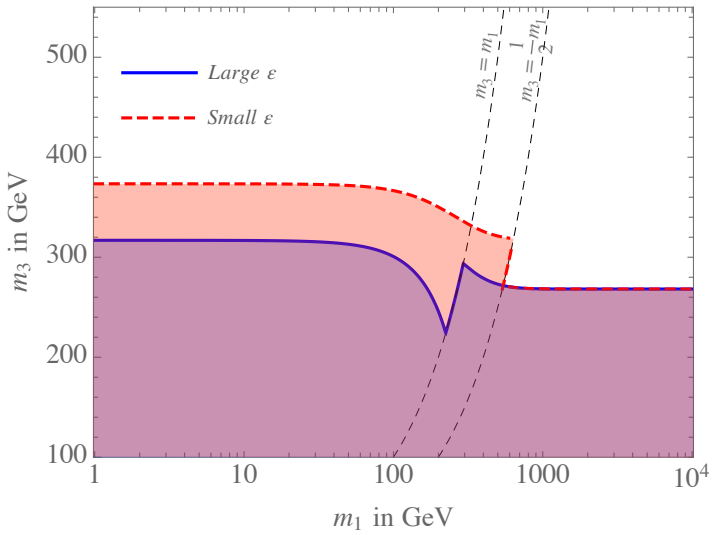

Figure 4.12: 95% probability exclusion regions in the (m_1, m_3) plane from collider searches of events with three leptons and missing energy (first row of Table 4.3). The dashed red curve assumes a value of ε sufficiently small to have dark photon decays outside the detector, while the solid blue one applies for larger values of ε. Both curves assume $m_1 = 2m_{\gamma_D}$. The gray thin dashed lines mark the different kinematic regions of Tab. 4.1.

our signal events. [9] Each search looks for decays occurring in different parts of the detector (inner tracker, calorimeter and muon spectrometer), at distances ranging from millimeters to several meters away from the primary vertex, and is thus sensitive to different lifetimes of the long-lived particle. Table 4.4 shows the number of observed and background events – or the number of displaced vertices, in the case of Ref. [195] – together with the upper bound on the signal derived within our Bayesian approach. Figure 4.13 shows the corresponding constraints in the (m_1, m_3) plane obtained for $\varepsilon = 10^{-8}$ by computing the number of signal events through a formula analogous to Eq. (4.25), where P now corresponds to the probability for the decay(s) to occur in the relevant part of the detector. We display only the exclusions set by the dilepton and dijet searches of Refs. [194, 196], since they give the strongest bounds; they were obtained by assuming an efficiency equal to $\delta_{eff} = 0.4$ and $\delta_{eff} = 0.03$ respectively. Notice that, differently from missing-energy searches, in this case final states with jets are competitive with leptons since they have equally suppressed backgrounds. The plot suggests that values of m_3 as large as the TeV can be excluded with displaced decays. The range of

[9] For example, the CMS search of Ref. [200] makes use of the timing information from the ECAL to identify long-lived particles and sets strong bounds. Deriving the constraints on our model from this and other searches would require a dedicated Montecarlo simulation and is beyond the scope of this work.

Search	Integrated Luminosity	N_b	N_{obs}	$N_s^{\max}$
ATLAS Dilepton [194]	$32.8\,\text{fb}^{-1}$ @ 13 TeV	0.27 ± 0.17	0	3.0
ATLAS Dimuon [195]	$32.9\,\text{fb}^{-1}$ @ 13 TeV	$0.5^{+1.4}_{-0.0}$	2	6.0
ATLAS Dijet [196]	$36.1\,\text{fb}^{-1}$ @ 13 TeV	0.027 ± 0.011	0	3.0
ATLAS Dijet [197]	$35.9\,\text{fb}^{-1}$ @ 13 TeV	8.5 ± 2.2	10	10.0

Table 4.4: 95% probability bounds on the number of signal events, $N_s^{\max}$, obtained from searches for displaced dilepton or dijet vertices performed by ATLAS. The number of expected background (N_b) and observed (N_{obs}) events is reported in the third and fourth columns respectively.

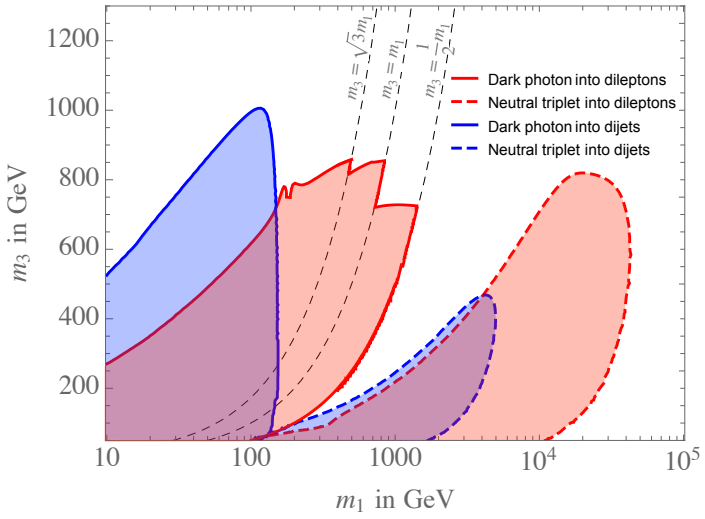

Figure 4.13: Bounds in the triplet-singlet mass plane for $\varepsilon = 10^{-8}$ and $m_1 = 2m_{\gamma_D}$ from searches performed by ATLAS that look for displaced dileptons in the inner tracker [194] and dijets in the muon spectrometer [196]. Regions with solid contours are excluded by the decay of the dark photons, while those with thick dashed contours are excluded by the decays of the $3_0'$. Since the latter has a smaller decay rate compared to the dark photon, its exclusion region extends to larger values of m_1. The thin dashed lines identify the different kinematic regions of Table 4.1, and can coincide with discontinuities in the value of the bounds.

excluded m_1 depends on the value of ε, as a combination of these two parameters controls the lifetime of the decaying particle, while the yield of signal events largely depends on m_3. Increasing (decreasing) ε, in particular, would deform the excluded regions and shift them towards smaller (larger) values of m_1.

The current bounds from collider searches are starting to test the thermal dark matter region of our model for values of $\varepsilon \sim 10^{-8}$, corresponding to dark photons behaving as long-lived particles on collider scales. A future hadronic circular collider operating at 100 TeV with an integrated luminosity of $20\,ab^{-1}$ will be able to improve on the current bounds by a factor of ten or slightly more, depending on the channel, testing a large portion of the available parameter space (see Figs. 3.3, 3.4 and 3.5).

5 Conclusions

Strongly coupled theories with composite dark matter candidates represent an interesting alternative to conventional weakly coupled dark matter models. They are well motivated from a UV perspective, reproducing the successful features of the Standard Model: global symmetries arise as accidental symmetries of the low energy dynamics of a gauge theory, explaining in a natural way the stability of dark matter, similarly to the stability of the proton in the Standard Model. The scenario of chiral gauge theories allows one to go one step further, explaining dynamically the origin of the dark matter mass scale and providing further protection for the accidental symmetry which explains dark matter stability.

From a low energy perspective, the phenomenological predictions for the dark matter candidates including the dark matter mass, annihilation cross section and experimental signatures are sensitive to the underlying strong dynamics, justifying the study of the gauge theories in terms of fundamental fields. This is particularly relevant for the models of gluequark dark matter discussed in Chapter 2, where the cosmological history and the present day annihilation cross section differ significantly from the case of an ordinary thermal relic in the case of dark fermions with a constituent mass larger than the dynamical confinement scale, see section 2.5 for a discussion. The study of chiral gauge theories with product gauge groups presented in Chapter 3 can be done systematically with the aid of chiral lagrangian techniques and reveals some interesting non generic features from a low energy perspective, presented in section 3.6. An accurate description of the IR phenomenology is not always captured by the dimension 4 effective lagrangian for the lowest lying states, SM singlet dark pion and dark photon, especially for what concerns the cosmological history and collider searches.

The inclusion of SM interactions can be done in such a way that it does not interfere with the electroweak symmetry breaking sector, currently strongly constrained with electroweak precision tests and the measurement of Higgs boson properties with ever increasing precision. Yet this can allow one to test this models with a variety of search strategies, complementing direct detection and indirect searches with collider experiments. Gluequark dark matter candidates can be tested mainly through indirect searches, while the models of chiral dark matter allow for a variety of search strategies, as described in chapter 4. For favourable choices of parameters the thermal dark matter region of chiral dark matter models can be tested through all the three available categories of dark matter searches. Even if the dark matter candidate is a Standard Model singlet, effective collider searches can be performed looking for the SM charged partners or the long-lived dark photons, rather than directly searching for dark matter in missing energy plus mono-X signals. Future experiments will be able to improve significantly the current limits, testing a large portion of the available parameter space of the model.

Further studies and improvements can be envisioned on many different aspects touched upon during this work. We would like to mention, in particular, improved phenomenological predictions for the gluequark candidate, the detailed exploration of some of the alternative scenarios for chiral dark matter described in section 3.5.5, more refined studies of collider bounds for chiral dark matter and further exploration of chiral models compatible with Grand Unification.

Bibliography

[1] R. Contino, A. Mitridate and A. Podo, *Beyond the standard model with strong dynamics*, *Frascati Phys. Ser.* **65** (2017) 1.

[2] R. Contino, A. Mitridate, A. Podo and M. Redi, *Gluequark Dark Matter*, *JHEP* **02** (2019) 187 [1811.06975].

[3] R. Contino, A. Podo and F. Revello, *Composite dark matter from strongly-interacting chiral dynamics*, *to appear* (2020) .

[4] A. Mitridate and A. Podo, *Bounds on Dark Matter decay from 21 cm line*, *JCAP* **05** (2018) 069 [1803.11169].

[5] R. Contino, A. Podo and F. Revello, *to appear*.

[6] L. Hui, J. P. Ostriker, S. Tremaine and E. Witten, *Ultralight scalars as cosmological dark matter*, *Phys. Rev. D* **95** (2017) 043541 [1610.08297].

[7] D. J. E. Marsh, *Axion Cosmology*, *Phys. Rept.* **643** (2016) 1 [1510.07633].

[8] M. Drewes et al., *A White Paper on keV Sterile Neutrino Dark Matter*, *JCAP* **01** (2017) 025 [1602.04816].

[9] K. M. Zurek, *Asymmetric Dark Matter: Theories, Signatures, and Constraints*, *Phys. Rept.* **537** (2014) 91 [1308.0338].

[10] K. Petraki and R. R. Volkas, *Review of asymmetric dark matter*, *Int. J. Mod. Phys. A* **28** (2013) 1330028 [1305.4939].

[11] L. J. Hall, K. Jedamzik, J. March-Russell and S. M. West, *Freeze-In Production of FIMP Dark Matter*, *JHEP* **03** (2010) 080 [0911.1120].

[12] N. Bernal, M. Heikinheimo, T. Tenkanen, K. Tuominen and V. Vaskonen, *The Dawn of FIMP Dark Matter: A Review of Models and Constraints*, *Int. J. Mod. Phys. A* **32** (2017) 1730023 [1706.07442].

[13] G. Jungman, M. Kamionkowski and K. Griest, *Supersymmetric dark matter*, *Phys. Rept.* **267** (1996) 195 [hep-ph/9506380].

[14] M. Cirelli, N. Fornengo and A. Strumia, *Minimal dark matter*, *Nucl. Phys.* **B753** (2006) 178 [hep-ph/0512090].

[15] B. Carr and F. Kuhnel, *Primordial Black Holes as Dark Matter: Recent Developments*, 2006.02838.

[16] C. Kilic, T. Okui and R. Sundrum, *Vectorlike Confinement at the LHC*, *JHEP* **02** (2010) 018 [0906.0577].

[17] Y. Bai and R. J. Hill, *Weakly Interacting Stable Pions*, *Phys. Rev. D* **82** (2010) 111701 [1005.0008].

[18] M. R. Buckley and E. T. Neil, *Thermal dark matter from a confining sector*, *Phys. Rev. D* **87** (2013) 043510 [1209.6054].

[19] Lattice Strong Dynamics (LSD) collaboration, T. Appelquist et al., *Composite bosonic baryon dark matter on the lattice: SU(4) baryon spectrum and the effective Higgs interaction*, *Phys. Rev. D* **89** (2014) 094508 [1402.6656].

[20] O. Antipin, M. Redi and A. Strumia, *Dynamical generation of the weak and Dark Matter scales from strong interactions*, *JHEP* **01** (2015) 157 [1410.1817].

[21] T. Appelquist et al., *Stealth Dark Matter: Dark scalar baryons through the Higgs portal*, *Phys. Rev. D* **92** (2015) 075030 [1503.04203].

[22] O. Antipin, M. Redi, A. Strumia and E. Vigiani, *Accidental Composite Dark Matter*, *JHEP* **07** (2015) 039 [1503.08749].

[23] A. Carmona and M. Chala, *Composite Dark Sectors*, *JHEP* **06** (2015) 105 [1504.00332].

[24] R. Huo, S. Matsumoto, Y.-L. Sming Tsai and T. T. Yanagida, *A scenario of heavy but visible baryonic dark matter*, *JHEP* **09** (2016) 162 [1506.06929].

[25] A. Mitridate, M. Redi, J. Smirnov and A. Strumia, *Dark Matter as a weakly coupled Dark Baryon*, *JHEP* **10** (2017) 210 [1707.05380].

[26] D. Buttazzo, L. Di Luzio, G. Landini, A. Strumia and D. Teresi, *Dark Matter from self-dual gauge/Higgs dynamics*, *JHEP* **10** (2019) 067 [1907.11228].

[27] D. Buttazzo, L. Di Luzio, P. Ghorbani, C. Gross, G. Landini, A. Strumia et al., *Scalar gauge dynamics and Dark Matter*, *JHEP* **01** (2020) 130 [1911.04502].

[28] D. Barducci, S. De Curtis, M. Redi and A. Tesi, *An almost elementary Higgs: Theory and Practice*, *JHEP* **08** (2018) 017 [1805.12578].

[29] G. D. Kribs, A. Martin, B. Ostdiek and T. Tong, *Dark Mesons at the LHC*, *JHEP* **07** (2019) 133 [1809.10184].

[30] A. Falkowski, J. Juknevich and J. Shelton, *Dark Matter Through the Neutrino Portal*, 0908.1790.

[31] K. K. Boddy, J. L. Feng, M. Kaplinghat and T. M. P. Tait, *Self-Interacting Dark Matter from a Non-Abelian Hidden Sector*, *Phys. Rev. D* **89** (2014) 115017 [1402.3629].

[32] K. K. Boddy, J. L. Feng, M. Kaplinghat, Y. Shadmi and T. M. P. Tait, *Strongly interacting dark matter: Self-interactions and keV lines*, *Phys. Rev. D* **90** (2014) 095016 [1408.6532].

[33] D. B. Kaplan and H. Georgi, *SU(2) x U(1) Breaking by Vacuum Misalignment*, *Phys. Lett.* **136B** (1984) 183.

[34] T. Banks, *CONSTRAINTS ON SU(2) x U(1) BREAKING BY VACUUM MISALIGNMENT*, *Nucl. Phys.* **B243** (1984) 125.

[35] D. B. Kaplan, H. Georgi and S. Dimopoulos, *Composite Higgs Scalars*, *Phys. Lett.* **136B** (1984) 187.

[36] H. Georgi, D. B. Kaplan and P. Galison, *Calculation of the Composite Higgs Mass*, *Phys. Lett.* **143B** (1984) 152.

[37] H. Georgi and D. B. Kaplan, *Composite Higgs and Custodial SU(2)*, *Phys. Lett.* **145B** (1984) 216.

[38] M. J. Dugan, H. Georgi and D. B. Kaplan, *Anatomy of a Composite Higgs Model*, *Nucl. Phys.* **B254** (1985) 299.

[39] L. E. Ibanez and G. G. Ross, *SU(2)-L x U(1) Symmetry Breaking as a Radiative Effect of Supersymmetry Breaking in Guts*, *Phys. Lett.* **110B** (1982) 215.

[40] K. Inoue, A. Kakuto, H. Komatsu and S. Takeshita, *Aspects of Grand Unified Models with Softly Broken Supersymmetry*, *Prog. Theor. Phys.* **68** (1982) 927.

[41] P. W. Graham, D. E. Kaplan and S. Rajendran, *Cosmological Relaxation of the Electroweak Scale*, *Phys. Rev. Lett.* **115** (2015) 221801 [1504.07551].

[42] G. D. Kribs and E. T. Neil, *Review of strongly-coupled composite dark matter models and lattice simulations*, *Int. J. Mod. Phys. A* **31** (2016) 1643004 [1604.04627].

[43] Z. Berezhiani, *Mirror world and its cosmological consequences*, *Int. J. Mod. Phys. A* **19** (2004) 3775 [hep-ph/0312335].

[44] P. Ciarcelluti, *Cosmology with mirror dark matter*, *Int. J. Mod. Phys. D* **19** (2010) 2151 [1102.5530].

[45] R. Foot, *Mirror dark matter: Cosmology, galaxy structure and direct detection*, *Int. J. Mod. Phys. A* **29** (2014) 1430013 [1401.3965].

[46] Z. Chacko, D. Curtin, M. Geller and Y. Tsai, *Cosmological Signatures of a Mirror Twin Higgs*, *JHEP* **09** (2018) 163 [1803.03263].

[47] K. Harigaya and Y. Nomura, *Light Chiral Dark Sector*, *Phys. Rev.* **D94** (2016) 035013 [1603.03430].

[48] R. T. Co, K. Harigaya and Y. Nomura, *Chiral Dark Sector*, *Phys. Rev. Lett.* **118** (2017) 101801 [1610.03848].

[49] M. P. Hertzberg and M. Sandora, *Dark Matter and Naturalness*, *JHEP* **12** (2019) 037 [1908.09841].

[50] S. B. Gudnason, C. Kouvaris and F. Sannino, *Towards working technicolor: Effective theories and dark matter*, *Phys. Rev. D* **73** (2006) 115003 [hep-ph/0603014].

[51] C. Kouvaris, *Dark Majorana Particles from the Minimal Walking Technicolor*, *Phys. Rev. D* **76** (2007) 015011 [hep-ph/0703266].

[52] V. De Luca, A. Mitridate, M. Redi, J. Smirnov and A. Strumia, *Colored Dark Matter*, *Phys. Rev.* **D97** (2018) 115024 [1801.01135].

[53] S. Catterall, L. Del Debbio, J. Giedt and L. Keegan, *MCRG Minimal Walking Technicolor*, *Phys. Rev. D* **85** (2012) 094501 [1108.3794].

[54] G. Bergner, P. Giudice, G. Münster, I. Montvay and S. Piemonte, *Spectrum and mass anomalous dimension of SU(2) adjoint QCD with two Dirac flavors*, *Phys. Rev. D* **96** (2017) 034504 [1610.01576].

[55] G. Bergner, P. Giudice, G. Münster, P. Scior, I. Montvay and S. Piemonte, *Low energy properties of SU(2) gauge theory with $N_f = 3/2$ flavours of adjoint fermions*, *JHEP* **01** (2018) 119 [1712.04692].

[56] A. Athenodorou, E. Bennett, G. Bergner and B. Lucini, *Infrared regime of SU(2) with one adjoint Dirac flavor*, *Phys. Rev. D* **91** (2015) 114508 [1412.5994].

[57] G. Bergner, P. Giudice, G. Münster, I. Montvay and S. Piemonte, *The light bound states of supersymmetric SU(2) Yang-Mills theory*, *JHEP* **03** (2016) 080 [1512.07014].

[58] T. DeGrand, *Lattice tests of beyond Standard Model dynamics*, *Rev. Mod. Phys.* **88** (2016) 015001 [1510.05018].

[59] S. Ali, G. Bergner, H. Gerber, P. Giudice, I. Montvay, G. Munster et al., *Simulations of N=1 supersymmetric Yang-Mills theory with three colours*, *PoS* **LATTICE2016** (2016) 222 [1610.10097].

[60] G. Bergner, P. Giudice, I. Montvay, G. Münster and S. Piemonte, *Spectrum and mass anomalous dimension of SU(2) gauge theories with fermions in the adjoint representation: from $N_f = 1/2$ to $N_f = 2$*, *PoS* **LATTICE2016** (2017) 237 [1701.08992].

[61] D. Nogradi and A. Patella, *Strong dynamics, composite Higgs and the conformal window*, *Int. J. Mod. Phys. A* **31** (2016) 1643003 [1607.07638].

[62] T. DeGrand, Y. Shamir and B. Svetitsky, *Near the Sill of the Conformal Window: Gauge Theories with Fermions in Two-Index Representations*, *Phys. Rev. D* **88** (2013) 054505 [1307.2425].

[63] UKQCD collaboration, M. Foster and C. Michael, *Hadrons with a heavy color adjoint particle*, *Phys. Rev. D* **59** (1999) 094509 [hep-lat/9811010].

[64] G. S. Bali and A. Pineda, *QCD phenomenology of static sources and gluonic excitations at short distances*, *Phys. Rev. D* **69** (2004) 094001 [hep-ph/0310130].

[65] C. J. Morningstar and M. J. Peardon, *The Glueball spectrum from an anisotropic lattice study*, *Phys. Rev. D* **60** (1999) 034509 [hep-lat/9901004].

[66] J. E. Juknevich, D. Melnikov and M. J. Strassler, *A Pure-Glue Hidden Valley I. States and Decays*, *JHEP* **07** (2009) 055 [0903.0883].

[67] J. E. Juknevich, *Pure-glue hidden valleys through the Higgs portal*, *JHEP* **08** (2010) 121 [0911.5616].

[68] H. B. Meyer, *Glueball matrix elements: A Lattice calculation and applications*, *JHEP* **01** (2009) 071 [0808.3151].

[69] O. Antipin and M. Redi, *The Half-composite Two Higgs Doublet Model and the Relaxion*, *JHEP* **12** (2015) 031 [1508.01112].

[70] S. Bolognesi and M. Shifman, *The Hopf Skyrmion in QCD with Adjoint Quarks*, *Phys. Rev. D* **75** (2007) 065020 [hep-th/0701065].

[71] R. Auzzi, S. Bolognesi and M. Shifman, *Skyrmions in Yang-Mills Theories with Massless Adjoint Quarks*, *Phys. Rev. D* **77** (2008) 125029 [0804.0229].

[72] R. J. Scherrer and M. S. Turner, *Decaying Particles Do Not Heat Up the Universe*, *Phys. Rev. D* **31** (1985) 681.

[73] M. Kamionkowski and M. S. Turner, *THERMAL RELICS: DO WE KNOW THEIR ABUNDANCES?*, *Phys. Rev. D* **42** (1990) 3310.

[74] J. McDonald, *WIMP Densities in Decaying Particle Dominated Cosmology*, *Phys. Rev. D* **43** (1991) 1063.

[75] R. T. Co, F. D'Eramo, L. J. Hall and D. Pappadopulo, *Freeze-In Dark Matter with Displaced Signatures at Colliders*, *JCAP* **12** (2015) 024 [1506.07532].

[76] A. Berlin, D. Hooper and G. Krnjaic, *PeV-Scale Dark Matter as a Thermal Relic of a Decoupled Sector*, *Phys. Lett. B* **760** (2016) 106 [1602.08490].

[77] M. Cirelli, Y. Gouttenoire, K. Petraki and F. Sala, *Homeopathic Dark Matter, or how diluted heavy substances produce high energy cosmic rays*, *JCAP* **02** (2019) 014 [1811.03608].

[78] N. Arkani-Hamed and S. Dimopoulos, *Supersymmetric unification without low energy supersymmetry and signatures for fine-tuning at the LHC*, *JHEP* **06** (2005) 073 [hep-th/0405159].

[79] J. Kang, M. A. Luty and S. Nasri, *The Relic abundance of long-lived heavy colored particles*, *JHEP* **09** (2008) 086 [hep-ph/0611322].

[80] C. Jacoby and S. Nussinov, *The Relic Abundance of Massive Colored Particles after a Late Hadronic Annihilation Stage*, 0712.2681.

[81] K. Harigaya, M. Ibe, K. Kaneta, W. Nakano and M. Suzuki, *Thermal Relic Dark Matter Beyond the Unitarity Limit*, *JHEP* **08** (2016) 151 [1606.00159].

[82] M. Geller, S. Iwamoto, G. Lee, Y. Shadmi and O. Telem, *Dark quarkonium formation in the early universe*, *JHEP* **06** (2018) 135 [1802.07720].

[83] D. Morgan and V. Hughes, *Atomic processes involved in matter-antimatter annihilation*, *Phys. Rev. D* **2** (1970) 1389.

[84] A. De Simone, G. F. Giudice and A. Strumia, *Benchmarks for Dark Matter Searches at the LHC*, *JHEP* **06** (2014) 081 [1402.6287].

[85] A. Mitridate, M. Redi, J. Smirnov and A. Strumia, *Cosmological Implications of Dark Matter Bound States*, *JCAP* **05** (2017) 006 [1702.01141].

[86] A. Zenoni et al., *New measurements of the anti-p p annihilation cross-section at very low-energy*, *Phys. Lett. B* **461** (1999) 405.

[87] G. Boyd, J. Engels, F. Karsch, E. Laermann, C. Legeland, M. Lutgemeier et al., *Thermodynamics of SU(3) lattice gauge theory*, *Nucl. Phys. B* **469** (1996) 419 [hep-lat/9602007].

[88] M. Redi and R. Sato, *Composite Accidental Axions*, *JHEP* **05** (2016) 104 [1602.05427].

[89] D. J. Chung, E. W. Kolb and A. Riotto, *Superheavy dark matter*, *Phys. Rev. D* **59** (1998) 023501 [hep-ph/9802238].

[90] S. Weinberg, *The Quantum theory of fields. Vol. 1: Foundations*. Cambridge University Press, 2005.

[91] D. B. Kaplan, *Five lectures on effective field theory*, 10, 2005, nucl-th/0510023.

[92] E. Eichten, K. Gottfried, T. Kinoshita, J. B. Kogut, K. D. Lane and T. M. Yan, *The Spectrum of Charmonium*, *Phys. Rev. Lett.* **34** (1975), 369-372.

[93] M. W. Goodman and E. Witten, *Detectability of Certain Dark Matter Candidates*, *Phys. Rev. D* **31** (1985) 3059.

[94] XENON collaboration, E. Aprile et al., *Dark Matter Search Results from a One Ton-Year Exposure of XENON1T*, *Phys. Rev. Lett.* **121** (2018) 111302 [1805.12562].

[95] P. Batra, B. A. Dobrescu and D. Spivak, *Anomaly-free sets of fermions*, *J. Math. Phys.* **47** (2006) 082301 [hep-ph/0510181].

[96] D. B. Costa, B. A. Dobrescu and P. J. Fox, *General Solution to the U(1) Anomaly Equations*, *Phys. Rev. Lett.* **123** (2019) 151601 [1905.13729].

[97] B. Allanach, B. Gripaios and J. Tooby-Smith, *Geometric General Solution to the $U(1)$ Anomaly Equations*, *JHEP* **05** (2020) 065 [1912.04804].

[98] J. M. Berryman, A. de Gouvêa, D. Hernández and K. J. Kelly, *Imperfect mirror copies of the standard model*, *Phys. Rev.* **D94** (2016) 035009 [1605.03610].

[99] T. DeGrand, *Lattice methods for students at a formal TASI*, in *Theoretical Advanced Study Institute in Elementary Particle Physics: The Many Dimensions of Quantum Field Theory*, 7, 2019, 1907.02988.

[100] M. Luscher, *Chiral gauge theories revisited*, *Subnucl. Ser.* **38** (2002) 41 [hep-th/0102028].

[101] S. Raby, S. Dimopoulos and L. Susskind, *Tumbling Gauge Theories*, *Nucl. Phys. B* **169** (1980) 373.

[102] F. A. Bais and J. M. Frere, *Composite Vector Fields and Tumbling Gauge Theories*, *Phys. Lett.* **98B** (1981) 431.

[103] B. Holdom, *Two U(1)'s and Epsilon Charge Shifts*, *Phys. Lett. B* **166** (1986) 196.

[104] C. Vafa and E. Witten, *Restrictions on Symmetry Breaking in Vector-Like Gauge Theories*, *Nucl. Phys.* **B234** (1984) 173.

[105] D. A. Kosower, *SYMMETRY BREAKING PATTERNS IN PSEUDOREAL AND REAL GAUGE THEORIES*, *Phys. Lett.* **144B** (1984) 215.

[106] M. E. Peskin, *The Alignment of the Vacuum in Theories of Technicolor*, *Nucl. Phys. B* **175** (1980) 197.

[107] J. Preskill, *Subgroup Alignment in Hypercolor Theories*, *Nucl. Phys. B* **177** (1981) 21.

[108] M. L. Perl, E. R. Lee and D. Loomba, *Searches for fractionally charged particles*, *Ann. Rev. Nucl. Part. Sci.* **59** (2009) 47.

[109] Y. Bai, J. Berger, J. Osborne and B. A. Stefanek, *Phenomenology of Strongly Coupled Chiral Gauge Theories*, *JHEP* **11** (2016) 153 [1605.07183].

[110] Y. Bai and R. J. Hill, *Weakly interacting stable hidden sector pions*, *Physical Review D* **82** (2010) .

[111] R. Contino, *The Higgs as a Composite Nambu-Goldstone Boson*, in *Physics of the large and the small, TASI 09, proceedings of the Theoretical Advanced Study Institute in Elementary Particle Physics, Boulder, Colorado, USA, 1-26 June 2009*, pp. 235–306, 2011, 1005.4269, DOI.

[112] OBELIX collaboration, A. Bertin et al., *anti-n p annihilation in flight in two mesons in the momentum range between 50-MeV/c and 400-MeV/c with OBELIX*, *Nucl. Phys. B Proc. Suppl.* **56** (1997) 227.

[113] A. Berlin, D. Hooper and G. Krnjaic, *Thermal Dark Matter From A Highly Decoupled Sector*, *Phys. Rev. D* **94** (2016) 095019 [1609.02555].

[114] Planck collaboration, N. Aghanim et al., *Planck 2018 results. VI. Cosmological parameters*, 1807.06209.

[115] CMB-S4 collaboration, K. N. Abazajian et al., *CMB-S4 Science Book, First Edition*, 1610.02743.

[116] J. Lesgourgues, G. Marques-Tavares and M. Schmaltz, *Evidence for dark matter interactions in cosmological precision data?*, *JCAP* **02** (2016) 037 [1507.04351].

[117] M. A. Buen-Abad, M. Schmaltz, J. Lesgourgues and T. Brinckmann, *Interacting Dark Sector and Precision Cosmology*, *JCAP* **01** (2018) 008 [1708.09406].

[118] Z. Chacko, Y. Cui, S. Hong, T. Okui and Y. Tsai, *Partially Acoustic Dark Matter, Interacting Dark Radiation, and Large Scale Structure*, *JHEP* **12** (2016) 108 [1609.03569].

[119] P. Ko, N. Nagata and Y. Tang, *Hidden Charged Dark Matter and Chiral Dark Radiation*, *Phys. Lett. B* **773** (2017) 513 [1706.05605].

[120] G. Salam and A. Weiler, "Collider reach (β)." http://collider-reach.web.cern.ch/collider-reach/.

[121] CTA collaboration, A. Acharyya et al., *Pre-construction estimates of the Cherenkov Telescope Array sensitivity to a dark matter signal from the Galactic centre*, 2007.16129.

[122] R. Contino, C. Grojean, M. Moretti, F. Piccinini and R. Rattazzi, *Strong Double Higgs Production at the LHC*, *JHEP* **05** (2010) 089 [1002.1011].

[123] J. M. Cline, G. Dupuis, Z. Liu and W. Xue, *The windows for kinetically mixed Z'-mediated dark matter and the galactic center gamma ray excess*, *JHEP* **08** (2014) 131 [1405.7691].

[124] D. Curtin, R. Essig, S. Gori and J. Shelton, *Illuminating Dark Photons with High-Energy Colliders*, *JHEP* **02** (2015) 157 [1412.0018].

[125] J. A. Evans, S. Gori and J. Shelton, *Looking for the WIMP Next Door*, *JHEP* **02** (2018) 100 [1712.03974].

[126] T. Bhattacharya and P. Roy, *Unitarity Limit on the Gaugino - Gravitino Mass Ratio*, *Phys. Lett. B* **206** (1988) 655.

[127] S. Clark, B. Dutta, Y. Gao, Y.-Z. Ma and L. E. Strigari, *21 cm limits on decaying dark matter and primordial black holes*, *Phys. Rev. D* **98** (2018) 043006 [1803.09390].

[128] H. Liu and T. R. Slatyer, *Implications of a 21-cm signal for dark matter annihilation and decay*, *Phys. Rev. D* **98** (2018) 023501 [1803.09739].

[129] S. R. Furlanetto, *The 21-cm Line as a Probe of Reionization*, 1511.01131.

[130] P. Madau, A. Meiksin and M. J. Rees, *21-CM tomography of the intergalactic medium at high redshift*, *Astrophys. J.* **475** (1997) 429 [astro-ph/9608010].

[131] M. Valdes, C. Evoli, A. Mesinger, A. Ferrara and N. Yoshida, *The nature of dark matter from the global high redshift HI 21 cm signal*, *Mon. Not. Roy. Astron. Soc.* **429** (2013) 1705 [1209.2120].

[132] C. Evoli, A. Mesinger and A. Ferrara, *Unveiling the nature of dark matter with high redshift 21 cm line experiments*, *JCAP* **11** (2014) 024 [1408.1109].

[133] L. Lopez-Honorez, O. Mena, A. Moline, S. Palomares-Ruiz and A. C. Vincent, *The 21 cm signal and the interplay between dark matter annihilations and astrophysical processes*, *JCAP* **08** (2016) 004 [1603.06795].

[134] G. D'Amico, P. Panci and A. Strumia, *Bounds on Dark Matter annihilations from 21 cm data*, *Phys. Rev. Lett.* **121** (2018) 011103 [1803.03629].

[135] J. D. Bowman, A. E. E. Rogers, R. A. Monsalve, T. J. Mozdzen and N. Mahesh, *An absorption profile centred at 78 megahertz in the sky-averaged spectrum*, *Nature* **555** (2018) 67 [1810.05912].

[136] J. B. Muñoz, E. D. Kovetz and Y. Ali-Haïmoud, *Heating of Baryons due to Scattering with Dark Matter During the Dark Ages*, *Phys. Rev. D* **92** (2015) 083528 [1509.00029].

[137] R. Barkana, *Possible interaction between baryons and dark-matter particles revealed by the first stars*, *Nature* **555** (2018) 71 [1803.06698].

[138] J. B. Muñoz and A. Loeb, *A small amount of mini-charged dark matter could cool the baryons in the early Universe*, *Nature* **557** (2018) 684 [1802.10094].

[139] M. Pospelov, J. Pradler, J. T. Ruderman and A. Urbano, *Room for New Physics in the Rayleigh-Jeans Tail of the Cosmic Microwave Background*, *Phys. Rev. Lett.* **121** (2018) 031103 [1803.07048].

[140] S. Fraser et al., *The EDGES 21 cm Anomaly and Properties of Dark Matter*, *Phys. Lett. B* **785** (2018) 159 [1803.03245].

[141] A. Berlin, D. Hooper, G. Krnjaic and S. D. McDermott, *Severely Constraining Dark Matter Interpretations of the 21-cm Anomaly*, *Phys. Rev. Lett.* **121** (2018) 011102 [1803.02804].

[142] R. Barkana, N. J. Outmezguine, D. Redigolo and T. Volansky, *Strong constraints on light dark matter interpretation of the EDGES signal*, *Phys. Rev. D* **98** (2018) 103005 [1803.03091].

[143] Planck collaboration, P. A. R. Ade et al., *Planck 2015 results. XIII. Cosmological parameters*, *Astron. Astrophys.* **594** (2016) A13 [1502.01589].

[144] T. R. Slatyer and C.-L. Wu, *General Constraints on Dark Matter Decay from the Cosmic Microwave Background*, *Phys. Rev. D* **95** (2017) 023010 [1610.06933].

[145] P. Peebles, *Recombination of the Primeval Plasma*, *Astrophys. J.* **153** (1968) 1.

[146] S. Galli, F. Iocco, G. Bertone and A. Melchiorri, *CMB constraints on Dark Matter models with large annihilation cross-section*, *Phys. Rev. D* **80** (2009) 023505 [0905.0003].

[147] J. Chluba, D. Paoletti, F. Finelli and J.-A. Rubiño-Martín, *Effect of primordial magnetic fields on the ionization history*, *Mon. Not. Roy. Astron. Soc.* **451** (2015) 2244 [1503.04827].

[148] D. E. Osterbrock, *Astrophysics of gaseous nebulae and active galactic nuclei*. 1989.

[149] X.-L. Chen and M. Kamionkowski, *Particle decays during the cosmic dark ages*, *Phys. Rev. D* **70** (2004) 043502 [astro-ph/0310473].

[150] J. Shull and M. van Steenberg, *The ionization equilibrium of astrophysically abundant elements*, *Astrophys. J. Suppl.* **48** (1982) 95.

[151] T. R. Slatyer, *Energy Injection And Absorption In The Cosmic Dark Ages*, *Phys. Rev. D* **87** (2013) 123513 [1211.0283].

[152] J. Miralda-Escude, M. Haehnelt and M. J. Rees, *Reionization of the inhomogeneous universe*, *Astrophys. J.* **530** (2000) 1 [astro-ph/9812306].

[153] R. Essig, E. Kuflik, S. D. McDermott, T. Volansky and K. M. Zurek, *Constraining Light Dark Matter with Diffuse X-Ray and Gamma-Ray Observations*, *JHEP* **11** (2013) 193 [1309.4091].

[154] M. G. Baring, T. Ghosh, F. S. Queiroz and K. Sinha, *New Limits on the Dark Matter Lifetime from Dwarf Spheroidal Galaxies using Fermi-LAT*, *Phys. Rev. D* **93** (2016) 103009 [1510.00389].

[155] M. Cirelli, G. Corcella, A. Hektor, G. Hutsi, M. Kadastik, P. Panci et al., *PPPC 4 DM ID: A Poor Particle Physicist Cookbook for Dark Matter Indirect Detection*, *JCAP* **03** (2011) 051 [1012.4515].

[156] P. Ciafaloni, D. Comelli, A. Riotto, F. Sala, A. Strumia and A. Urbano, *Weak Corrections are Relevant for Dark Matter Indirect Detection*, *JCAP* **03** (2011) 019 [1009.0224].

[157] M. Kawasaki, K. Kohri, T. Moroi and Y. Takaesu, *Revisiting Big-Bang Nucleosynthesis Constraints on Long-Lived Decaying Particles*, *Phys. Rev. D* **97** (2018) 023502 [1709.01211].

[158] V. Poulin, J. Lesgourgues and P. D. Serpico, *Cosmological constraints on exotic injection of electromagnetic energy*, *JCAP* **03** (2017) 043 [1610.10051].

[159] A. Albert et al., *Results from the search for dark matter in the Milky Way with 9 years of data of the ANTARES neutrino telescope*, *Phys. Lett. B* **769** (2017) 249 [1612.04595].

[160] H.E.S.S. collaboration, H. Abdallah et al., *Search for dark matter annihilations towards the inner Galactic halo from 10 years of observations with H.E.S.S*, *Phys. Rev. Lett.* **117** (2016) 111301 [1607.08142].

[161] K. Murase and J. F. Beacom, *Constraining Very Heavy Dark Matter Using Diffuse Backgrounds of Neutrinos and Cascaded Gamma Rays*, *JCAP* **10** (2012) 043 [1206.2595].

[162] IceCube collaboration, M. Aartsen et al., *Search for neutrinos from decaying dark matter with IceCube*, *Eur. Phys. J. C* **78** (2018) 831 [1804.03848].

[163] S. Profumo, F. S. Queiroz, J. Silk and C. Siqueira, *Searching for Secluded Dark Matter with H.E.S.S., Fermi-LAT, and Planck*, *JCAP* **03** (2018) 010 [1711.03133].

[164] Fermi-LAT collaboration, M. Ackermann et al., *Searching for Dark Matter Annihilation from Milky Way Dwarf Spheroidal Galaxies with Six Years of Fermi Large Area Telescope Data*, *Phys. Rev. Lett.* **115** (2015) 231301 [1503.02641].

[165] M. Cirelli, P. Panci, K. Petraki, F. Sala and M. Taoso, *Dark Matter's secret liaisons: phenomenology of a dark U(1) sector with bound states*, *JCAP* **1705** (2017) 036 [1612.07295].

[166] LSST Dark Matter Group collaboration, A. Drlica-Wagner et al., *Probing the Fundamental Nature of Dark Matter with the Large Synoptic Survey Telescope*, 1902.01055.

[167] M. Escudero, S. J. Witte and D. Hooper, *Hidden Sector Dark Matter and the Galactic Center Gamma-Ray Excess: A Closer Look*, *JCAP* **11** (2017) 042 [1709.07002].

[168] B. J. Kavanagh, P. Panci and R. Ziegler, *Faint Light from Dark Matter: Classifying and Constraining Dark Matter-Photon Effective Operators*, *JHEP* **04** (2019) 089 [1810.00033].

[169] PandaX-II collaboration, X. Cui et al., *Dark Matter Results From 54-Ton-Day Exposure of PandaX-II Experiment*, *Phys. Rev. Lett.* **119** (2017) 181302 [1708.06917].

[170] LUX collaboration, D. Akerib et al., *Results from a search for dark matter in the complete LUX exposure*, *Phys. Rev. Lett.* **118** (2017) 021303 [1608.07648].

[171] LZ collaboration, D. Akerib et al., *LUX-ZEPLIN (LZ) Conceptual Design Report*, 1509.02910.

[172] A. Dolgov, S. Dubovsky, G. Rubtsov and I. Tkachev, *Constraints on millicharged particles from Planck data*, *Phys. Rev. D* **88** (2013) 117701 [1310.2376].

[173] R. de Putter, O. Doré, J. Gleyzes, D. Green and J. Meyers, *Dark Matter Interactions, Helium, and the Cosmic Microwave Background*, *Phys. Rev. Lett.* **122** (2019) 041301 [1805.11616].

[174] L. Chuzhoy and E. W. Kolb, *Reopening the window on charged dark matter*, *JCAP* **07** (2009) 014 [0809.0436].

[175] D. Dunsky, L. J. Hall and K. Harigaya, *CHAMP Cosmic Rays*, *JCAP* **07** (2019) 015 [1812.11116].

[176] K. Cheung and Z. S. Wang, *Probing Long-lived Particles at Higgs Factories* *Phys. Rev. D* **101** (2020) 035003 [1911.08721].

[177] ATLAS collaboration, *Search for new high-mass phenomena in the dilepton final state using 36.1 fb^{-1} of proton-proton collision data at $\sqrt{s}$ = 13 TeV with the ATLAS detector*, .

[178] T. Han, S. Mukhopadhyay and X. Wang, *Electroweak Dark Matter at Future Hadron Colliders*, *Phys. Rev. D* **98** (2018) 035026 [1805.00015].

[179] R. Contino, T. Kramer, M. Son and R. Sundrum, *Warped/composite phenomenology simplified*, *JHEP* **05** (2007) 074 [hep-ph/0612180].

[180] J. Kang and M. A. Luty, *Macroscopic Strings and 'Quirks' at Colliders*, *JHEP* **11** (2009) 065 [0805.4642].

[181] M. J. Strassler and K. M. Zurek, *Echoes of a hidden valley at hadron colliders*, *Phys. Lett. B* **651** (2007) 374 [hep-ph/0604261].

[182] L. A. Harland-Lang, A. D. Martin, P. Motylinski and R. S. Thorne, *Parton distributions in the LHC era: MMHT 2014 PDFs*, *Eur. Phys. J.* **C75** (2015) 204 [1412.3989].

[183] CMS Collaboration collaboration, *Search for a narrow resonance decaying to a pair of muons in proton-proton collisions at 13 TeV*, Tech. Rep. CMS-PAS-EXO-19-018, CERN, Geneva, 2019.

[184] C.-W. Chiang, G. Cottin, Y. Du, K. Fuyuto and M. J. Ramsey-Musolf, *Collider Probes of Real Triplet Scalar Dark Matter*, 2003.07867.

[185] CMS Collaboration collaboration, *Search for a narrow resonance in high-mass dilepton final states in proton-proton collisions using 140* fb^{-1} *of data at* $\sqrt{s}$ = 13 TeV, Tech. Rep. CMS-PAS-EXO-19-019, CERN, Geneva, 2019.

[186] ATLAS collaboration, G. Aad et al., *Search for high-mass dilepton resonances using 139* fb^{-1} *of pp collision data collected at* $\sqrt{s}$ *=13 TeV with the ATLAS detector*, *Phys. Lett.* **B796** (2019) 68 [1903.06248].

[187] CMS collaboration, A. M. Sirunyan et al., *Search for narrow and broad dijet resonances in proton-proton collisions at* $\sqrt{s}$ = 13 *TeV and constraints on dark matter mediators and other new particles*, *JHEP* **08** (2018) 130 [1806.00843].

[188] CMS collaboration, A. M. Sirunyan et al., *Search for pair-produced resonances decaying to quark pairs in proton-proton collisions at* $\sqrt{s}$ = *13 TeV*, *Phys. Rev.* **D98** (2018) 112014 [1808.03124].

[189] ATLAS collaboration, G. Aad et al., *Search for new resonances in mass distributions of jet pairs using 139* fb^{-1} *of pp collisions at* $\sqrt{s}$ = 13 *TeV with the ATLAS detector*, 1910.08447.

[190] ATLAS collaboration, G. Aad et al., *Search for electroweak production of charginos and sleptons decaying into final states with two leptons and missing transverse momentum in* $\sqrt{s}$ = 13 *TeV pp collisions using the ATLAS detector*, *Eur. Phys. J. C* **80** (2020) 123 [1908.08215].

[191] ATLAS collaboration, G. Aad et al., *Search for chargino-neutralino production with mass splittings near the electroweak scale in three-lepton final states in* $\sqrt{s}$*=13 TeV pp collisions with the ATLAS detector*, *Phys. Rev. D* **101** (2020) 072001 [1912.08479].

[192] CMS collaboration, A. M. Sirunyan et al., *Search for supersymmetry in events with a photon, a lepton, and missing transverse momentum in proton-proton collisions at* $\sqrt{s} = 13$ *TeV*, *JHEP* **01** (2019) 154 [1812.04066].

[193] CMS collaboration, A. M. Sirunyan et al., *Search for supersymmetry in proton-proton collisions at 13 TeV in final states with jets and missing transverse momentum*, *JHEP* **10** (2019) 244 [1908.04722].

[194] ATLAS collaboration, G. Aad et al., *Search for displaced vertices of oppositely charged leptons from decays of long-lived particles in pp collisions at* $\sqrt{s} = 13$ *TeV with the ATLAS detector*, 1907.10037.

[195] ATLAS collaboration, M. Aaboud et al., *Search for long-lived particles in final states with displaced dimuon vertices in pp collisions at* $\sqrt{s} = 13$ *TeV with the ATLAS detector*, *Phys. Rev.* **D99** (2019) 012001 [1808.03057].

[196] ATLAS collaboration, M. Aaboud et al., *Search for long-lived particles produced in pp collisions at* $\sqrt{s} = 13$ *TeV that decay into displaced hadronic jets in the ATLAS muon spectrometer*, *Phys. Rev. D* **99** (2019) 052005 [1811.07370].

[197] ATLAS collaboration, M. Aaboud et al., *Search for long-lived neutral particles in pp collisions at* $\sqrt{s} = 13$ *TeV that decay into displaced hadronic jets in the ATLAS calorimeter*, *Eur. Phys. J.* **C79** (2019) 481 [1902.03094].

[198] CMS collaboration, A. M. Sirunyan et al., *Search for long-lived particles decaying into displaced jets in proton-proton collisions at* $\sqrt{s} = 13$ *TeV*, *Phys. Rev.* **D99** (2019) 032011 [1811.07991].

[199] J. Liu, Z. Liu and L.-T. Wang, *Enhancing Long-Lived Particles Searches at the LHC with Precision Timing Information*, *Phys. Rev. Lett.* **122** (2019) 131801 [1805.05957].

[200] CMS collaboration, A. M. Sirunyan et al., *Search for long-lived particles using nonprompt jets and missing transverse momentum with proton-proton collisions at* $\sqrt{s} = 13$ *TeV*, *Phys. Lett. B* **797** (2019) 134876 [1906.06441].